

Aus dem Walther-Straub-Institut für Pharmakologie und Toxikologie

Institut der Ludwig-Maximilians-Universität München

Vorstand: Prof. Dr. med. Thomas Gudermann

# **Role of kinase-coupled TRPM6 ion channels in the lung**



Dissertation zum Erwerb des Doktorgrades der  
Humanbiologie (Dr. rer. biol. hum.) an der  
Medizinischen Fakultät der  
Ludwig-Maximilians-Universität München

vorgelegt von

**Banu Akdogan**

aus

Karabük, Türkei

2021

Mit Genehmigung der Medizinischen Fakultät der Universität München

Berichterstatter: Prof. Dr. Thomas Gudermann

Mitberichterstatter: Prof. Dr. Nikolaus Kneidinger  
PD Dr. Tobias Heer

Mitbetreuung durch den  
promovierten Mitarbeiter: Dr. Vladimir Chubanov

Dekan: Prof. Dr. med. dent. Reinhard Hickel

Tag der mündlichen Prüfung: 26.04.2021

## Abstract

The alveolar surface of the lung is formed by a continuous epithelium layer comprising alveolar type 1 and type 2 cells (AT1 and AT2 cells) covered by the airway lining fluid (ALF) and the surfactant film. It was demonstrated that concentrations of Na<sup>+</sup>, K<sup>+</sup> and Cl<sup>-</sup> in ALF are controlled by a numerous epithelial Na<sup>+</sup>, K<sup>+</sup> and Cl<sup>-</sup> channels and transporters and that acquired or inherited defects in transepithelial transport of these ions lead to severe diseases such as cystic fibrosis, pulmonary oedema and impaired protection of the lung from pathogenic species or pollutants. However, molecular identities, and cellular mechanisms controlling the balance of divalent cations in ALF, as well as the clinical relevance of such processes, remain unknown. Previous studies of our laboratory have established that homologous kinase-coupled channels, TRPM6 and TRPM7, co-function together in control of the cellular uptake of divalent cations, including Ca<sup>2+</sup>, Mg<sup>2+</sup> and Zn<sup>2+</sup>. The physiological relevance of such function was demonstrated in experiments with genetically modified animal models showing that TRPM6 and TRPM7 are vital for the placental and intestinal transport of divalent cations. Earlier, our group has also shown that global deletion of *Trpm6* in mice resulted in morphological changes in the alveolar surface, suggesting that TRPM6 operates in respiratory epithelial cells to regulate the balance of Mg<sup>2+</sup>.

Therefore, the main aim of this study was to assess the function of *Trpm6* in the lung by examining genetically modified mouse strains and primary isolated respiratory cells. Using *Trpm6*<sup>Cre/+</sup>; *Rosa26*<sup>GFP/+</sup> reporter mouse strain, we found that TRPM6 is expressed explicitly in AT2 cells but not in other alveolar cells. Assessment of lung tissues and primary alveolar AT2 cells obtained from mice with a global *Trpm6* null mutation revealed that disruption of *Trpm6* is associated with impaired release of pulmonary surfactants, likely in an ATP-dependent fashion. Examination of respiratory parameters of living *Trpm6*-deficient mice showed a profound lung emphysema in 12-weeks old mice. Inductively coupled plasma mass spectroscopy (ICP-MS) assessment of main minerals in ALF samples demonstrated that levels of Mg<sup>2+</sup> were significantly increased in *Trpm6*-deficient mice. These findings suggest that TRPM6 controls Mg<sup>2+</sup> uptake in AT2 cells from ALF and that ablation of these pathways leads to Mg<sup>2+</sup> deprivation and metabolic failure of AT2 cells. In line with this idea, an increase of dietary Mg<sup>2+</sup> uptake fully ameliorated the respiratory phenotypes of *Trpm6*-deficient mice. In contrast to the null mutation, a "kinase-dead" point mutation in *Trpm6* did not affect functional and metabolic characteristics of the lung, reinforcing the importance of the channel activity of TRPM6.

Together, our results support the new concept that TRPM6 operates in AT2 cells to regulate the alveolar balance of  $Mg^{2+}$  and that this mechanism is vital for maintaining the air-liquid interface and tissue homeostasis. Our data suggest that patients may be protected from the development of a lung emphysema by dietary  $Mg^{2+}$  supplementation or treatment with TRPM6-specific agonists.

# Zusammenfassung

Die Alveolaroberfläche der Lunge wird von einer durchgehenden Epithelschicht gebildet, die aus Alveolarepithelzellen des Typs 1 und des Typs 2 (AT1- und AT2-Zellen) besteht, welche mit der Atemwegsflüssigkeit (ALF) und einem Film von Lungensurfactant überzogen sind. Es ist bereits bekannt, dass die Na<sup>+</sup>-, K<sup>+</sup>- und Cl<sup>-</sup>-Konzentrationen in ALF durch eine Ansammlung von epithelständigen Na<sup>+</sup>-, K<sup>+</sup>- und Cl<sup>-</sup>-Kanälen sowie -Transportern kontrolliert werden und dass erworbene oder vererbte Defekte beim transepithelialen Transports dieser Ionen zu schweren Krankheiten wie zystischer Fibrose und Lungenödem führen sowie den Schutz der Lunge vor pathogenen Spezies oder Schadstoffen beeinträchtigen. Allerdings sind die molekularen und zellulären Mechanismen, die das Gleichgewicht zweiwertiger Kationen in ALF kontrollieren, sowie die klinische Relevanz solcher Prozesse nach wie vor unbekannt. Frühere Studien unseres Labors haben gezeigt, dass die homologen Kinase-gekoppelte Kanäle, TRPM6 und TRPM7, bei der Kontrolle der zellulären Aufnahme von zweiwertigen Kationen wie Ca<sup>2+</sup>, Mg<sup>2+</sup> und Zn<sup>2+</sup> zusammenwirken. Die physiologische Tragweite dieser Funktion wurde in den Experimenten mit genetisch veränderten Tiermodellen demonstriert, die verdeutlichen, dass TRPM6 und TRPM7 für den Transport der zweiwertigen Kationen in Plazenta und Darm lebensnotwendig sind. Zuvor zeigte unsere Gruppe außerdem, dass die globale Deletion von *Trpm6* in Mäusen zu morphologischen Veränderungen der Alveolaroberfläche führte, was darauf hindeutet, dass TRPM6 in Atemwegsepithelzellen regulierend auf das Mg<sup>2+</sup>-Gleichgewicht wirkt.

Daher war das Hauptziel dieser Arbeit, die Funktion von *Trpm6* in der Lunge durch Untersuchung genetisch veränderter Mausstämmen und primär isolierter Atemwegszellen zu identifizieren. Mit Hilfe des *Trpm6*<sup>Cre/+</sup>; *Rosa26*<sup>rGFP/+</sup>-Reporter-Mausstamms fanden wir heraus, dass TRPM6 explizit in AT2-Zellen, aber nicht in anderen alveolären Zellen exprimiert wird. Die Untersuchung von Lungengewebe und primären alveolären AT2-Zellen, die aus Mäusen mit einer globalen *Trpm6*-Nullmutation gewonnen wurden, offenbarte, dass die Störung der TRPM6-Kanalaktivität mit einer reduzierten wahrscheinlich ATP-abhängigen Freisetzung von Lungensurfactant verbunden ist. Durch Auswertung der Atmungsparameter von lebenden *Trpm6*-defizienten Mäusen konnten wir die Entwicklung eines ausgeprägten Lungenemphysems in 12 Wochen alten Mäusen beobachten.

Die ICP-MS-Analyse der wichtigsten Mineralien in ALF-Proben ergab, dass die Mg<sup>2+</sup>-Werte in *Trpm6*-Null-Mäusen signifikant erhöht waren. Diese Ergebnisse deuten darauf hin, dass

TRPM6 die Aufnahme von  $Mg^{2+}$  in AT2-Zellen aus ALF reguliert und dass die Ablation dieser Übertragungswege zu  $Mg^{2+}$ -Deprivation und Stoffwechselstörungen in AT2-Zellen führt.

In Übereinstimmung mit dieser Annahme wurde der respiratorische Phänotyp der *Trpm6*-defizitären Mäuse durch diätetische Anreicherung von  $Mg^{2+}$ - Ionen vollständig gelindert. Im Gegensatz zur Nullmutation beeinträchtigte eine sog. „Kinase-tote“-Punktmutation in *Trpm6* funktionale und metabolische Eigenschaften der Lunge nicht, was die Bedeutung der TRPM6-Kanalaktivität für den geschilderten Phänotyp weiter bekräftigt.

Unsere Ergebnisse unterstützen ein neues Konzept, in dem TRPM6 in AT2-Zellen regulierend auf das alveoläre Gleichgewicht von  $Mg^{2+}$  - Ionen wirkt und dieser Mechanismus für die Aufrechterhaltung der Grenzfläche zwischen Luft und Flüssigkeit sowie für die Gewebemöostase essentiell ist. In Zukunft könnten Patienten durch eine Nahrungsergänzung mit  $Mg^{2+}$  - Mineralien oder einer Behandlung mit TRPM6-spezifischen Agonisten vor der Ausbildung eines Lungenemphysems geschützt werden.

# Index of Figures

Figure 1. Phylogenetic tree of the TRP superfamily.....	18
Figure 2. Domain topology of TRPM6 and TRPM7.....	20
Figure 3. Anatomy and morphology of the lung. ....	23
Figure 4. Morphology of the pulmonary alveolus. ....	24
Figure 5. Production and recycling of lung surfactants.....	25
Figure 6. Targeting strategy used for the generation of mice with the kinase-dead mutation in <i>Trpm6</i> .....	52
Figure 7. Breeding strategy to generate <i>Trpm6<sup>R/R</sup></i> mice. ....	52
Figure 8. Determination of mean linear intercept ( $L_m$ ) by using design-based stereology.....	63
Figure 9. Expression of $\tau$ GFP in the lung of <i>Trpm6<sup>Cre/+</sup>; Rosa26<sup><math>\tau</math>GFP/+</sup></i> .....	76
Figure 10. Co-localization of $\tau$ GFP and ABCa3 in lung tissue sections of <i>Trpm6<sup>Cre/+</sup>; Rosa26<sup><math>\tau</math>GFP/+</sup></i> mice. ....	77
Figure 11. In situ hybridization (ISH) of <i>Trpm6<sup>fl/+</sup></i> (Control) lungs with <i>Trpm6</i> sense and antisense probes.....	78
Figure 12. Relative <i>Trpm6</i> mRNA levels in whole lungs of <i>Trpm6<sup>fl/+</sup></i> (Control) and <i>Trpm6<sup><math>\Delta</math>17/<math>\Delta</math>17</sup>;Sox2-Cre</i> (KO) mice analyzed by qRT-PCR.....	79
Figure 13. Histological examination of lungs of <i>Trpm6<sup>fl/+</sup></i> (Control) and <i>Trpm6<sup><math>\Delta</math>17/<math>\Delta</math>17</sup>;Sox2-Cre</i> (KO) mice.....	80
Figure 14. Mean chord length analysis of morphological lung sections of 4-, 8- and 12-weeks old <i>Trpm6<sup>fl/+</sup></i> (Control) and <i>Trpm6<sup><math>\Delta</math>17/<math>\Delta</math>17</sup>;Sox2-Cre</i> (KO) mice.....	81
Figure 15. Lung function parameters performed with <i>Trpm6<sup>fl/+</sup></i> (Control) and <i>Trpm6<sup><math>\Delta</math>17/<math>\Delta</math>17</sup>;Sox2-Cre</i> (KO) mice. ....	82
Figure 16. Histological examination of lungs from <i>Trpm6<sup>fl/+</sup></i> (Control) and <i>Trpm6<sup><math>\Delta</math>17/<math>\Delta</math>17</sup>;Sox2-Cre</i> (KO) mice fed with a high $Mg^{2+}$ diet. ....	83
Figure 17. Mean chord length analysis of morphological lung sections of <i>Trpm6<sup>fl/+</sup></i> (Control) and <i>Trpm6<sup><math>\Delta</math>17/<math>\Delta</math>17</sup>;Sox2-Cre</i> (KO) mice fed with a high $Mg^{2+}$ diet.....	84
Figure 18. Lung function parameters performed with <i>Trpm6<sup>fl/+</sup></i> (Control) and <i>Trpm6<sup><math>\Delta</math>17/<math>\Delta</math>17</sup>;Sox2-Cre</i> (KO) mice fed with a high $Mg^{2+}$ diet. ....	85

Figure 19. Electron microscopic (EM) analysis of alveolar regions from lungs of <i>Trpm6<sup>fl/+</sup></i> (Control) and <i>Trpm6<sup>Δ17/Δ17</sup>;Sox2-Cre</i> (KO) mice.....	86
Figure 20. Surfactant protein A (SP-A) levels in bronchoalveolar alveolar lavage (BAL) of <i>Trpm6<sup>fl/+</sup></i> (Control) and <i>Trpm6<sup>Δ17/Δ17</sup>;Sox2-Cre</i> (KO) mice.....	87
Figure 21. Surfactant protein B (SP-B) and C (SP-C) levels in bronchoalveolar alveolar lavage (BAL) of <i>Trpm6<sup>fl/+</sup></i> (Control) and <i>Trpm6<sup>Δ17/Δ17</sup>;Sox2-Cre</i> (KO) mice.....	88
Figure 22. Surfactant protein D (SP-D) levels in bronchoalveolar alveolar lavage (BAL) of <i>Trpm6<sup>fl/+</sup></i> (Control) and <i>Trpm6<sup>Δ17/Δ17</sup>;Sox2-Cre</i> (KO) mice. (A) BAL samples were collected from 12-weeks old mice and analyzed by Western blot using the anti-SP-D antibody. ....	89
Figure 23. Quantification of AT2 cells in the lung parenchyma of 4-weeks old <i>Trpm6<sup>fl/+</sup></i> (Control) and <i>Trpm6<sup>Δ17/Δ17</sup>;Sox2-Cre</i> (KO) mice. ....	90
Figure 24. Quantification of AT2 cells in the lung parenchyma of 8-weeks old <i>Trpm6<sup>fl/+</sup></i> (Control) and <i>Trpm6<sup>Δ17/Δ17</sup>;Sox2-Cre</i> (KO) mice. ....	91
Figure 25. Analysis of divalent cations in blood serum samples collected from <i>Trpm6<sup>fl/+</sup></i> (Control) and <i>Trpm6<sup>Δ17/Δ17</sup>;Sox2-Cre</i> (KO) mice.....	93
Figure 26. Analysis of divalent cations in ALF samples collected from <i>Trpm6<sup>fl/+</sup></i> (Control) and <i>Trpm6<sup>Δ17/Δ17</sup>;Sox2-Cre</i> (KO) mice. ....	94
Figure 27. Analysis of divalent cations in blood serum and ALF samples collected from <i>Trpm6<sup>fl/+</sup></i> (Control) and <i>Trpm6<sup>Δ17/Δ17</sup>;Sox2-Cre</i> (KO) mice fed with a high Mg <sup>2+</sup> diet.....	95
Figure 28. Ratios of Mg <sup>2+</sup> concentrations in the serum to ALF of <i>Trpm6<sup>fl/+</sup></i> (Control) and <i>Trpm6<sup>Δ17/Δ17</sup>;Sox2-Cre</i> (KO) mice. ....	96
Figure 29. Genotyping of <i>Trpm6<sup>R/R</sup></i> , <i>Trpm6<sup>R/+</sup></i> and <i>Trpm6<sup>+/+</sup></i> mice.....	98
Figure 30. Body weights of <i>Trpm6<sup>+/+</sup></i> (Control) and <i>Trpm6<sup>R/R</sup></i> (KI) mice .....	98
Figure 31. Morphological analysis of lungs from <i>Trpm6<sup>+/+</sup></i> (Control) and <i>Trpm6<sup>R/R</sup></i> (KI) mice. ....	99
Figure 32. Functional analysis of lungs from <i>Trpm6<sup>+/+</sup></i> (Control) and <i>Trpm6<sup>R/R</sup></i> (KI) mice.....	100
Figure 33. Analysis of divalent cations in blood serum and ALF samples collected from <i>Trpm6<sup>+/+</sup></i> (Control) and <i>Trpm6<sup>R/R</sup></i> (KI) mice.....	100
Figure 34. Representative light microscopy images obtained from primary isolated murine alveolar type 2 (AT2) cells .....	101
Figure 35. Relative expression levels of <i>Sp-C</i> , <i>Trpm6</i> , <i>Aqp-5</i> and <i>α-Sma</i> mRNA in <i>Trpm6<sup>fl/+</sup></i> (Control) primary AT2 cells. ....	102

---

Figure 36. Imaging of living cells from the A549 cell line stained with the fluorescent LyTR and Hoechst dye. ....	103
Figure 37. Imaging of living primary AT2 cells .....	103
Figure 38. Immunofluorescence staining of primary AT2 cells obtained from <i>Rosa26<sup>+/+</sup></i> (Control) and <i>Trpm6<sup>Cre/+</sup>; Rosa26<sup>TGFP/+</sup></i> .....	104
Figure 39. Imaging of living primary AT2 cells obtained from <i>Trpm6<sup>fl/+</sup></i> (Control) and <i>Trpm6<sup>Δ17/Δ17</sup>; Sox2-Cre</i> (KO) mice stained with fluorescent LyTR dye in vitro. ....	105
Figure 40. Immunofluorescence staining of primary AT2 cells obtained <i>Trpm6<sup>fl/+</sup></i> (Control) and <i>Trpm6<sup>Δ17/Δ17</sup>; Sox2-Cre</i> (KO) mice. ....	105
Figure 41. Images obtained by electron microscopy (EM) of primary AT2 cells from <i>Trpm6<sup>fl/+</sup></i> (Control) and <i>Trpm6<sup>Δ17/Δ17</sup>; Sox2-Cre</i> (KO) mice. ....	106
Figure 42. Labelling of ATP stores in lamellar bodies (LB) of cells from A549 cell line and primary AT2 cells from <i>Trpm6<sup>fl/+</sup></i> (Control) mice. ....	108
Figure 43. Staining of primary AT2 cells isolated from <i>Trpm6<sup>fl/+</sup></i> (Control) and <i>Trpm6<sup>Δ17/Δ17</sup>; Sox2-Cre</i> (KO) mice with fluorescent dyes. ....	109
Figure 44. A proposed model for the role of TRPM6 channels in respiratory balance of Mg <sup>2+</sup> . ....	119

# Index of Tables

Table 1. List of reagents used in the present study.....	33
Table 2. List of primers used for genotyping mouse strains. ....	38
Table 3. List of primers used for qPCR analysis. ....	39
Table 4. Primers used to generate In situ hybridization (ISH) probe. ....	39
Table 5. Kits used in the present study.....	40
Table 6. Buffers and solutions used for western blot analysis.....	41
Table 7. Buffers and solutions used for immunostaining of cells and tissue sections. ....	42
Table 8. Buffers and solutions used for electron microscopic analysis (EM). ....	42
Table 9. Buffers and solutions used for alveolar epithelial Type 2 cell isolation. ....	43
Table 10. Buffers and solutions used for PCR.....	43
Table 11. Buffers and solutions used for atomic absorption spectroscopy. ....	44
Table 12. List of consumables used in the present study.....	45
Table 13. Equipment used in the present study. ....	48
Table 14. Software used in this project.....	50
Table 15. Breeding of mouse strains used in this project.....	53
Table 16. Master mix composition for PCR reaction. ....	54
Table 17. Primer pairs and PCR amplicons used for genotyping of mice.....	54
Table 18. PCR settings for <i>Rosa26</i> . ....	56
Table 19. PCR settings for <i>Sox2-Cre</i> .....	56
Table 20. PCR settings for <i>Trpm6<sup>fl</sup></i> allele. ....	57
Table 21. PCR settings for <i>Trpm6<sup>R</sup></i> allele. ....	57
Table 22. PCR settings for <i>Trpm6<sup>A17</sup></i> allele. ....	58
Table 23. PCR settings for both <i>Trpm6<sup>fl</sup></i> and <i>Trpm6<sup>+</sup></i> alleles.....	58
Table 24. PCR settings for <i>Trpm6<sup>+</sup></i> allele. ....	59
Table 25. PCR settings for <i>Rosa26<sup>rtGFP</sup></i> and <i>Rosa26<sup>+</sup></i> alleles. ....	59

---

Table 26. PCR settings for <i>Trpm6</i> <sup>Cre</sup> allele.....	60
Table 27. Procedure for H&E staining of lung tissue sections.....	62
Table 28. Parameters measured by a pulmonary function test. ....	64
Table 29. Primary anti surfactant protein (SP) antibodies used for Western blot experiments. .....	66
Table 30. Secondary antibodies used for Western blot experiments.....	66
Table 31. Antibodies used for the staining of lung tissue sections. ....	67
Table 32. Master mix for qPCR. ....	69
Table 33. Settings used for qPCR. ....	69
Table 34. cDNA templates Sequence of primers used to generate ISH <i>Trpm6</i> probes. ....	70
Table 35. Antibodies and dyes used for IF staining of cells.....	71

---

# Abbreviations

$\alpha$ -SMA	alpha smooth muscle actin
AAS	atomic absorption spectroscopy
AAT	Alpha-1 antitrypsin
ABCa3	ATP-binding cassette sub-family A, member 3
ALF	alveolar lining fluid
AM	alveolar macrophages
AT1	alveolar epithelial type 1 cell
AT2	alveolar epithelial type 2 cell
ATP	adenosine triphosphate
AQP5	aquaporin-5 water channel
BAL	bronchoalveolar lavage
CC	coiled-coil domain
COPD	chronic obstructive pulmonary diseases
DCT	distal convoluted tubule
ECL	enhanced chemiluminescence
eEF2K	eukaryotic elongation factor 2 kinase
EM	electron microscopy
$\tau$ GFP	tau green fluorescent protein
FOT	forced oscillation technique
H&E	hematoxylin and eosin
HNE	human neutrophilic elastase
HSH	hypomagnesemia with secondary hypocalcemia
ICP-MS	inductively coupled plasma mass spectroscopy
IRES	internal ribosome entry site
ISH	<i>in situ</i> hybridization
KD	kinase domain
KI	knock in
KO	knock out
$L_m$	mean chord length
LB	lamellar body
LyTR	Lysotracker Red
MCL	mean chord length
PC	phosphatidylcholine

PCR	polymerase chain reaction
PL	phospholipids
PPE	porcine pancreatic elastase
pro-SPC	pro-surfactant protein C
P-V	pressure-volume curves
qRT-PCR	quantitative real time PCR
ROS	reactive oxygen species
SD	substrate domain
SP-A	surfactant protein A
SP-B	surfactant protein B
SP-C	surfactant protein C
SP-D	surfactant protein D
TM	tubular myelin
TRP	transient receptor potential channels
TRPA1	transient receptor potential ankyrin 1
TRPC6	transient receptor potential canonical 6
TRPM6	transient receptor potential melastatin 6
TRPM7	transient receptor potential melastatin 7
TRPV1	transient receptor potential vanilloid 1
TRPV4	transient receptor potential vanilloid 4
WB	western blot
WT	wild type

---

# Table of contents

Abstract.....	3
Zusammenfassung.....	5
Index of Figures.....	7
Index of Tables.....	10
Abbreviations .....	12
Table of contents.....	14
1. Introduction .....	17
1.1. The transient receptor potential (TRP) gene family .....	17
1.2. The transient receptor potential melastatin family (TRPM) and its two members TRPM6 and TRPM7 .....	19
1.3. TRP channels in chronic obstructive pulmonary disease (COPD) .....	22
1.3.1. Anatomy and functions of the air-liquid interface in the respiratory system .....	23
1.3.2. Chronic obstructive pulmonary diseases (COPD) .....	27
1.3.3. Pathophysiological roles of TRP channels in COPD .....	29
2. Aims of the present study .....	32
3. Materials.....	33
3.1. Chemicals .....	33
3.2. PCR primers .....	38
3.3. Kits.....	40
3.4. Buffers and solutions .....	41
3.5. Consumables .....	45
3.6. Technical devices .....	48
3.7. Software.....	50
4. Methods .....	51
4.1. Genetic mouse strains used in the present study .....	51
4.1.1. Production of mice with a global null mutation in <i>Trpm6</i> .....	51

---

4.1.2. Generation of mice with a global kinase-dead point mutation in <i>Trpm6</i> .....	51
4.1.3. Production of mice carrying a <i>Trpm6</i> <sup>Cre</sup> allele .....	52
4.2. Genotyping of mouse strains.....	53
4.3. Housing of mice .....	60
4.4. Histological examination of lungs .....	61
4.4.1. Preparation of lungs and Hematoxylin and Eosin (H&E) staining of tissue sections .....	61
4.4.2. Quantitative morphometry of lung tissue sections.....	62
4.5. Functional analysis of the lung .....	63
4.6. Collection of murine samples .....	64
4.6.1. Collection of serum and bronchoalveolar lavage (BAL).....	64
4.7. Western blot analysis of bronchoalveolar lavage.....	65
4.8. Immunohistochemistry of the tissue sections .....	67
4.9. Molecular biology and biochemical methods .....	68
4.9.1. RNA isolation and cDNA synthesis .....	68
4.9.2. Quantitative polymerase chain reaction (qPCR) .....	68
4.9.3. In-situ hybridization (ISH) .....	69
4.10. Isolation and culture of primary AT2 cells and cell culture of A549 cell line .....	70
4.11. Staining of cultured cells .....	71
4.12. EM (Electron Microscopy) analysis of cells and lung tissue sections.....	72
4.13. Determination of elementary Mg, Ca and Zn using inductively coupled plasma mass spectrometry (ICP-MS) and atomic absorption spectroscopy (AAS) .....	73
4.14. Statistical analysis.....	74
5. Results .....	75
5.1. Expression pattern of <i>Trpm6</i> in the mouse lung .....	75
5.2. Morphological and functional alterations in the lung of <i>Trpm6</i> -deficient mice .....	79
5.3. Effect of Mg <sup>2+</sup> supplementation on the respiratory phenotype of <i>Trpm6</i> -deficient mice .....	83
5.4. Electron microscopy (EM) assessment of the lung tissues from <i>Trpm6</i> -deficient mice .....	85

---

5.5. Assessment of surfactant proteins in bronchoalveolar lavage (BAL) of <i>Trpm6</i> -deficient mice.....	87
5.6. Assessment of AT2 cells in the lungs of <i>Trpm6</i> -deficient mice.....	90
5.7. Determination of elementary levels of divalent cations in serum and alveolar lining fluid (ALF) of <i>Trpm6</i> -deficient mice.....	92
5.8. Generation and phenotypic evaluation of a kinase-dead <i>Trpm6</i> mice.....	97
5.9. Morphological changes in primary AT2 cells isolated from <i>Trpm6</i> -deficient mice.....	101
6. Discussion.....	110
6.1. Expression patterns of TRPM6 in the lung.....	110
6.2. Pulmonary emphysema in <i>Trpm6</i> -deficient mice.....	111
6.3. Mg <sup>2+</sup> dependency of the respiratory phenotype of <i>Trpm6</i> -deficient mice.....	112
6.4. No involvement of TRPM6 kinase activity in the respiratory phenotype of <i>Trpm6</i> -deficient mice.....	114
6.5. Impaired production of respiratory surfactants in the lung of <i>Trpm6</i> -deficient mice ..	115
6.6. Mg <sup>2+</sup> homeostasis and COPD.....	117
6.7. The suggested model for the role of TRPM6 in AT2 cells.....	118
7. Conclusions.....	120
References.....	121
Acknowledgements.....	138
Eidesstattliche Versicherung.....	140
Curriculum vitae.....	141

# 1. Introduction

## 1.1. The transient receptor potential (TRP) gene family

Transient receptor potential (TRP) channels were discovered during the characterization of new mutant strains of *Drosophila* fruit flies with defective functional characteristics (transient receptor potential) of photoreceptor cells (reviewed in [1, 2]). In follow up studies, TRP proteins were found in many invertebrate species and mammals. In humans, the TRP superfamily comprises 27 cation channels. TRP channels are remarkably divergent in channel characteristics such as activation mechanism and ion selectivity [3-5]. However, TRP channels share several common features. The most TRP channel proteins contain six transmembrane helices, forming tetrameric channel units, which are often not selective for a particular cation and referred to as nonselective cation cations [3].

Based on amino acid sequence homology, the TRP superfamily was divided into six families (Figure 1): TRPC (Canonical), TRPV (Vanilloid), TRPM (Melastatin), TRPA (Ankyrin), TRPP (Polycystin) and TRPML (Mucolipin) [2, 5-7].

In mammals, the TRPC family consists of seven proteins (TRPC1–7) while the TRPM subfamily contains eight channels (TRPM1–8). The TRPV subfamily comprises six members (TRPV1–6). In humans, the TRPA group has only one member (TRPA1). The TRPP and TRPML subfamilies contain three functional proteins in humans [8].

Most of the TRP channels are localized in the plasma membrane [9], but some proteins are also found in cell organelles [10]. TRP channels contain six transmembrane helices (6 TMs) with a short stretch of hydrophobic residues located between TM5 and TM6, which form the channel pore [11]. Besides, TRP channels contain large cytosolic C- and N-terminal domains. Similar to many other channels, TRP proteins form homo or hetero-tetrameric channel complexes [12].

The N-terminal segments of TRPC, TRPV and TRPA proteins contain multiple so-called ankyrin repeats [13]. 33 conserved amino-acid residues form one ankyrin domain. In many proteins, ankyrin repeats form a site involved in protein-protein interactions [3, 7, 12]. The C-terminal segment of most TRP channels contains a characteristic TRP domain encoded by 23-25 amino-acid residues [7]. The TRP domain harbours a TRP box sequence of six conserved residues (EWKFAR in TRPC channels) [1, 3, 4]. Coiled-coil (CC) domains, which play a role

in channel assembly are present in most TRP channels [14-16]. The TRPP and TRPML proteins have a large extracellular loop linking the first two transmembrane helices [3].

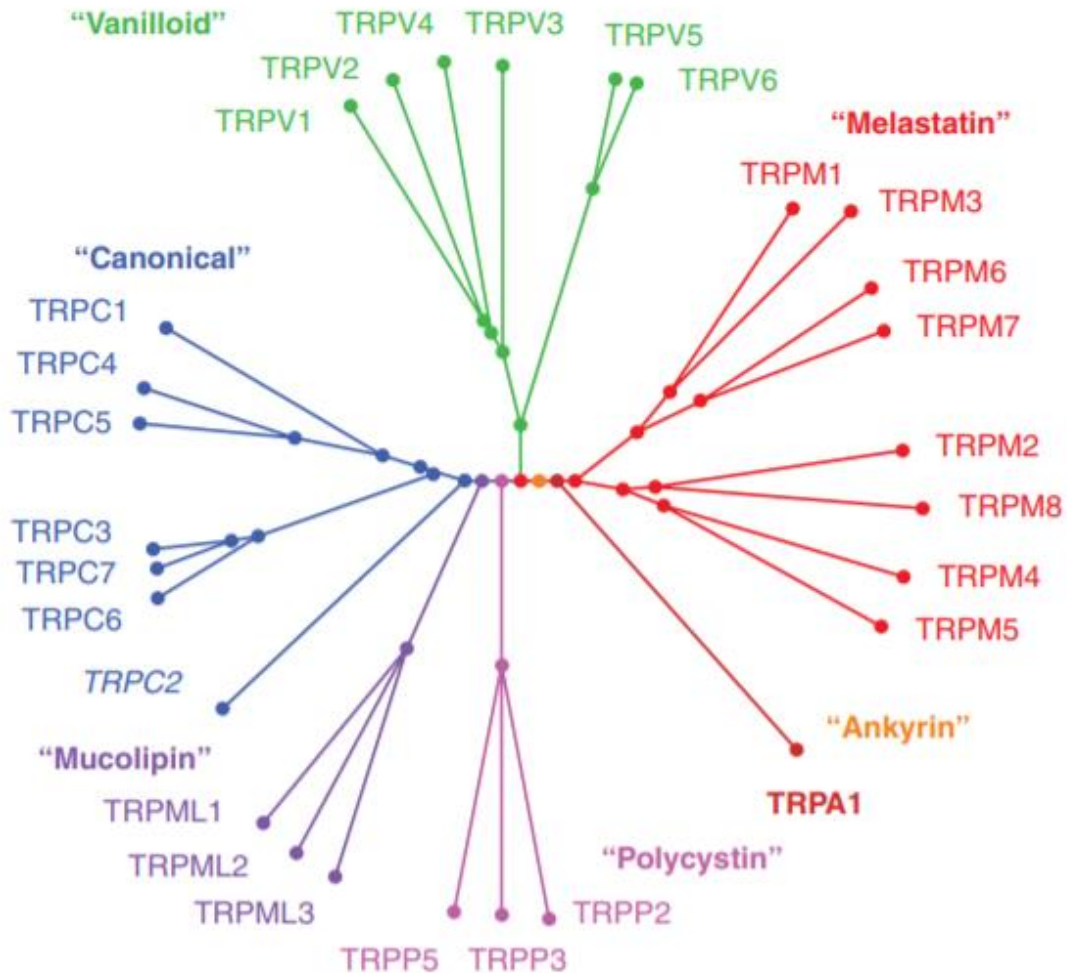


**Figure 1. Phylogenetic tree of the TRP superfamily.** The tree outlines homology of human TRP proteins and mouse TRPC2 (TRPC2 is only a not expressed pseudogene in humans). The figure is taken from Gees *et al.* [2]

Many TRP channels play a critical role in sensory cells function mediating responses to touch, sound, light, taste and temperature [3]. Several TRP channels are abundantly expressed in sensory neurons controlling pain responses [4] and accumulating evidence indicates that TRP channels also regulate the variety of physiological processes beyond sensory systems [7].

## 1.2. The transient receptor potential melastatin family (TRPM) and its two members TRPM6 and TRPM7

The TRPM group of TRP channels was named after its founding member melastatin or TRPM1. The TRPM group is encoded by eight genes in mammals [17]. Within the TRPM family, two proteins, TRPM6 and its closest homologue TRPM7 contain a C-terminal kinase domain belonging to an atypical type of protein kinases entitled as alpha-kinases [17-23].

TRPM6 mRNA was first identified by Ryazanova *et al.* [24] in the cloning of homologues of the eukaryotic elongation factor 2 kinase (eEF2K). TRPM6 is also known as TRP-PLIK2 (TRP-phospholipase C Interacting Kinase2), LTRPC6 (Long TRP Channel 6) or Chak2 (Channel-Kinase 2) [17].

Several research groups independently discovered TRPM7. One laboratory identified TRPM7 in a screen for new phospholipase C (PLC)-interacting proteins [25]. Another group identified TRPM7 by a search for homologues of the eEF2K [24]. Moreover, TRPM7 was identified as a new ion channel expressed in haematopoietic cells [19]. TRPM7 is also named TRP-PLIK (TRP-Phospholipase C Interacting Kinase), LTRPC7 (Long TRP Channel 7) or Chak1 (Channel-Kinase 1) [17].

The human *TRPM6* gene comprises 39 exons [17] and the full-length mRNA variant encodes a 2.022 amino acid protein [20, 22, 23, 26]. The human *TRPM7* gene spans 39 exons and encodes a 1.865 amino acid protein. TRPM6 and TRPM7 display 52% amino acid sequence identity [27]. Orthologues of TRPM6 and TRPM7 were found in all vertebrate species [14, 26].

Multiple tissue Northern blot analysis detected TRPM6 transcripts in human kidney, colon, lung and testis [21]. An *in situ* hybridization (ISH) approach identified transcripts of *TRPM6* in the duodenum, colon as well as in the distal convoluted tubule (DCT) of the kidney [20]. Groenestege *et al.* [28] detected TRPM6 protein in the DCT of kidneys and enterocytes of the intestine.

Northern blot analysis and quantitative reverse transcription PCR (qRT-PCR) suggested that *TRPM7* is ubiquitously expressed [25]. Human *TRPM7* was found to be extensively expressed in the heart and bone [29]. In mice, TRPM7 transcripts were detected in the kidney, intestine, lung and brain [30]. Mittermeier *et al.* [31] detected the high levels of *Trpm7* mRNA in DCT and colon epithelial cells.

TRPM6 and TRPM7 form tetrameric channel complexes in the plasma membrane [32]. In analogy to other TRP channels, TRPM6 and TRPM7 channels have six transmembrane domain with a channel unit located between transmembrane domain 5 and 6 [12, 33]. TRPM6

and TRPM7 contain large N-terminal domains lacking ankyrin repeats [34]. The C-terminal segments of TRPM6 and TRPM7 comprise the TRP domain, followed by a coiled-coil domain, the autophosphorylation segment (or “substrate” domain, SD) and the alpha-kinase domain (KD) (Figure 2) [34].

TRPM6 and TRPM7 channels form channel complexes selective for divalent cations [32]. Activation of the TRPM6 and TRPM7 channels leads to an influx of divalent cations, mainly  $Zn^{2+}$ ,  $Ca^{2+}$  and  $Mg^{2+}$  [35]. Intracellular  $Mg^{2+}$  and  $Mg\cdot ATP$  regulate both the TRPM6 and TRPM7 channels [19, 27].

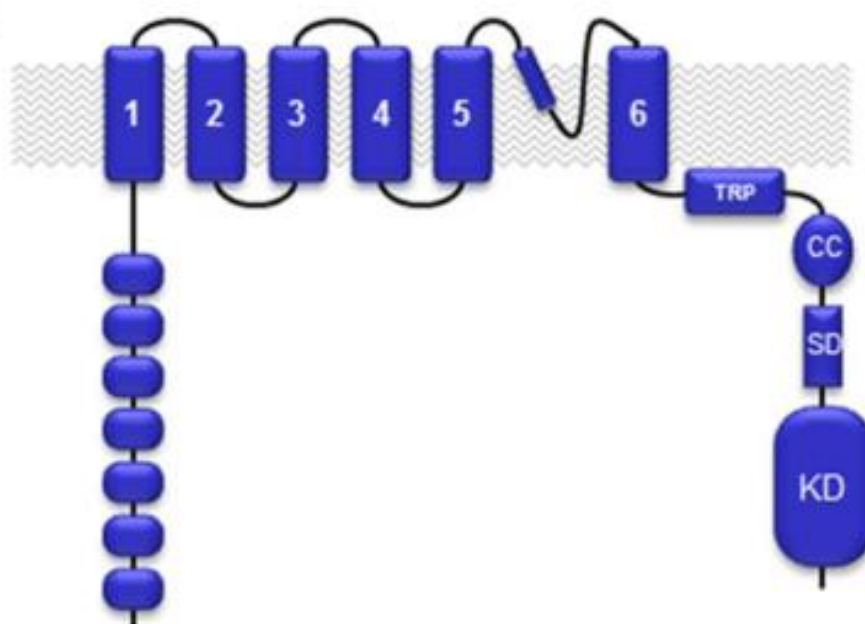


**Figure 2. Domain topology of TRPM6 and TRPM7.** TRPM6 and TRPM7 proteins possess six transmembrane domains (1–6) with a channel unit located between TM5 and TM6. The C-terminus of TRPM6 and TRPM7 channels comprises four domains which are transient receptor potential (TRP) domain, a coiled-coil (CC) domain, a kinase substrate domain (SD) as well as a kinase domain (KD). The figure is taken from Ferioli *et al.* [34].

Clinical studies and experiments with gene-modified animal models revealed that TRPM6 plays a crucial role in systemic  $Mg^{2+}$  homeostasis [36]. Two independent groups have found that in humans, loss-of-function mutations in the *TRPM6* gene lead to an autosomal recessive syndrome, which is known as Hypomagnesemia with secondary hypocalcemia (HSH) [20, 21]. HSH disorder is detected at the very early ages by very low  $Mg^{2+}$  and  $Ca^{2+}$  serum levels, accompanied by muscle spasms and severe seizures [20, 21]. When the disease is untreated,

HSH can result in neurological damage followed by mortality [20, 21]. However, oral Mg<sup>2+</sup> supplementation relieves all the symptoms associated with the disease [20, 21].

In contrast to HSH patients, genetic inactivation of *Trpm6* in mice lead to neural tube closure defects and early embryonic death [37]. Our group also found that mouse embryos lacking *Trpm6* (*Trpm6*<sup>βgeo/βgeo</sup> mice, *Trpm6*-deficient mice) could not survive [36]. *Trpm6*<sup>Δ17/Δ17</sup> embryos failed to grow and died at the embryonic day 12-5 (e12.5) [36].

To investigate possible mechanisms of early mortality of *Trpm6*-deficient mice, our group established a new animal model based on an epiblast-specific ablation of *Trpm6* using a conditional inactivation of the floxed *Trpm6* locus [36]. Such an approach resulted in a deletion of *Trpm6* in the whole early embryo, but not in maternal tissues, including placental trophoblasts [36]. This strategy allowed to produce viable *Trpm6*KO embryos, supporting the idea that the function of TRPM6 in extraembryonic cells is vital for the prenatal development of mice [36]. Furthermore, our group reported that adult *Trpm6*-deficient mice displayed short lifespans, multiple morphological changes of their internal organs and a severe Mg<sup>2+</sup> deficiency [36]. Similar to HSH patients, dietary Mg<sup>2+</sup> supplementation of *Trpm6*-deficient mice reversed all these phenotypes [36].

Several laboratories suggested that TRPM7 is essential to maintain cellular Mg<sup>2+</sup> levels [19, 38-40]. Nadler *et al.* [19] demonstrated that targeted deletion of the *Trpm7* gene in DT40 B lymphocytes resulted in Mg<sup>2+</sup> deficiency and proliferation defects. However, *Trpm7* KO cells could proliferate when Mg<sup>2+</sup> levels were increased in the culture medium [38].

Moreover, many studies identified several processes regulated by TRPM7 channel such as cell motility [41-43], mechanosensitivity [43-45] and cell cycle [19, 38, 40, 46]. TRPM7 was found to be associated with cardiac fibrosis [47], cancer [48-50], hypertension [51] and neurogenerative disorders [19, 38, 52, 53].

In mice, global deletion of *Trpm7* resulted in early embryonic mortality at e7.5 for unknown reasons [54]. In contrast to the experiments with *Trpm6*-deficient mice, the epiblast-specific inactivation of *Trpm7* failed to generate viable KO offspring, which indicates that *Trpm7* is vital for embryonic development [54]. The kinase-dead mice with a K1646R point mutation in the *Trpm7* gene were generated and characterized by two groups (Kaitsuka *et al.* and Ryazanova *et al.*) generated mice with [55, 56]. Both studies revealed that *Trpm7* kinase-dead mice developed normally and that serum Mg<sup>2+</sup> levels in adult mice were not changed, indicating the importance of the channel activity of TRPM7 [55, 56].

In mouse embryos, tissue-specific inactivation of *Trpm7* affected the development of internal organs for unknown reasons [54, 57]. For instance, Jin *et al.* [57] reported that *Trpm7* is indispensable for kidney morphogenesis.

Recently, our group conducted tissue-specific mutagenesis of *Trpm7* in the kidney and intestine [31]. When *Trpm7* was inactivated in kidneys, systemic homeostasis of divalent cations was not affected [31]. However, postnatal development of mice was altered after deletion of *Trpm7* in the intestine [31]. When *Trpm7* was deleted in intestinal epithelial cells, 5-6 days-old pups displayed growth failure and death due to insufficient nutritional intake of  $Mg^{2+}$ ,  $Ca^{2+}$  and  $Zn^{2+}$  [31].

Taken together, TRPM6 and TRPM7 contain both an ion channel domain linked to a kinase domain. Both TRPM6 and TRPM7 channels are selective for divalent cations and display high permeability to  $Mg^{2+}$  and  $Ca^{2+}$ . TRPM7 has been detected to be ubiquitously expressed in all mammalian cells, while TRPM6 is mostly expressed in kidney, intestine and placenta. Both TRPM6 and TRPM7 are essential for systemic  $Mg^{2+}$  homeostasis and other divalent cations such as  $Ca^{2+}$  and  $Zn^{2+}$ . Previously, our group has shown that null mutation of *Trpm6* in mice resulted in morphological changes of internal organs including the lung. Histological analysis of lung tissue revealed that *Trpm6* KO mice develop emphysema; however, the function of *Trpm6* in the lung remains unknown.

### **1.3. TRP channels in chronic obstructive pulmonary disease (COPD)**

Chronic obstructive pulmonary disease (COPD) comprises a group of respiratory diseases with several clinical symptoms such as dyspnea, chronic cough, airway limitation as well as inflammation, obstruction and destruction of the lung parenchyma [58-61]. According to the World Health Organization (WHO) report in 2019, 328 million people were diagnosed with COPD and 3 million people died due to COPD worldwide [58, 59, 62]. Hence, COPD is estimated to be the 3rd leading cause of death in the world [58, 59, 63-66].

Many TRP channels were found to be expressed in the respiratory epithelium whose function is crucial for the pathogenesis of a variety of lung diseases. Recent literature indicates that several TRP channels have been linked to common lung diseases, including COPD [67, 68].

### 1.3.1. Anatomy and functions of the air-liquid interface in the respiratory system

The airways of the respiratory system consist of the trachea linked to the bronchial tree of the left and right lungs, as outlined in Figure 3. Terminal bronchioles are connected to alveolar ducts associated with multiple alveoli (Figure 3) [69-72]. The bronchial epithelium is a complex structure primarily containing goblet, ciliated and basal cells [73]. The primary function of goblet cells is to produce and secrete mucin glycoproteins, which are the major macromolecular components of the protective mucus [74]. Ciliated cells maintain mucociliary clearance flow. These cells also sense and respond to mechanical and irritant stimuli [75]. Basal cells function as progenitors of goblet and ciliated cells [75].

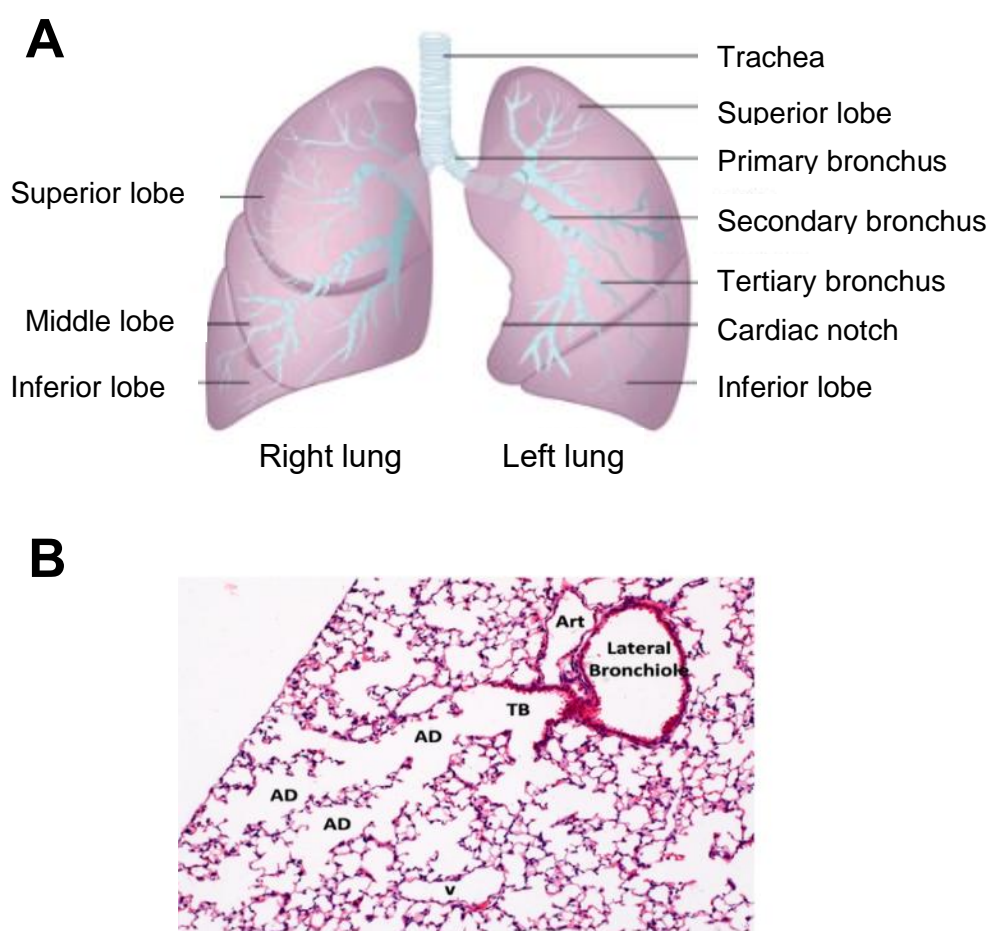


**Figure 3. Anatomy and morphology of the lung.** (A) The lungs are connected to the trachea by the right and left bronchi on the interior surface and composed of segments called lobes. In humans, right lung comprises of superior, middle and inferior lobes whereas left lung contains only two lobes. The cardiac notch is an indentation of the left lung allowing space for the heart. Bronchioles branch into multiple alveolar ducts that are lined entirely by alveoli. (B) Histology of the bronchioles in mouse lungs stained with hematoxylin and eosin (H&E) is shown. TB, terminal bronchiole; AD, alveolar duct. The figure is modified from Pan *et al.* [72].

The lung alveolar epithelium forms a physical barrier involved in gas exchange between the air and the blood to protect the organism from inhaled exogenous agents [76, 77]. Each alveolus comprises three cell types: Alveolar type 1 (AT1) and type 2 (AT2) cells, and alveolar macrophages (AM) (Figure 4) [78-80].

AT1 cells are large squamous cells covering ~95% of the alveolar surface [78, 81]. These epithelial cells are relatively thin, enabling to reduce the diffusion distance between the alveolar air space and pulmonary capillary blood (Figure 4) [82]. AT1 cells are mainly involved in gas exchange and form a protective barrier against pathogenic microorganisms and their toxins [76, 79, 83, 84].

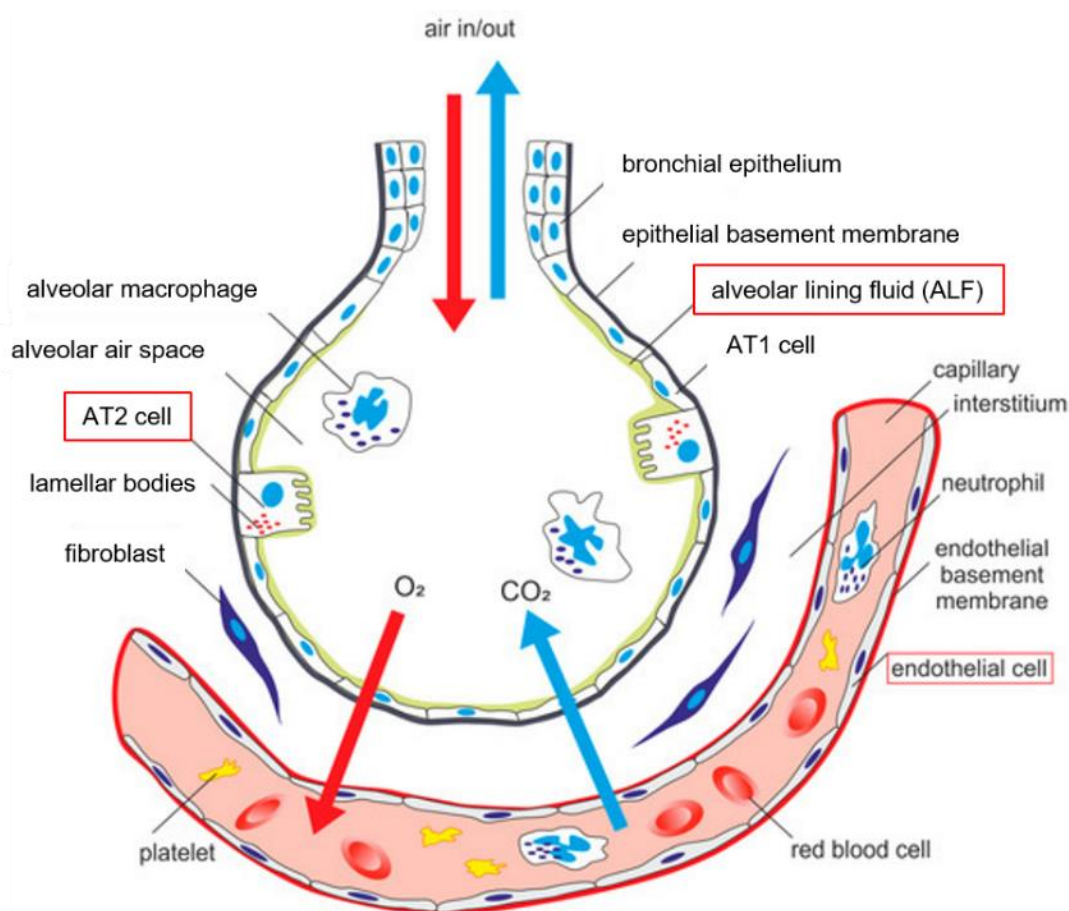


**Figure 4. Morphology of the pulmonary alveolus.** In the alveolar region, the airway epithelium is formed by alveolar epithelial type 1 (AT1), type 2 (AT2) cells and alveolar macrophages (AM). One characteristic of the alveolus is the formation of the alveolar lining fluid (ALF). The ALF is the medium to spread the surfactant, which is crucial for maintaining alveolar stability by facilitating alveolar gas exchange processes and host defense. Alveolar macrophages also contribute to the clearance of invading microorganisms. The figure is modified from Nova *et al.* [80].

AT2 cells are cuboidal cells covering ~5% of the alveolar surface (Figure 4) [78, 85]. AT2 cells contribute to epithelium repair upon injury by their capability to proliferate and transdifferentiate into AT1 cells [84, 86, 87]. AT2 cells are responsible for synthesis, release and recycling of pulmonary surfactants [88-91] and also maintain transepithelial movement of water, metabolites and ions [82].

Alveolar macrophages (AM) are responsible for the initiation of inflammatory responses in the alveoli (Figure 4) [92]. AM are located at the air-tissue interface of the lung as well in the pulmonary alveoli in close proximity with AT2 cells. AM provide the first line of phagocytic defence against microbial agents in the lower respiratory tract [93]. Besides their phagocytic and anti-microbial activities, upon stimulation AM secrete chemical mediators such as TNF- $\alpha$ , IL-1 $\beta$ , IL-6, IL-8, PGE<sub>2</sub>, PAF, and LTB<sub>4</sub> upon stimulation, thereby regulating inflammatory reactions in the lung [93].

Alveolar lining fluid (ALF) covers the entire alveolar epithelium (Figure 4) [78]. In the literature, several different names are used for this fluid, such as alveolar wall liquid (AWL) [79], epithelial lining fluid (ELF) [94], airway surface liquid (ASL) [95]. Components of ALF are secreted and recycled by AT2 cells [96]. ALF is rich in lipid-protein complexes known as surfactants, which are mainly composed of phospholipids (PL) (~90%), surfactant proteins (5-10%) and other lipids [97, 98]. The major phospholipid of respiratory surfactants is phosphatidylcholine (PC) [88, 89]. Surfactants contain four major proteins: surfactant protein A, B, C, and D (SP-A, SP-B, SP-C, and SP-D). Respiratory surfactants form a film (Figure 5), which reduces alveolar

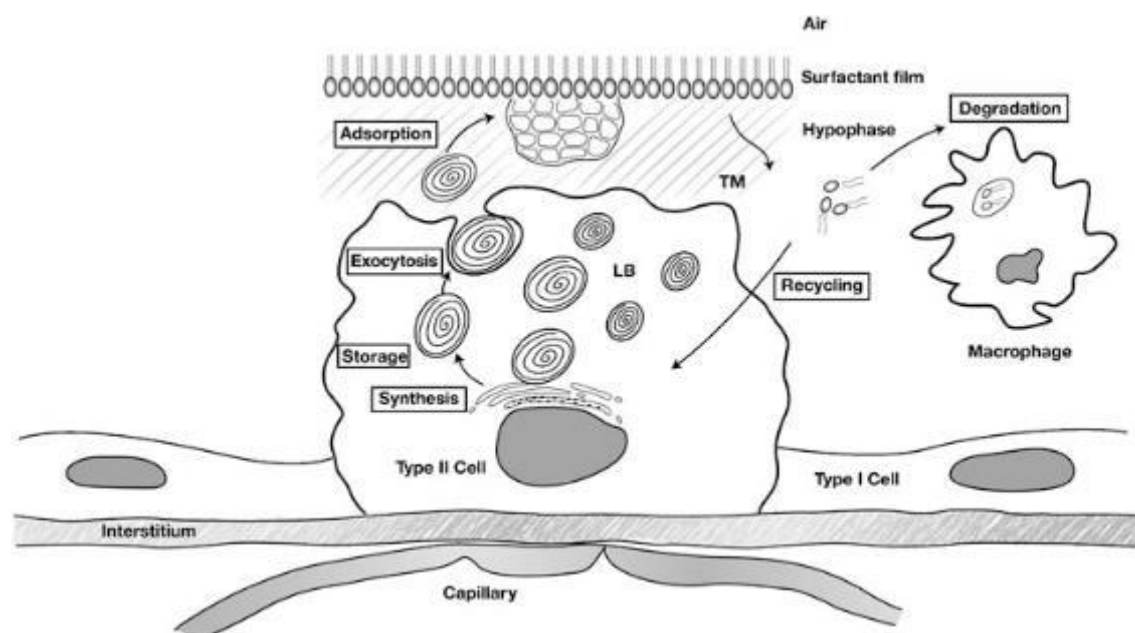


**Figure 5. Production and recycling of lung surfactants.** Surfactants are produced and stored in AT2 cells as lamellar bodies (LB) and exocytosed to the alveolar space as tubular myelin (TM) where they form a surfactant film. The figure is taken from Christmann *et al.* [99].

surface tension during lung expansion due to inspiration and prevents lung collapse during expiration [99]. The four surfactant proteins are classified into two groups based on their affinity to water as hydrophilic and hydrophobic [100]. SP-A and SP-D are known to be hydrophilic surfactant proteins and their primary function is to participate in innate immune defences [101-103]. In the alveolar space, SP-A protein is the most abundantly detected and SP-A monomer has a molecular weight of 32 kDa [97, 100, 101, 104, 105]. Extracellular SP-A plays an essential role in the lamellar body exocytosis and tubular myelin formation [106-110]. SP-D is a glycoprotein, synthesized and secreted by pulmonary AT2 cells and plays a crucial role in pulmonary host defence by mediating clearance of pathogens [111]. The molecular weight of SP-D monomer is 42 kDa [97, 112].

SP-B and SP-C are hydrophobic surfactant proteins [113]. SP-B is found mainly as dimers in the alveolar space [113]. The mature protein has a molecular weight of 8 kDa whereas unprocessed isoforms (proSP-B) have MWs of 26 and 15 kDa [113]. SP-B forms lamellar bodies by packing of lipids and transformation into tubular myelin [114]. The central role of SP-B is to increase the adsorption rate of PLs at the air-water interface [97, 115]. SP-C is synthesized in AT2 cells as 21 and 12 kDa integral membrane precursor proteins and processed to a 4 kDa mature protein [97, 114, 116]. SP-C stabilizes the surfactant film by enhancing the adsorption rate of phospholipids [113]. SP-C functions similar to SP-B [116].

In AT2 cells, surfactant proteins and phospholipids are synthesized in the endoplasmic reticulum [99]. After further processing in the Golgi apparatus, they are packed into lamellar bodies (LB) which are intracellular storage organelles [99, 117]. Surfactants are exocytosed into ALF in structures called tubular myelin (TM) (Figure 5) [99, 118]. TM represents a network of phospholipid bilayers, which maintains continuous delivery of surfactants from AT2 cells to the surfactant film which is placed at the air-liquid interface [99]. Most of the surfactant is recycled by AT2 cells, whereas ~15% is metabolized by alveolar macrophages [99, 118, 119].

Interestingly, the ionic composition of ALF is not well understood. The current literature primarily describes the main elements of the bronchoalveolar lavage (BAL) collected from humans, rats, rabbits, pigs and dogs [120-126]. Qamar *et al.* [120] analyzed the elemental profile of BAL samples obtained from rats by inductively coupled plasma mass spectrometry (ICP-MS). In BAL of healthy rats, ICP-MS analysis revealed the presence of 11 essential elements [120], including Ca > Mg > Fe > Br > I > Cr > Ni > Zn > Mn > Se > Cu (from high to low concentration). The concentration of Mg<sup>2+</sup>, Ca<sup>2+</sup> and Zn<sup>2+</sup> in BAL of rats was 4.3 µM, 157 µM and 0.07 µM, respectively [120]. Govindaraju *et al.* [123] analyzed the anions and cations in rat ALF and reported Mg<sup>2+</sup> and Ca<sup>2+</sup> contents in ALF from healthy rats of 0.67 mM and 1.01 mM, respectively. Nielson *et al.* [124] investigated concentrations of several ions including Ca<sup>2+</sup> in the aqueous subphase of the alveolar lining of the lungs of healthy rabbits. The authors

reported a  $\text{Ca}^{2+}$  content of 1.8 mM in ALF of rabbits [124]. Juettner *et al.* [125] studied the degree and time relationship for exchange of solutes between the lung lavage fluid and the serum in pigs. In this study, the authors reported a concentration of 2.33 mM for  $\text{Ca}^{2+}$  in BAL of healthy pigs [125]. Bargagli *et al.* [126] assessed trace elements in BAL of healthy subjects by atomic absorption spectroscopy (AAS). The authors reported a  $\text{Zn}^{2+}$  concentration of 1.25  $\mu\text{M}$  in BAL of healthy controls [126].

### **1.3.2. Chronic obstructive pulmonary diseases (COPD)**

The American Thoracic Society (ATS) outlines COPD's two common forms: chronic bronchitis (CB) and emphysema [127]. CB is defined as sputum production and chronic cough for a minimum of three months per year within the two years [128]. CB is caused by increased secretion of mucus by goblet cells, which leads to obstruction in the small airways and alterations of the airway surface tension [128, 129]. The clinical consequences of CB include a severe and decline of lung function, increased airflow obstruction, higher exacerbation frequency and mortality [128, 130]. It is well documented that many patients with severe emphysema also developed CB [128].

Lung emphysema is a pathological condition characterized by the progressive disruption of lung parenchyma associated with shortness of breath due to over-inflation of the alveoli [131-133]. ATS defines emphysema as follows "Emphysema is a disease condition of the lung which is characterized by enlargement of the air spaces followed by the destruction of their walls." [134, 135].

The aetiology of emphysema is not well understood and is most likely associated with a combination of both genetic and environmental elements. The widespread cause of emphysema in humans is cigarette smoke [60, 64, 65, 133]. Besides cigarette smoke, additional risk factors are ageing and gender [136], a previous history of asthma [137] and early respiratory infections [138]. Mechanistically, inflammatory processes, oxidative stress and an imbalance of protease-antiprotease trigger lung emphysema [61, 139, 140]. In the lung parenchyma, various proteases including neutrophil elastase (NE), cathepsins and matrix metalloproteinases (MMP-1, 2, 9, 12) disrupts the delicate connective tissue components [141]. This results in an imbalance between proteases and antiproteases such as alpha-1 antitrypsin (AAT), secretory leukoprotease inhibitor (SLPI), tissue inhibitor of matrix metalloproteinases (TIMP1-4) whose function is to protect against protease-mediated effects [142, 143].

The lungs are exposed to oxidants either endogenously produced by metabolic reactions and exogenously air pollutants. Exposure to cigarette smoke is a complex mixture of several compounds containing approximately 1014 oxidative free radicals [144, 145]. Oxidative stress activates transcription factors such as NF- $\kappa$ B leading to the release of inflammatory mediators including cytokines such as IL-8 and TNF- $\alpha$  [146]. The most significant pathogenesis COPD is the airway inflammation which results from exposure to several pollutants. Upon activation, inflammatory mediators are released from alveolar epithelial cells and neutrophils, macrophages and lymphocytes contributing to the progression of lung tissue destruction. The exposure to cigarette smoke activates alveolar epithelial cells to liberate inflammatory mediators including IL-1 $\beta$  and TNF- $\alpha$  capable of initiating chronic lung inflammation and airway remodelling [147, 148]. Moreover, ozone (O<sub>3</sub>) contributes to airway inflammation leading to the generation of reactive oxygen species (ROS) [149].

Ca<sup>2+</sup> is a critical intracellular mediator of airway inflammatory responses. For instance, dysregulation of Ca<sup>2+</sup> homeostasis in bronchial epithelia contributes to pulmonary disease [149, 150], and rises in cytosolic Ca<sup>2+</sup> trigger inflammatory signalling [149, 151, 152].

Neutrophil elastase (NE) belongs to serine proteases regulated by alpha-1 antitrypsin (AAT) [153]. AAT protein is mainly produced in the liver and protects the delicate lung tissue from the possible destructions by NE [153-155]. Patients with inherited AAT deficiency and loss of function mutations of AAT develop early-onset emphysema at childhood due to an imbalance between neutrophil elastase and AAT in the lung [61, 140, 156, 157].

COPD is considered as the age-associated disease since it is frequently diagnosed after the age of ~45 [156]. COPD is not curable [156]. However, available medical and physical treatments can relieve the symptoms, improve life quality and reduce the risk of mortality. In several patients diagnosed with COPD, treatment with inhaled corticosteroid medicines such as bronchodilators including  $\beta$ -Agonists, anticholinergics and phosphodiesterase inhibitor inhaled as aerosol sprays or taken orally relieve symptoms by relaxing and opening the airways of the lungs [58, 158-160]. In severe cases, lung transplantation is an option for some patients [161].

Several mouse models of emphysema were developed to study the pathomechanisms and search for new therapeutic options [162-167]. Several animal models are based on the induction of emphysema by challenging mice with exogenous agents like a single dose of elastase injection into the trachea [166, 168-170]. Common intratracheally delivered elastases include papain, porcine pancreatic elastase and human neutrophil elastase [169-171]. As a result, the lung parenchyma is destroyed, leading to irreversible tissue damage and emphysema. Many studies rely on chronic exposure of mice to cigarette smoke. After four

months of exposure, the mice display significant pathological changes in the lung mimicking emphysema after smoking in humans [172-176].

There are several genetic mouse strains, which spontaneously develop lung emphysema [168, 177]. Thus, independent studies have shown that genetic ablation of SP-A, SP-C, and SP-D resulted in a gradual appearance of alveolar emphysema in the mutant mice [112, 178-183]. Botas *et al.* [112] reported a diminished the number of AT2 cells in lungs of SP-D deficient mice lungs. Moreover, alveolar size increased while alveolar surface areas decreased. As expected, homeostasis of surfactants is disturbed in SP-D deficient mice, which is visible by the presence of giant lamellar bodies in AT2 cells [112, 184]. Stereological analysis of lung tissue sections revealed an increased intracellular pool of surfactants [112, 184]. SP-C-deficient mice developed emphysema associated with accumulations of intracellular lipids in AT2 cells [183]. Along these lines, SP-C deficient mice developed abnormal respiratory parameters typical for emphysema [183]. SP-B deficiency in mice was associated with lung injury susceptibility without signs of emphysema [185].

To summarize, emphysema represents a common form of COPD, characterized by severe parenchymal destruction and gradual decline in lung mechanics. To date, there is no existing therapy available to reverse lung tissue destruction.

### 1.3.3. Pathophysiological roles of TRP channels in COPD

Recently, several TRP channels were found to be associated with COPD [67, 68] such as TRPA1, TRPC6, TRPV1 and TRPV4.

TRPA1 is a  $\text{Ca}^{2+}$  permeable cation channel, activated by endogenous and exogenous toxic compounds [186]. Accordingly, it was suggested that TRPA1 could function as a trigger of pathophysiological processes in many cell types, including respiratory cells. Consequently, TRPA1 was identified in several respiratory cells including human lung fibroblasts (CCD19-Lu) and human AT2 cells (A549), human small airway epithelial cells (SAEC), human embryonic lung fibroblasts (IMR90), normal human lung fibroblasts (NHLF) and primary human bronchial smooth muscle cells (HBSMC) [187, 188]. Conklin *et al.* [189] assessed a protective role of TRPA1 by monitoring respiratory parameters of *Trpa1* null mice exposed to a toxic chemical component of cigarette smoke acrolein. The challenged *Trpa1* null mice displayed a slower onset of breathing rate suppression as compared to WT mice, suggesting that TRPA1 mediates the protective response [189]. Furthermore, Lin *et al.* [190] analyzed the protective role of TRPA1 in lung inflammation in a smoke exposure model. After four weeks of chronic exposure to cigarette smoke, TRPA1<sup>-/-</sup> mice displayed reduced inflammation in the lung which

was identified by reducing inflammatory cell infiltration and a decrease in inflammatory cytokine levels. Based on these findings, the authors proposed that TRPA1 plays a crucial role in regulating inflammatory pathways in respiratory epithelial cells.

TRPC6 is a redox-sensitive  $\text{Ca}^{2+}$  permeable cation channel of the canonical transient receptor potential (TRPC) family [149] expressed in a broad range of cell types which are thought to play a vital role in respiratory diseases such as COPD. Accordingly, Corteling *et al.* [191] identified TRPC6 mRNA in primary isolated respiratory cells including bronchial epithelial cells, alveolar smooth muscle cells and AM. Finney-Hayward *et al.* [192] detected the expression of human TRPC6 in primary macrophages, isolated from non-smokers and smokers with stable COPD and found significantly increased TRPC6 mRNA levels in AM from patients with COPD. The authors concluded that increased expression of TRPC6 in macrophages could be used as a diagnostic marker of COPD. Chen *et al.* [149] investigated the relevance of TRPC6 in  $\text{O}_3$ -induced airway inflammation in mice and identified an increased expression of TRPC6 in human bronchial epithelial cells (HBECs). Moreover, they reported that *Trpc6* KO mice and mice treated with a TRPC6 inhibitor, SAR7334, were protected from  $\text{O}_3$ -induced airway inflammation [149]. In the same study, *in vitro* experiments revealed that knockdown of TRPC6 expression and pharmacological blockage significantly diminished the release of inflammatory cytokines IL-6 and IL-8 induced by  $\text{O}_3$  in the human bronchial epithelial cell line 16HBE. These data reinforce the idea that oxidative stress generated by  $\text{O}_3$  upregulates the expression and activates TRPC6, which leads to the disruption of intracellular  $\text{Ca}^{2+}$  homeostasis and triggers the inflammatory response [149].

TRPV1 is a  $\text{Ca}^{2+}$  permeable cation channel activated by heat, capsaicin and several toxic compounds [193]. Hence, it was suggested that the broad expression pattern of TRPV1 in the airway epithelium could contribute to its role in COPD development. Accordingly, Reilly *et al.* [194] identified TRPV1 in the cultured human bronchial epithelial cell line (BEAS-2B) and AT2 cells (A549). Baxter *et al.* [195] investigated the role of TRPV1 in cigarette smoke-induced release of ATP from bronchial epithelia by comparing responses of WT and *Trpv1* KO mice. After acute smoke exposure, *Trpv1* KO mice exhibited reduced levels of ATP and IL-1 $\beta$  in the BAL [195]. In the same study, the authors examined expression levels of TRPV1 in human lung parenchyma from non-smokers and smokers with COPD. TRPV1 expression was significantly increased in patients with COPD compared with non-smokers [195]. Moreover, *in vitro* experiments revealed that cigarette smoke stimulated ATP release from HBEC cells, which was inhibited by pretreatment with a TRPV1 antagonist, JNJ-17203212 [195]. Choi *et al.* [196] investigated the role of TRPV1 in airway inflammation using WT mice treated with the TRPV1 antagonist, capsazepine. The authors detected reduced airway hyperresponsiveness and airway inflammation in WT mice which were evidenced by reduced levels of cytokines in

BAL fluids, indicating a protective role of TRPV1 in the respiratory system. Groneberg *et al.* [197] investigated the pathophysiological role of TRPV1 in triggering chronic cough and whether its antagonists can be used as a therapeutic option. In this study, patients with chronic cough and healthy subjects were challenged with capsaicin inhalation in different doses and coughs were counted for 1 min after a single breath. Normal subjects showed no evidence of airflow obstruction. However, a 30-fold less concentration of capsaicin was enough to initiate more than five coughs per min in patients, showing that patients with chronic cough were more sensitive to the tussive irritation by capsaicin [197]. Experiments with guinea pigs showed that capsaicin trigger cough indicating that TRPV1 plays a role in mediating the cough responses [197].

TRPV4 channels are non-selective cation channels activated by heat, mechanical stress, acidic pH, the synthetic phorbol ester 4 $\alpha$ -phorbol 12, 13-didecanoate (4 $\alpha$ -PDD) and epoxyeicosatrienoic acids (EETs) (metabolites of arachidonic acids AAs) [187, 198]. Literature indicates the involvement of TRPV4 channels, expressed in the lung, in pathways of diseases like COPD. Accordingly, TRPV4 is expressed in human bronchial epithelial cells, AT1 and AT2 cells and AM [68, 195, 199-201]. Weber *et al.* [201] assessed essential functions of TRPV4 in primary alveolar epithelial cells isolated from murine lungs. The authors identified a reduced production of SP-C in AT2 cells of TRPV4<sup>-/-</sup> mice, which also displayed more extensive mean chord lengths. Moreover, mutant mice showed altered lung function, evidenced by increased compliance compared with WT mice. The overall conclusion of this study was that TRPV4<sup>-/-</sup> mice develop emphysema suggesting a protective function of TRPV4 against pulmonary emphysema. Baxter *et al.* [195] investigated the role of TRPV4 in the mechanism for cigarette smoke-induced release of ATP in the pathogenesis of COPD. The authors reported that after acute smoke exposure, TRPV4<sup>-/-</sup> mice exhibited decreased levels of ATP and inflammatory mediator IL-1 $\beta$  in BAL, suggesting that TRPV4 is implicated in cigarette smoke-induced airway inflammation. Moreover, when HBEC were treated with the TRPV4 blocker HC067047 and exposed to cigarette smoke, ATP release from HBEC was inhibited compared to control cells, indicating a crucial role of TRPV4 channel in the release of ATP in response to acute smoke exposure [195]. Finally, the expression of TRPV4 mRNA was increased in lung biopsies from COPD patients reinforcing the conclusion that TRPV4 plays a role in COPD susceptibility [195].

To summarize, the existing data strongly indicate that TRP channels play a significant role in pathophysiology and the development of symptoms in various chronic lung diseases, including COPD. Therefore, TRP channels with widespread expression profiles in the respiratory epithelium may be promising pharmaceutical targets and specific modulators of TRP channels may serve as new therapeutic options in COPD.

## 2. Aims of the present study

Our previous systematic assessment of *Trpm6*-deficient mice [36] revealed that the *Trpm6*-deficient mice develop characteristic morphological changes in the lung parenchyma resembling pulmonary emphysema.

Therefore, we aimed to answer the following key questions in my Ph.D. thesis:

1. What is the expression pattern of *Trpm6* in the lung?
2. When and why do *Trpm6*-deficient mice develop pulmonary emphysema?
3. Is the respiratory phenotype of *Trpm6*-deficient mice associated with Mg<sup>2+</sup> homeostasis?
4. What is the contribution of the kinase activity of TRPM6 to the respiratory phenotype of *Trpm6*-deficient mice?
5. Which functional role(s) do perform TRPM6 channels in respiratory cells?

## 3. Materials

### 3.1. Chemicals

**Table 1. List of reagents used in the present study.**

Chemicals	Source
2-Mercaptoethanol	Carl Roth, # 4227
2-Propanol	Sigma Aldrich, # I9516
Absolute qPCR CYBR	Thermo Fisher Scientific, # AB1220A
Acetylene	Linde, # UN1001
Agarose	Carl Roth, # 3810
Ammonium peroxydisulphate (APS)	Carl Roth, # 9592
Anti-ATP-binding cassette sub family A member 3 antibody	Abcam, # ab24751
anti-Goat IgG HRP-linked (H+L chain)	R&D Systems, # HAF017
anti-Mouse CD 16/32 antibody	BD Biosciences, # 553142
anti-Mouse CD 45 antibody	BD Biosciences, # 553076
anti-Prosurfactant protein B antibody	Merck, # AB3430
anti-Prosurfactant protein C antibody	Abcam, # ab90716
anti-Prosurfactant protein C (pro-SPC) antibody	Merck, # AB3786
Anti-rabbit IgG HRP-linked (H+L chain)	Cell Signaling, # 7074
Anti-surfactant protein A antibody	Merck, # AB3420-I
BODIPY <sup>TM</sup> FL ATP	Thermo Fisher Scientific, # A12410
Bovine serum albumin (BSA)	Sigma-Aldrich, # A2153
Bromophenol blue sodium salt	Carl Roth, # A512
Calcium (Ca) pure standard	PerkinElmer, # N9303763

Chloroform	Sigma-Aldrich, # C2432
complete EDTA-free protease inhibitor cocktail	Sigma-Aldrich, # 04693159001
D-(+)-Glucose	Sigma-Aldrich, # G7528
Dako fluorescent mounting medium	Agilent, # S302380-2
Diethylpyrocarbonate (DEPC)	Sigma-Aldrich, # 159220
Dimethylsulfoxide (DMSO)	Carl Roth, # A994.2
Disodium hydrogen phosphate (Na <sub>2</sub> HPO <sub>4</sub> )	Sigma-Aldrich, # 255793
Dispase	Fischer scientific, # 11553550
Dulbecco's modified eagle's medium (DMEM) – low glucose	Sigma-Aldrich, # D5546
DNA gel loading dye (6X)	Thermo Fisher Scientific, # R0611
DNaseI	Appllichem, # A3778,0100
Dulbecco's phosphate-buffered saline (DPBS) divalent free	Gibco, # 14190-094
Eosin Y	Sigma-Aldrich, # 318906
Ethanol (EtOH, ≥ 99.5)	Carl Roth, # P075.2
Fetal bovine serum (FBS)	Thermo Fisher Scientific, # 10270-106
GeneRuler 100 bp DNA ladder	Thermo Fisher Scientific, # SM0241
GeneRuler Low Range DNA ladder	Thermo Fisher Scientific, # SM1193
GlutaMAX	Thermo Fisher Scientific, # 35050-061
Glutardialdehyd 25 %	Carl Roth, # 3778
Goat anti-mouse antibody Alexa Fluor 488	Invitrogen, # A11073
Goat anti-mouse antibody Alexa Fluor 633	Invitrogen, # A21050
Goat anti-rabbit antibody Alexa Fluor 488	Invitrogen, # A11008
Goat Serum	Ratiolab, # B15-035
Ham's F-12K (Kaighn's) Medium	Thermo Fisher Scientific, # 21127022
Hoechst 33342	Invitrogen, # H1399

Human/Mouse/Rat SPD antibody	R&D Systems, # AF1920
Hydrochloric acid (HCl) (37%)	Merck Millipore, # 100317
Hydrogen peroxide solution	Sigma-Aldrich, # 16911
Isoflurane (1000 mg/g)	Dechra, # G113H18B
Jung tissue freezing medium	Leica, # 14020108926
Ketamine 10%	Medistar Arzneimittelvertrieb GmbH
Luminol	Sigma-Aldrich, # 123072
Lyso tracker red DND-99	Invitrogen, # L7528
Magnesium (Mg) pure standard	PerkinElmer, # N9300179
Mayer´s hematoxylin	Sigma-Aldrich, # MHS1
Methanol	Carl Roth, # 4627
Mouse tissue lysis buffer	Vazyme, # PD101-01-AA
N-2-hydroxyethylpiperazine-N-2-ethane sulfonic acid (HEPES)	Thermo Fisher Scientific, # 15630080
Nitric acid 65% Suprapur	Merck, # 1004410250
Paraffin	Sigma-Aldrich, # 76242
Paraformaldehyde (PFA)	Sigma-Aldrich, # 441244
Paraformaldehyde (16%)	Electron Microscopy Sciences, # 15700
p-coumaric acid	Sigma-Aldrich, # C9008
Penicillin-streptomycin (10 mg/ml)	Thermo Fisher Scientific, # 15140122
Potassium chloride (KCl)	Sigma-Aldrich, # P3911
Potassium dihydrogen phosphate (KH <sub>2</sub> PO <sub>4</sub> )	Carl Roth, # 3904.1
Powdered milk	Carl Roth, # T145
Proteinase K	Vazyme, # PD101-01-AB
Quinacrine dihydrochloride	Sigma-Aldrich, # Q3251
RNAlater RNA stabilization reagent	Qiagen, # 76104

Roticlear	Carl Roth, # A538.1
Roti-GelStain	Carl Roth, # 3865
Rotiphorese gel 30	Carl Roth, # 3029
Schinkel solution	Merck, # 1167551000
Sodium dodecyl sulfate (SDS)	Carl Roth, # 2326
Sodium azide (NaN <sub>3</sub> )	Sigma-Aldrich, # 71289
Sodium chloride (NaCl)	Carl Roth, # 3957
Sodium dihydrogen phosphate dehydrate (NaH <sub>2</sub> PO <sub>4</sub> * 2 H <sub>2</sub> O)	Carl Roth, # T879.1
Sodium hydroxide (NaOH)	Carl Roth, # 6771
Spectra multicolor broad range protein ladder	Thermo Fisher Scientific, # 26634
Spectra multicolor high range protein ladder	Thermo Fisher Scientific, # 26625
Spectra multicolor low range protein ladder	Thermo Fisher Scientific, # 26628
Sucrose	Sigma-Aldrich, # S5016
Taq plus master mix	Vazyme, # PD101-01-AC
Tetramethylethylenediamine (TEMED)	Carl Roth, # 2367
Tissue freezing medium	Leica, # 14020108926
TRI reagent	Sigma-Aldrich, # T9424
Tris (hydroxymethyl)-aminomethane (TRIS)	Carl Roth, # 4855
Tris-HCl (2-Amino-2-hydroxymethyl- propane-1,3-diol hydrochloride)	Sigma-Aldrich, # 10812846001
Triton X-100	Merck, # 11869
Triton® X-100 wetting agent	PerkinElmer, # N9300260
Trypsin-EDTA solution	Sigma-Aldrich, # T3924

---

TWEEN 20 (Polyethylene glycol sorbitan monolaurate)	Sigma-Aldrich, # P1379
Xylazine 2%	Bela-pharm, #402650.00.00
Xylene	Sigma-Aldrich, # 214736
Zinc (Zn) pure standard	PerkinElmer, # N9300178

### 3.2. PCR primers

All primers used in the present study were obtained from Metabion, Planegg-Martinsried, Germany.

**Table 2. List of primers used for genotyping mouse strains.**

Name	Sequence	Amplicon
ROSA wt-rev	5'- CTT TAA GCC TGC CCA GAA GAC TC - 3'	495 bp (eROSA $\tau$ GFP) 256 bp (ROSA wt)
ROSA $\tau$ GFP-for	5'- GGA AGC ACT TGC TCT CCC AAA G - 3'	
ROSA $\tau$ GFP-rev	5'- GGG CGT ACT TGG CAT ATG ATA CAC - 3'	
Sox2-Cre-for	5'- TCC GGG CTG CCA CGA CCA A - 3'	446 bp
Sox2-Cre-rev	5'- GGC GCG GCA ACA CCA TTT TT - 3'	
Trpm6 cond-for	5'- GCA AAT ACA AGC AAC ACC TCC - 3'	368 bp
Trpm6 cond-rev	5'- TGT CTT CCA TGT TGC TAC GA - 3'	
Trpm6 kinase cre-del-for	5'- AGG GGG CTA GTA ATG AAT AA - 3'	240 bp (ki del)
Trpm6 kinase cre-del-rev	5'- GTC CGT TTG CCC TAC CTC CTG - 3'	153 bp (wt)
Trpm6 Null-for	5'- TGT CTT CCA TGT TGC TAC GA - 3'	362 bp
Trpm6 Null-rev	5'- CTT CCG GTC CAC AGT TCA T - 3'	
Trpm6 WC3-for	5'- AGC TCG CCC TGG ATG TAT - 3'	411 bp
Trpm6 WC3-rev	5'- TGT GGT GGC AGA GCA GGT A - 3'	
Trpm6 wt-for	5'- AGA GAC GTG CAG TGT AGG ACA GAG - 3'	549 bp
Trpm6 wt-rev	5'- ACG GCA CAC AGA AAA CAC CAG - 3'	
Trpm6 $\tau$ GFP-for1	5'- AAA TCG GCT CCA CGG AAA ACC TGA - 3'	435 bp ( $\tau$ GFP1)
Trpm6 $\tau$ GFP-for2	5'- CGT CCA GGA GCG CAC CAT CTT CTT - 3'	373 bp ( $\tau$ GFP2)
Trpm6 $\tau$ GFP-rev1	5'- CCT CGC CGG ACA CGC TGA ACT TG - 3'	
Trpm6 $\tau$ GFP-rev2	5'- ATC GCG CTT CTC GTT GGG GTC TTT - 3'	

**Table 3. List of primers used for qPCR analysis.**

Name	Sequence
AQP-5 for	5'- CTT TGG CCT GGC CAT AGG TAC CT -3'
AQP-5 rev	5'- CCA GAG TAA TGG CCG GAT TGA TGT G -3'
$\alpha$ -SMA for	5'- GAC GTA CAA CTG GTA TTG TG -3'
$\alpha$ -SMA rev	5'- TCA GGA TCT TCA TGA GGT AG -3'
SPC for	5'- AAG CCC TCC ACA CCC ACC TCT A -3'
SPC rev	5'- CTC TCC CGG AAG AAT CGG ACT CG -3'
Trpm6 ex17 for	5'- AAA GAG TAA AAG TCT GCG GG -3'
Trpm6 ex17 rev	5'- GGG TAG TAA AAC TGT AAC CTT -3'
HPRT for	5'-CTC ATG GAC TGA TTA TGG ACA GG-3
HPRT rev	5'-TTA ATG TAA TCC AGC AGG TCA GC-3'

**Table 4. Primers used to generate In situ hybridization (ISH) probe.**

Name	Sequence
Probe1 for	5'-aattaaccctcactaaagggGAGAGGAGGCCACAGTCAAG-3'
Probe2 for	5'-taatacgactcactatagggGCTCAAAGACGATGTCACGA-3'
Probe1 rev	5'-aattaaccctcactaaagggCCTGTCAAAGAAGAAGAGGAA-3'
Probe2 rev	5'-taatacgactcactatagggAGAAAAGACTTCACAATG-3'

### 3.3. Kits

**Table 5. Kits used in the present study.**

<b>Name</b>	<b>Source</b>
2x Absolute qPCR SYBR Green Mix	Thermo Fisher Scientific, # AB1220A
GenElute Mammalian Total RNA Miniprep Kit	Sigma-Aldrich, # RTN70
Mouse Direct PCR Kit	Vazyme, # PD101-01
Pierce Classic IP Kit	Thermo Fisher Scientific, # 26146
QIAshredder	Qiagen, # 79654
RevertAid H Minus First Strand cDNA Synthesis Kit	Thermo Fisher Scientific, # K1632
Urea Assay Kit	Sigma-Aldrich, # MAK006

### 3.4. Buffers and solutions

**Table 6. Buffers and solutions used for western blot analysis.**

Name	Composition
Loading buffer (2X Laemmli buffer)	250 mM Tris-HCl (pH 6.8), 40% Glycerin, 8% SDS, 0.04% Bromophenol blue, 1% $\beta$ -mercaptoethanol
Running gel	6% acrylamide/bisacrylamide, 375 mM Tris-HCl (pH 8.8), 0.1% SDS, 0.1% APS, TEMED (1:1000)
Stacking gel	3% acrylamide/bisacrylamide, 125 mM Tris-HCl (pH 6.8), 0.1% SDS, 0.1% APS, TEMED (1:1000)
Tris-glycine-SDS running buffer	25 mM Tris (pH 7.6), 190 mM glycine, 0,1% SDS
Tris-glycine-methanol transfer buffer	25 mM Tris (pH 7.6), 190 mM glycine, 20% methanol
Tris-buffered saline with Tween 20 (TBST)	20 mM Tris (pH 7.6), 137 mM NaCl, 0,1% Tween 20
Blocking solution	5% non-fat milk in TBST
Stripping solution	60 mM Tris-HCl (pH 6.8), 2% SDS, 0.7% $\beta$ -mercaptoethanol
Enhanced chemiluminescence (ECL) solution	Solution 1: 100 mM Tris-HCl (pH 8.5), 2.5 mM luminol, 0.4 mM p-coumaric acid Solution 2: 100 mM Tris-HCl (pH 8.5), 0.06% H <sub>2</sub> O <sub>2</sub> (Solution 1 and 2 were mixed 1:1 and used immediately for WB detection)

**Table 7. Buffers and solutions used for immunostaining of cells and tissue sections.**

Name	Composition
PBS buffer	137 mM NaCl, 2.7 mM KCl, 10 mM Na <sub>2</sub> HPO <sub>4</sub> , 1.8 mM KH <sub>2</sub> PO <sub>4</sub> (pH 7.4)
Fixation solution for IHC	4% paraformaldehyde (PFA) in PBS (pH 7.4)
Fixation solution for IF	3.7% paraformaldehyde (PFA) in PBS (pH 7.4)
Permeabilization solution	0.5% Triton X-100 in PBS
Blocking solution	4% BSA, 4% goat serum in PBS
Antibody incubation solution	2% BSA in PBS
Washing solution	0.1% BSA in PBS
Nuclei staining solution	2 µg/ml Hoechst 33342 in PBS

**Table 8. Buffers and solutions used for electron microscopic analysis (EM).**

Name	Composition
10X Phosphate-buffered saline (PBS)	100 g NaCl, 2.5 g KCl, 28 g Na <sub>2</sub> HPO <sub>4</sub> * 2 H <sub>2</sub> O, 3 g KH <sub>2</sub> PO <sub>4</sub> , add up to 1000 ml ddH <sub>2</sub> O (pH 7.4 )
1X Phosphate-buffered saline (PBS)	diluted from 10X PBS in ddH <sub>2</sub> O
EM fixative solution	5 g PFA, 150 ml ddH <sub>2</sub> O, 10 ml Glutardialdehyd (25%), 25 ml 10X PBS, add up to 250 ml ddH <sub>2</sub> O (pH 7.4)

**Table 9. Buffers and solutions used for alveolar epithelial Type 2 cell isolation.**

Name	Composition
Bronchoalveolar lavage (BAL) buffer	Dissolve 1 tablet of protease inhibitor complete mini EDTA free in 10 ml PBS.
Cardiac lung perfusion solution	0.9% NaCl
Agarose solution	1% Agarose in low-glucose DMEM. Heat in the microwave shortly to dissolve agarose
Minus medium	250 ml low-glucose DMEM, 5 ml GlutaMAX, 2.5 ml HEPES, 2.5 ml Penicillin-streptomycin solution.
Plus medium	250 ml low-glucose DMEM, 5 ml GlutaMAX, 2.5 ml HEPES, 2.5 ml Penicillin-streptomycin solution, 10 mg DnaseI.

**Table 10. Buffers and solutions used for PCR**

Name	Composition
50X Tris-acetate-EDTA (pH 8.5, TAE buffer)	242 g Tris, 100 ml 0.5 mM EDTA, 57 ml 20 mM Acetic acid, add 1000 ml ddH <sub>2</sub> O (pH 8.5)
1 % Agarose gel	2 g Agarose in 200 ml 1X TAE

**Table 11. Buffers and solutions used for atomic absorption spectroscopy.**

Name	Composition
Blank solution	500 $\mu\text{l}$ Schinkel solution (Cesium chloride - lanthanum chloride buffer solution), 500 $\mu\text{l}$ nitric acid (supra pure), add up to 50 ml ddH <sub>2</sub> O
0.2% Triton X-100 solution	1 ml Triton X-100 in 500 ml ddH <sub>2</sub> O
Mg <sup>2+</sup> standard solutions	Stock solution: 41 mM Following Mg <sup>2+</sup> standard solutions were prepared: 4 $\mu\text{M}$ , 8 $\mu\text{M}$ and 16 $\mu\text{M}$ with 500 $\mu\text{l}$ Schinkel solution, 500 $\mu\text{l}$ nitric acid (supra pure) and ddH <sub>2</sub> O
Ca <sup>2+</sup> standard solutions	Stock solution: 25 mM Following Ca <sup>2+</sup> standard solutions were prepared: 2.5 $\mu\text{M}$ , 5 $\mu\text{M}$ and 10 $\mu\text{M}$ with 500 $\mu\text{l}$ Schinkel solution, 500 $\mu\text{l}$ nitric acid (supra pure) and ddH <sub>2</sub> O
Zn <sup>2+</sup> standard solutions	Stock solution: 15 mM Following Zn <sup>2+</sup> standard solutions were prepared: 0.8 $\mu\text{M}$ , 1.5 $\mu\text{M}$ and 3 $\mu\text{M}$ with 500 $\mu\text{l}$ Schinkel solution, 500 $\mu\text{l}$ nitric acid (supra pure) and ddH <sub>2</sub> O
Serum and lavage samples	From the sample add: 10 $\mu\text{l}$ for 1:500 dilution 25 $\mu\text{l}$ for 1:200 dilution 500 $\mu\text{l}$ for 1:10 dilution add 50 $\mu\text{l}$ Schinkel solution and fill up to 5 ml with 0.2% Triton X-100/ddH <sub>2</sub> O

### 3.5. Consumables

**Table 12. List of consumables used in the present study.**

Name	Source
Adhesion slides (Superfrost plus)	Thermo Fischer Scientific, # J1800AMNZ
Amicon Ultra-0.5 centrifugal filter devices	Merck, # UFC501024
Biosphere tips with filters (10 $\mu$ l, 100 $\mu$ l, 200 $\mu$ l and 1000 $\mu$ l)	Sarstedt, #70.1116.210, # 70.1116, # 70.760.002, # 70.762
Cell scrapers 25 cm	Sarstedt, # 83.1830
Cellulose swab roll	B Braun, # 9051015
Ceramic ball for flame photometry	Perkin Elmer, # B0505086
Cover slips (20x20 mm)	Carl Roth, # H 873
Cover slips (24x60 mm)	Carl Roth, # H 878
Dako (hydrophobic) pen	Agilent, # S2002
Disposable sterile scalpels	Paragon, # 9000-10
Embedding cassettes	Carl Roth, # AA78.1
Eppendorf pipettes (10 $\mu$ l, 100 $\mu$ l, 200 $\mu$ l and 1000 $\mu$ l)	Eppendorf, # N52258H, # P21910H, # I41302I, # O34046H
Eppendorf Safe-Lock tubes 1.5 ml	Eppendorf, # 0030120086
Eppendorf Safe-Lock tubes 2 ml	Eppendorf, # 0030120094
Hollow cathode Lamp Element Ca	Perkin Elmer, # N305-0114
Hollow cathode Lamp Element Mg	Perkin Elmer, # N305-0144
Hollow cathode Lamp Element Zn	Perkin Elmer, # N305-0191
Hypodermic needle, Nr.14	Henke Sass Wolf, # 4710006030
Intravenous intubation cannula	B Braun, # 11226486
LightCycler 480 Multiwell Plate 96	Roche, # 04729692001
LightCycler 480 Sealing Foil	Roche, # 04729757001

Multiply- $\mu$ Strip Pro 8-strips	Sarstedt, #72.991.002
Microscope cover slips ( $\varnothing$ 22mm)	Thermo Fischer Scientific, # P235.1
Microtome disposable blades	Leica, # 14035838925
Mounting glass (20x20 mm)	Carl Roth, # H873
Mounting glass (24x60 mm)	Carl Roth, # H878
Nalgene rapid flow filter units	Thermo Fischer Scientific, # 595-4520
Neubauer chamber	Paul Marienfeld, # 0640111
Nitrocellulose membrane (0.45 $\mu$ M)	GE Healthcare Life Sciences, # 10600002
Nylon filters 10 $\mu$ m	Sefar, # 3A03-0010-102-00
Nylon filters 20 $\mu$ m	Sefar, # 3A03-0020-102-10
Nylon filters 100 $\mu$ m	Sefar, # 3A03-0100-115-01
Paper boxes for mouse transport	Janvier, # ET-EM-VIDE
Parafilm M	Pechiney Plastic Packaging, # PM992
Pasteur pipettes	Carl Roth, # 4522
Precision wipes	Kimtech Science, # 7552
Rotilabo disposable weighing tray	Carl Roth, # 2149.2
Pipettes (10 $\mu$ l, 100 $\mu$ l, 200 $\mu$ l and 1000 $\mu$ l)	Peqlab, # 245420133, # 245445121, # 245440122, # 245460326
Serological pipettes (2 ml, 5 ml, 10 ml and 25 ml)	Sarstedt, # 86.1252.001, # 86.1253.001, # 86.1254.001, # 86.1685.001
Slide boxes	Carl Roth, # K532.1
Superfrost Plus slides	Thermo Fischer Scientific, # 10149870
Sterican needles $\varnothing$ 0.40 x 20 mm, 27 G X $\frac{3}{4}$	B Braun, # 4657705
Syringe, sterile 1 ml	B Braun, # 9166017V
Syringe, sterile 5 ml	B Braun, # 4606051V
Syringe, sterile 10 ml	B Braun, # 4606108V

---

Syringe, sterile 20 ml	B Braun, # 4606205V
T25 flasks	Sarstedt, # 20003526
T75 flasks	Sarstedt, # 83.3911.002
TC dishes (10 cm)	Sarstedt, # 83.3902
Tips (10 $\mu$ l, 100 $\mu$ l, 200 $\mu$ l and 1000 $\mu$ l)	Sarstedt, # 70.1130, # 70.1116, # 70.760.002, # 70.762
Tissue Culture plates 6-well	Sarstedt, # 83.3920
Tissue Culture plates 96-well	Sarstedt, # 83.3924
Tube 15 ml, 120x17 mm, PP	Sarstedt, # 62.554.502
Tube 50 ml, 114x128 mm, PP	Sarstedt, # 62.547.254

### 3.6. Technical devices

**Table 13. Equipment used in the present study.**

Instrument	Model	Source
Atomic absorption spectrometer	PinAAcle 500	Perkin Elmer
Balances	Analytical balance KERN ALT220	Kern & Sohn
	Precision balance 572	Kern & Sohn
Cell culture incubator	HERA 240 CO <sub>2</sub>	Thermo Fisher Scientific
Cell culture bench	Heraeus Pico 17	Thermo Fisher Scientific
Centrifuges	Heraeus Labofuge 400	Thermo Fisher Scientific
	Heraeus Pico 17	Thermo Fisher Scientific
	Heraeus Biofuge Stratos	Thermo Fisher Scientific
Cryo-microtome for tissue sections	CM3050 S	Leica
Freezer	Forma 900 freezer (-80°C)	Thermo Fisher Scientific
Genomic DNA gel electrophoresis imaging system	Infinity-3026WL/26MX	PeqLab
Ice machine	Ziegra	ZIEGRA
Light cycler	Light Cycler 480	Roche
Microplate reader	CLARIOstar	BMG Labtech
Micropipettes	10, 100, 200 and 1000 µl	PeqLab
Microscopes	ZEISS LSM 880 Confocal Laser scanning microscope	ZEISS
	Axiovert 40 CFL	Carl Zeiss

	Olympus CX41	Olympus
Microwave	Microwave & Grill	Severin
Paraffin-microtome for tissue sections	Hyrax M55	Carl Zeiss
pH Meter	Lab 850	Schott Instruments
Power supply	PowerPac HC	Bio-Rad
	EV231	PeqLab
Shakers	MAXQ 6000	Thermo Fisher Scientific
	Mini Rocker MR-1	PeqLab
Spectrophotometer	BioPhotometer plus	Eppendorf
Thermocyclers	Biometra Professional TRIO	Biometra
	TProfessional TRIO	Analytik Jena
Vortexer	IKA MS3 basic	Ika
Western blot electrophoresis chamber	Mini-PROTEAN Tetra Cell	Bio-rad
Western blot imaging system	Chemi-Smart-5100	PeqLab
	Chemi Doc	Bio-Rad

### 3.7. Software

**Table 14. Software used in this project.**

Software	Version	Source
Case Viewer	V2.2	3D HISTECH
CellSens cell imaging	V1.7.1	Olympus
Chemi-Capt 5000	V15.02	Vilber
CLARIOstar Mars	V3.32	BMG Labtech
GraphPad Prism	V8.02	GraphPad Software, Inc.
Infinity-Capt	V14.2	Vilber
IrfanView	V4.51	Irfan Skiljan
Image J	1.52i	Wayne Rasband
Image Studio Lite	V5.2	LI-COR
Light Cyclor 480	V1.5.0 SP3	Roche
Microsoft Office	V2016	Microsoft
Panoramic Viewer	V1.15.4	3D HISTECH
Syngistik Touch	V1.1.1.0003	Perkin Elmer
Universal Probe Library System Assay Design	VWeb	Roche
ZEN Blue edition	V3.1	ZEISS Microscopy

## 4. Methods

### 4.1. Genetic mouse strains used in the present study

#### 4.1.1. Production of mice with a global null mutation in *Trpm6*

Mice with a conditional mutation in *Trpm6* (*Trpm6<sup>fl</sup>*) were generated as reported previously [36]. Since constitutive inactivation of *Trpm6* leads to embryonic mortality, our group established a new genetic model allowing to produce adult mice lacking *Trpm6* in the whole body. Specifically, we established an epiblast-specific inactivation of the *Trpm6<sup>fl</sup>* allele using *Sox2-Cre* transgenic mice ubiquitously expressing Cre recombinase from *Sox2-Cre* transgene [36]. Cre recombinase enabled the deletion of the genomic sequence between LoxP sites (referred as 'floxed' sequence) which drove Cre-mediated deletion of the floxed sequence in all epiblast cells (embryo at an early stage), but not in extraembryonic cells including placental trophoblasts of the mother [36, 202].

We crossed *Trpm6<sup>fl/fl</sup>* females and *Trpm6<sup>Δ17/+</sup>; Sox2-Cre* males to produce viable *Trpm6<sup>Δ17/Δ17</sup>; Sox2-Cre* (KO) offspring and corresponding *Trpm6<sup>fl/+</sup>* (control) littermates (Table 15) [36]. *Trpm6*-deficient (*Trpm6<sup>Δ17/Δ17</sup>; Sox2-Cre*) 4-, 8- and 12-weeks old male littermates were used for experiments.

#### 4.1.2. Generation of mice with a global kinase-dead point mutation in *Trpm6*

A mouse line (C57BL/6) carrying a conditional kinase-dead point mutation in *Trpm6* was generated by Taconic Artemis (Köln, Germany). Figure 6 outlines the corresponding targeting strategy. In analogy to the K1646R mutation in TRPM7 [55], K1810R in TRPM6 inactivates its kinase activity [34]. By homologous recombination in embryonic stem (ES) cells, exon 34 of *Trpm6* was replaced with a cDNA sequence encoding for the WT kinase domain of *Trpm6* (exons 34-39 with a STOP codon) flanked by LoxP sites and followed by an additional sequence coding for exon 34 harbouring a K1810R point mutation (Figure 6). Consequently, such floxed (*fl*) allele will express the WT TRPM6 protein, whereas Cre-mediated deletion of the floxed sequence will introduce the K1810R mutation into the *Trpm6* locus. Chimeric mice were crossed with *Fip* deleter mice to remove the neomycin resistance cassette (Neo), and

the animals displaying germ-line transmission were selected to produce mice homozygous for the *fl* allele. In order to generate mice heterozygous for the *K1810R* allele (*Trpm6<sup>R</sup>*), we used mice with the *Sox2-Cre* transgene. Finally, we bred *Trpm6<sup>R/+</sup>* couples to generate *Trpm6<sup>R/R</sup>* and *Trpm6<sup>+/+</sup>* (Figure 7) (Table 15).

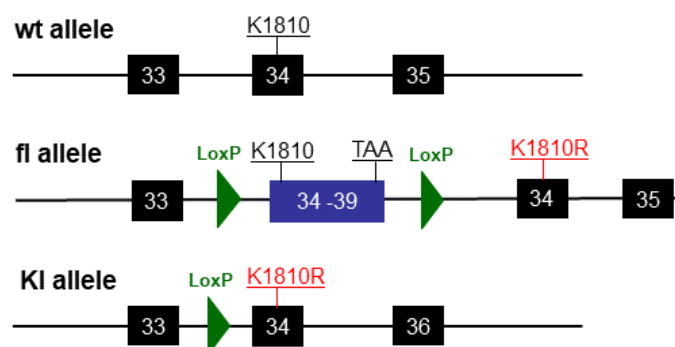


**Figure 6. Targeting strategy used for the generation of mice with the kinase-dead mutation in *Trpm6*.** wt, wild-type; TAA, stop codon; LoxP, 34 bp DNA sequence recognition sites.

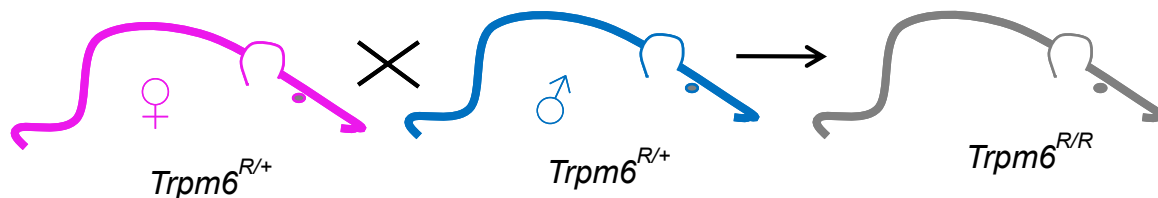


**Figure 7. Breeding strategy to generate *Trpm6<sup>R/R</sup>* mice.** *Trpm6<sup>R/+</sup>*, mice heterozygous for the *K1810R* allele; *Trpm6<sup>R/R</sup>*, mice carrying global kinase-dead point mutation in *Trpm6*.

#### 4.1.3. Production of mice carrying a *Trpm6<sup>Cre</sup>* allele

A mouse line carrying a *Trpm6<sup>Cre</sup>* allele was reported earlier [203]. *Trpm6<sup>Cre</sup>* mice in which Cre recombinase is co-expressed with individual *Trpm6* gene allows visualizing TRPM6 channel expressing cells at a single cell resolution [203]. In order to generate these mice, an internal ribosome entry site (IRES) followed by Cre sequence was inserted immediately 3' of the stop-codon of *Trpm6*. The IRES ensures simultaneous expression of TRPM6 and Cre proteins from a single bicistronic mRNA. Next, we crossed *Trpm6<sup>Cre/Cre</sup>* animals with transgenic mice containing *floxed-stop-τGFP* sequence in *Rosa26 locus* (*Rosa26<sup>τGFP</sup>* mice). The *Rosa26 locus*

is ubiquitously expressed has been proven to be a reliable locus used for the insertion of Cre-dependent transgenes. Rosa26 reporter mice provides fluorescent labeling with a fusion of the microtubule-associated protein  $\tau$  with GFP ( $\tau$ GFP- green fluorescent protein). *Floxed-stop- $\tau$ GFP* protein is not expressed from the *Rosa26* locus in the absence of Cre. However, in the presence of *Trpm6<sup>Cre</sup>*, Cre will delete the floxed stop-codon sequence from *Rosa26<sup>GFP</sup>* and will induce expression of  $\tau$ GFP protein specifically in the cells expressing TRPM6.

**Table 15. Breeding of mouse strains used in this project.**

Outcome	Breeding strategy	Expected and observed F1 outcomes <sup>a</sup>
Global null mutation	$\text{♂ } Trpm6^{\Delta 17/+}; Sox2-Cre \times \text{♀ } Trpm6^{fl/fl}$	<u>25% <math>Trpm6^{\Delta 17/\Delta 17}; Sox2-Cre</math></u> 25% $Trpm6^{\Delta 17/fl}$ 25% $Trpm6^{\Delta 17/+}; Sox2-Cre$ 25% $Trpm6^{fl/+}$
Global kinase-dead mutation	$\text{♂ } Trpm6^{R/+} \times \text{♀ } Trpm6^{R/+}$	<u>25% <math>Trpm6^{R/R}</math></u> 50% $Trpm6^{R/+}$ 25% $Trpm6^{+/+}$
$\tau$ GFP expression under the control of <i>Trpm6</i>	$\text{♂ } Trpm6^{Cre/Cre}; Rosa26^{+/+} \times$ $\text{♀ } Trpm6^{+/+}; Rosa26^{\tau GFP/+}$	<u>50% <math>Trpm6^{Cre/+}; Rosa26^{\tau GFP/+}</math></u> 50% $Trpm6^{Cre/+}$

<sup>a</sup>Genotypes were determined using genomic DNA extracted from ear fragments.

## 4.2. Genotyping of mouse strains

The genomic DNA was recovered from the mouse ear fragments. The extraction of DNA was performed using a One-Step Mouse Genotyping Kit (Vazyme, Catalog # PD101-01) according to the manufacturer's instructions. DNA was extracted by adding the lysis buffer mixture (100

µl Mouse tissue lysis buffer + 2 µl Proteinase K) to the sample, and incubation at 55°C for 30 min. After the digestion, the samples were incubated at 95°C for 5 min to inactivate proteases and stored at -20°C.

The DNA extracts from ear fragments were examined using a polymerase chain reaction (PCR) approach. To the master mix, 2 µl extracted DNA was added as outlined in Table 16. The corresponding primers and PCR settings are shown in Tables 17-26.

**Table 16. Master mix composition for PCR reaction.**

Reagent	Volume
DNA extract	2 µl
2 X M-PCR Optimix*	10 µl
Forward primer	0.1 µl
Reverse primer	0.1 µl
ddH <sub>2</sub> O	9.3 µl

\*from One-Step Mouse Genotyping Kit

**Table 17. Primer pairs and PCR amplicons used for genotyping of mice.**

Allele	Primer	Amplicon
<i>Rosa26</i>	Forward primer: 5'- GGA AGC ACT TGC TCT CCC AAA G -3', Reverse primer: 5'- GGG CGT ACT TGG CAT ATG ATA CAC -3' WT Reverse primer: 5'- CTT TAA GCC TGC CCA GAA GAC TC -3'	WT: 365 bp τGFP: 495 bp
<i>Sox2-Cre</i>	Forward primer: 5'- TCC GGG CTG CCA CGA CCA A -3' Reverse primer: 5'- GGC GCG GCA ACA CCA TTT TT -3'	446 bp

<i>Trpm6<sup>fl</sup></i>	Forward primer: 5'- GCA AAT ACA AGC AAC ACC TCC -3' Reverse primer: 5'- TGT CTT CCA TGT TGC TAC GA -3'	368 bp
<i>Trpm6<sup>R/R</sup></i>	Forward primer: 5'- AGG GGG CTA GTA ATG AAT AA -3' Reverse primer: 5'- GTC CGT TTG CCC TAC CTC CTG -3'	208 bp
<i>Trpm6<sup>Δ17</sup></i>	Forward primer: 5'- TGT CTT CCA TGT TGC TAC GA -3' Reverse primer: 5'- CTT CCG GTC CAC AGT TCA T -3'	362 bp
<i>Trpm6<sup>fl/+</sup></i>	Forward primer: 5'- AGC TCG CCC TGG ATG TAT -3' Reverse primer: 5'- TGT GGT GGC AGA GCA GGT A -3'	411 bp
<i>Trpm6<sup>+</sup></i>	Forward primer: 5'- AGA GAC GTG CAG TGT AGG ACA GAG -3' Reverse primer: 5'- ACG GCA CAC AGA AAA CAC CAG -3'	549 bp
<i>Trpm6<sup>Cre</sup></i>	Forward1 primer: 5'- AAA TCG GCT CCA CGG AAA ACC TGA-3' Reverse1 primer: 5'- CCT CGC CGG ACA CGC TGA ACT TG-3' Forward2 primer: 5'- CGT CCA GGA GCG CAC CAT CT TCTT-3' Reverse2 primer: 5'- ATC GCG CTT CTC GTT GGG GTC TTT-3'.	435 bp (τGFP1) 373 bp (τGFP2)

**Table 18. PCR settings for *Rosa26*.**

Phase	Temperature	Time	Number of cycles
Initialization step	94°C	5 min	1
Denaturation	94°C	30 s	10
Annealing	75°C (-1°C per cycle)	60 s	
Elongation	72°C	90 s	
Denaturation	94°C	30 s	35
Annealing	64°C	60 s	
Elongation	72°C	60 s	
Final extension	72°C	5 min	1
Cooling	16°C	continuous	1

**Table 19. PCR settings for *Sox2-Cre*.**

Phase	Temperature	Time	Number of cycles
Initialization step	94°C	5 min	1
Denaturation	94°C	30 s	10
Annealing	70°C (-1°C per cycle)	30 s	
Elongation	72°C	60 s	
Denaturation	95°C	30 s	35
Annealing	59°C	30 s	
Elongation	72°C	60 s	
Final extension	72°C	5 min	1
Cooling	16°C	continuous	1

**Table 20. PCR settings for *Trpm6<sup>f</sup>* allele.**

Phase	Temperature	Time	Number of cycles
Initialization step	95°C	5 min	1
Denaturation	95°C	30 s	10
Annealing	64°C (-1°C per cycle)	60 s	
Elongation	72°C	90 s	
Denaturation	95°C	30 s	35
Annealing	53°C	60 s	
Elongation	72°C	90 s	
Final extension	72°C	5 min	1
Cooling	16°C	continuous	1

**Table 21. PCR settings for *Trpm6<sup>R</sup>* allele.**

Phase	Temperature	Time	Number of cycles
Initialization step	95°C	5 min	1
Denaturation	95°C	30 s	10
Annealing	65°C (-1°C per cycle)	60 s	
Elongation	72°C	60 s	
Denaturation	95°C	30 s	35
Annealing	55°C	60 s	
Elongation	72°C	60 s	
Final extension	72°C	5 min	1
Cooling	16°C	continuous	1

**Table 22. PCR settings for *Trpm6*<sup>Δ17</sup> allele.**

Phase	Temperature	Time	Number of cycles
Initialization step	95°C	5 min	1
Denaturation	95°C	30 s	10
Annealing	64°C (-1°C per cycle)	60 s	
Elongation	72°C	90 s	
Denaturation	95°C	30 s	35
Annealing	53°C	60 s	
Elongation	72°C	60 s	
Final extension	72°C	5 min	1
Cooling	16°C	continuous	1

**Table 23. PCR settings for both *Trpm6*<sup>fl</sup> and *Trpm6*<sup>+</sup> alleles.**

Phase	Temperature	Time	Number of cycles
Initialization step	94°C	5 min	1
Denaturation	94°C	30 s	10
Annealing	70°C (-1°C per cycle)	30 s	
Elongation	72°C	60 s	
Denaturation	95°C	30 s	35
Annealing	59°C	30 s	
Elongation	72°C	60 s	
Final extension	72°C	5 min	1
Cooling	16°C	continuous	1

**Table 24. PCR settings for *Trpm6*<sup>+</sup> allele.**

Phase	Temperature	Time	Number of cycles
Initialization step	94°C	5 min	1
Denaturation	94°C	30 s	10
Annealing	75°C (-1°C per cycle)	60 s	
Elongation	72°C	90 s	
Denaturation	94°C	30 s	35
Annealing	64°C	60 s	
Elongation	72°C	60 s	
Final extension	72°C	5 min	1
Cooling	16°C	continuous	1

**Table 25. PCR settings for *Rosa26*<sup>GFP</sup> and *Rosa26*<sup>+</sup> alleles.**

Phase	Temperature	Time	Number of cycles
Initialization step	95°C	5 min	1
Denaturation	95°C	30 s	10
Annealing	66°C (-1°C per cycle)	30 s	
Elongation	72°C	60 s	
Denaturation	95°C	30 s	35
Annealing	61°C	30 s	
Elongation	72°C	60 s	
Final extension	72°C	5 min	1
Cooling	16°C	continuous	1

**Table 26. PCR settings for *Trpm6*<sup>Cre</sup> allele.**

Phase	Temperature	Time	Number of cycles
Initialization step	95°C	5 min	1
Denaturation	95°C	30 s	10
Annealing	60°C (-1°C per cycle)	30 s	
Elongation	72°C	60 s	
Denaturation	95°C	30 s	35
Annealing	55°C	30 s	
Elongation	72°C	60 s	
Final extension	72°C	5 min	1
Cooling	16°C	continuous	1

PCR reactions were carried out with a TProfessional TRIO thermocycler (Analytik Jena). PCR products were separated by electrophoresis using 1% agarose gels in Tris-acetate-EDTA (TAE) buffer and stained with Roti-GelStain (Carl Roth). Gels were run with 100 bp DNA Ladders (GeneRuler) and imaged using an Infinity-3026WL/26MX documentation system (PeqLab). IrfanView software was used to analyze obtained images.

### 4.3. Housing of mice

All animal experiments were approved by the Government of Upper Bavaria (ROB-55.2-2532.Vet\_02-18-160) and carried out in compliance with the EU-directive 2010/63 on the protection of animals used for scientific purposes.

Animals were housed in individually ventilated polycarbonate cages (IVC System, Techniplast, Germany) in the animal facility of the WSI, LMU Munich, Germany. Cages were changed weekly. Mice were kept under a 12:12h light-dark cycle with artificial lighting. Temperature and relative humidities were 22+/-1°C and 50+/-5%, respectively. All mice had free access to multigrain chow (#V1125, ssniff Spezialdiäten GmbH, containing 0.22% Mg<sup>2+</sup>) and drinking

water (*ad libitum*). For Mg<sup>2+</sup> supplementation, *Trpm6*-deficient mice and control group were fed with an MgCl<sub>2</sub>-enriched chow containing 0.52 % Mg<sup>2+</sup>.

## 4.4. Histological examination of lungs

### 4.4.1. Preparation of lungs and Hematoxylin and Eosin (H&E) staining of tissue sections

Mice were dissected and examined at the Institute of Lung Biology and Disease (ILBD) of the Helmholtz Centrum Munich (German Research Center for Health and Environment, Neuherberg, Germany) after anesthesia by intraperitoneal (i.p.) injection of ketamine (270 mg/kg) and xylazine (11 mg/kg). After Tracheostomy, mice were cannulated with a 20-gauge intravenous intubation cannula.

The right lung was excised and snap-frozen in liquid nitrogen prior to extraction of mRNA and proteins. The left lung was fixed by intratracheal instillation of PBS-buffered 6% paraformaldehyde (PFA) at a constant pressure of 20 cm fluid column. The removed tissues were incubated in 6% PFA at 4°C for 24 h. Next, the tissues were placed into 20 ml of 2% (w/v) lukewarm agar and allowed to be embedded at 4°C for 60 min. The tissues were cut into 2 mm thick sections using a cutting apparatus. The tissue fragments were placed in cassettes and stored in 4% PFA at 4°C. The tissue fragments in cassettes were subjected to serial dehydration steps using 70%, 80%, 96% (3x), 100% (3x) ethanol in Leica TP1020 processor. The alcohol was removed from the tissues by incubation of the cassettes in Roticlear (Carl Roth) solvent for 1 h at RT.

The fragments were embedded in paraffin wax to saturate the tissue cavities and cells. The paraffin-embedded tissues were sectioned (3 µm) using a microtome (Hyrax M55). The obtained sections were transferred onto Superfrost glass slides, incubated at 38°C for 24 h and stored at 4°C.

The paraffin-embedded tissue sections were deparaffinized using xylol and rehydrated in descending alcohol series, as outlined in Table 27. Next, the sections were stained in Mayer's hematoxylin and exposed to eosin followed by dehydration using different ethanol solutions and xylol (Table 27). Finally, the stained tissue sections were covered with mounting medium (Entellan) and mounted on glass slides.

**Table 27. Procedure for H&E staining of lung tissue sections.**

<b>Chemical</b>	<b>Time</b>
100% xylol	2 x 5 min
100% ethanol	2 x 1 min
90% ethanol	1 min
80% ethanol	1 min
70% ethanol	1 min
ddH <sub>2</sub> O	30 s
Mayer's hematoxylin solution	8 min
0.5% aqueous eosin solution	8 min
ddH <sub>2</sub> O	1 min
70% ethanol	3 x 10 s
80% ethanol	3 x 10 s
90% ethanol	3 x 10 s
96% ethanol	3 x 10 s
100% ethanol	2 x 1 min
100% xylol	2 x 5 min

#### **4.4.2. Quantitative morphometry of lung tissue sections**

Pulmonary emphysema is associated with an irreversible enlargement of alveolar air space. In the present study, alveolar air space enlargement was examined by determining the mean linear chord length (MCL) in H&E stained lung tissue sections (prepared as described in Section 4.4.1). An Olympus BX51 light microscope equipped with 20x fold objective, and the Computer Assisted Stereological Toolbox software (newCAST, Visiopharm) were used as described previously [65]. Briefly, 20 frames were selected randomly across a tissue section

by the software, and superimposed by a line grid and points as exemplified in Figure 8. The images were analyzed by the following formula:

$$\text{MCL} = \Sigma P_{\text{air}} \times L(p) / \Sigma I_{\text{septa}} \times 0.5,$$

where; MCL ( $L_m$ ,  $\mu\text{m}$ ) is the mean linear chord length;  $L(p)$  is the line length per test point (99.3  $\mu\text{m}$ ),  $I_{\text{septa}}$  are intercepts of alveolar septa with the grid lines,  $P_{\text{air}}$  counts the points of the grid lines hitting air spaces.

The lung tissue sections were assessed by quantifying mean linear chord length ( $L_m$ ) on 20 randomly selected regions per lung section.

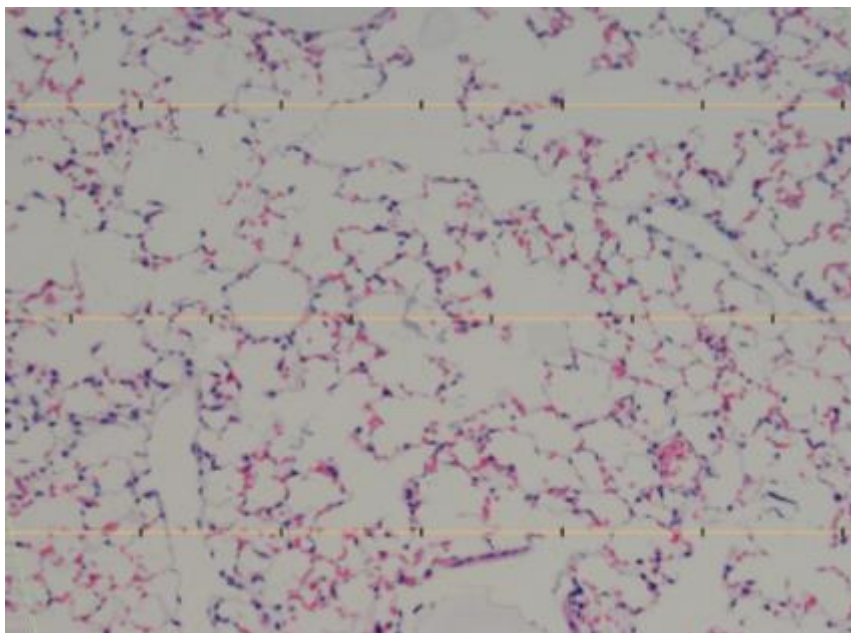


**Figure 8. Determination of mean linear intercept ( $L_m$ ) by using design-based stereology.** On each lung tissue section, a grid with points and lines was superimposed. Points (shown as black points on orange line segments) representing the alveolar air space volume ( $\Sigma P_{\text{air}}$ ) and the total number of intercepts of the line segments (orange lines) intercepting the alveolar septal surfaces ( $\Sigma I_{\text{septa}}$ ) were counted. This image is a screenshot of the CAST system during MCL measurement.

#### 4.5. Functional analysis of the lung

8- and 12-weeks old male mice were analyzed at the Institute of Lung Biology and Disease (ILBD) of the Helmholtz Centrum Munich, Germany as reported previously [65]. Mice were

anaesthetized using ketamine-xylazine (14% Ketamine / 3% xylazine) by intraperitoneal (i.p.) application at a dosage of 0.1 ml/10 g body weight. Once sedated, mice were tracheostomized using a 20-gauge cannula and connected to a FlexiVent system (Scireq, Montréal, Canada). Mice were ventilated with a tidal volume of 10 ml/kg at a frequency of 150 breaths/min to reach a mean lung volume similar to that of spontaneous breathing. Several lung parameters (Table 28) including compliance and resistance were examined using a software-generated script from the FinePointe Software (version 6, Data Sciences International). Measurements were repeated four times per animal.

**Table 28. Parameters measured by a pulmonary function test.**

Parameter	Abbreviation	Description
Dynamic compliance	$C_{dyn}$	Reflects the elasticity of the lung parenchyma
Lung resistance	R	Determines the level of obstruction in the lung
Elastance	E	Assesses the elastic rigidity of the lung
Tissue damping	G	Reflects the destructive properties of the lung
Tissue elastance	H	Mirrors the elastic properties of lung
Hysteresivity	$\eta$	Describes mechanical coupling between tissue damping (G) and tissue elastance (H), calculated as $\eta=G/H$

## 4.6. Collection of murine samples

### 4.6.1. Collection of serum and bronchoalveolar lavage (BAL)

8- and 12-weeks old mice were anaesthetized by isoflurane, euthanatized by cervical dislocation and blood samples were immediately collected by cardiac puncture technique using an 18-gauge needle and an Omnifix U-40 syringe. Blood samples were incubated at room temperature for 20 min and centrifuged 45 min at 2.000 rpm (Heraeus Pico 17 centrifuge) at RT. The obtained serum fractions were collected in a separate 1.5 ml tube, stored at  $-80^{\circ}\text{C}$ .

For collections of bronchoalveolar lavage (BAL), mice were anaesthetized as described above, and lungs were lavaged by using a 20-gauge needle and an Omnifix U-40 syringe with 3x500  $\mu$ l PBS supplemented with protease inhibitor cocktail tablets (Roche Diagnostics). BAL samples were centrifuged 20 min at 1.500 rpm (Heraeus Labofuge 400) at 4°C and supernatants were transferred to new tubes. In some experiments, BAL samples were concentrated by centrifugation using Amicon Ultra-0.5 centrifugal filters (Merck). Protein content in BAL samples were determined using a Bradford assay and an Eppendorf Biophotometer.

#### **4.7. Western blot analysis of bronchoalveolar lavage**

BAL samples were diluted with 2x Laemmli buffer (with 1%  $\beta$ -mercaptoethanol) followed by heating at 70°C for 10 min and subjected to a sodium dodecyl sulfate-polyacrylamide gel electrophoresis (SDS-PAGE) at +150 V in a Mini-PROTEAN Tetra Cell unit (Bio-rad) using TGS running buffer. 13% or 15% polyacrylamide gels (Rotiphorese gel 30, Carl Roth) were used. Separated proteins were transferred from the SDS-PAGE gel to a nitrocellulose membrane (GE Healthcare Life Sciences) in TGM buffer using a Mini-PROTEAN Tetra Cell transfer unit for ~12h at 150 mA. Next, the membrane was incubated in TBST buffer supplemented with 5% non-fat dry milk (Carl Roth) for 1 h at RT. Membranes were incubated for ~12h at 4°C with primary antibodies diluted in TBST with 5% BSA (Table 29).

Next, membranes were washed 3x in TBST and incubated for 1 h at RT with corresponding horseradish peroxidase (HPR) labelled second antibodies (Table 30) in TBST with 5% BSA. After washing with 3x TBST, the membranes were examined using the enhanced chemiluminescence (ECL) reagent and a Chemi-Doc imaging system (Bio-Rad).

**Table 29. Primary anti surfactant protein (SP) antibodies used for Western blot experiments.**

Name	Host / Specificity	Dilution	Supplier
Anti-SP-A	Rabbit polyclonal Ab, detects human and mouse surfactant Protein A	3 µg/ml	Merck Millipore, #AB3420-I
Anti-SP-B	Rabbit polyclonal Ab, detects human and mouse surfactant Protein B	1:1000	Merck Millipore, #AB3430
Anti-SP-C	Rabbit polyclonal Ab, recognizes human and mouse prosurfactant Protein C	1 µg/ml	Abcam, #ab90716
Anti-SP-D	Goat polyclonal Ab, detects human and mouse surfactant protein D	0.2 µg/ml	R&D Systems, # AF1920

**Table 30. Secondary antibodies used for Western blot experiments.**

Name	Host / Specificity	Dilution	Supplier
Anti-rabbit IgG HRP-linked (H+L chain)	Goat Ab against rabbit Ig-G	1:2000	Cell Signaling, # 7074
Anti-goat IgG HRP-linked (H+L chain)	Rabbit Ab against goat Ig-G	1:2000	R&D Systems, # HAF017

## 4.8. Immunohistochemistry of the tissue sections

8- and 12-weeks old male mice were euthanized by cervical dislocation. The organs to be examined were collected and transferred to 4% paraformaldehyde in PBS. After 2 h (at RT), the tissues were placed in PBS for 1 h (at RT). Finally, the tissues were incubated overnight in 18% sucrose for 24 h, embedded in ice-cold freezing tissue medium (Leica). 10-12  $\mu$ m tissue sections were prepared using a CM3050 S cryotome (Leica), placed on Superfrost Plus slides and stored at -80°C.

Immunohistochemical staining of the tissue sections was carried as reported previously. Tissue sections were washed in 2x PBS and incubated 1 h at RT in PBS containing 10% normal goat serum and 0.5% Triton X 100. Next, tissue sections were probed by various primary antibodies (Table 31) diluted in PBS with 10% goat serum and 0.5% Triton X 100 for 2 h at RT. Afterwards, tissue sections were washed 3x with PBS, incubated in the presence of the corresponding secondary antibody (Table 31) in the same buffer for 1 h at RT. Next, slides were washed 3x with PBS and covered with Mounting Medium (Dako Cytomation).

**Table 31. Antibodies used for the staining of lung tissue sections.**

Name	Dilution	Supplier
Anti-Prosurfactant Protein C	1:1000	Merck Millipore, #AB3786
Anti-ATP-binding cassette sub-family A member 3 (ABCa3)	1:300	Abcam, ab24751
Alexa Fluor 488 goat anti-rabbit IgG (H+L)	1:2000	Invitrogen, #A11008
Alexa Fluor 488 goat anti-mouse IgG (H+L)	1:400	Invitrogen, #A11029
Alexa Fluor 633 goat anti-rabbit IgG (H+L)	1:2000	Invitrogen, #A21071
Alexa Fluor 633 goat anti-mouse IgG (H+L)	1:400	Invitrogen, #A21050

Stained sections were examined using confocal laser-scanning microscopes Zeiss LSM 880 AxioObserver) driven by ZEN Version 3.1 software (WSI, Munich Germany) and Zeiss Axio Scan.Z1. (University of Homburg, Germany). All images were acquired at identical settings (Zeiss LSM 880: C-Apochromat 63x/1.2 W objective, 410–501 nm and 493–630 nm

filters; 488 nm, 405 nm and 633 nm laser excitation wavelengths and Zeiss Axio Scan.Z1: Plan-Apochromat 10x/0.45 M27, 353-465 nm and 650-673 nm filters; 405 nm and 673 nm laser excitation wavelengths).

In some experiments, Image J software was used to quantify the number of  $\tau$ GFP-positive AT2 cells in lung tissue sections cells in the randomly selected field.

## 4.9. Molecular biology and biochemical methods

### 4.9.1. RNA isolation and cDNA synthesis

Total RNA was extracted from lung tissues using TRI Reagent (Trizol, Sigma Aldrich). RNA content was determined by using a BioPhotometer (Eppendorf) spectrophotometer. Complementary DNA (cDNA) was synthesized by the RevertAid H Minus M-MuLV reverse transcriptase (Thermo Fisher Scientific). 1  $\mu$ g of total RNA was processed using a mix of 0.2  $\mu$ g random hexamer primers, 1 mM dNTPs in a reaction buffer containing 250 mM Tris-HCl pH 8.3, 250 mM KCl, 20 mM MgCl<sub>2</sub>, 50 mM DTT, 20 U RiboLock RNase inhibitor and 200 U RevertAid H Minus M-MuLV reverse transcriptase. The reverse-transcription reaction was performed for 5 min at 25°C, followed by 60 min incubation at 42°C and heat-termination for 5 min at 72°C.

### 4.9.2. Quantitative polymerase chain reaction (qPCR)

qPCR analysis was conducted using a Maxima Cyber green master mix (Thermo Fischer Scientific) (Table 32) and LightCycler 480 Multiwell Plates (Roche). The set of PCR primers is listed in Table 3. qPCR was performed using a LightCycler 480 (Roche) with conditions listed in Table 33. Expression levels of target genes were normalized to expression levels of the reference gene, *Hprt*. Analysis of the data was performed with the LightCycler 480 software. The relative mRNA expression levels were calculated using the  $2^{-\Delta\Delta C_t}$  approach.

**Table 32. Master mix for qPCR.**

Reagent	Volume
Template DNA	5 $\mu$ l
2x Absolute qPCR SYBR Green Mix	12.5 $\mu$ l
Primer forward	0.1 $\mu$ l
Primer reverse	0.1 $\mu$ l
Nuclease-free water	7.3 $\mu$ l

**Table 33. Settings used for qPCR.**

Phase	Temperature	Time	Number of cycles
Initialization step	95°C	15 min	1
Denaturation	95°C	15 min	40
Annealing	60°C	15 min	
Elongation	72°C	30 min	
Melting curve analysis	95°C	10 min	1
	60°C	1 min	
Cooling	40°C	continuous	1

#### 4.9.3. In-situ hybridization (ISH)

In-situ hybridization (ISH) was performed in collaboration with by Dr. David Simmons (University of Queensland, Australia) as reported earlier [36]. ISH *Trpm6* probes were produced by PCR using primers with T7 or T3 RNA polymerase sites recognition sites (Table 34). PCR products were gel-purified (Qiagen Gel Extraction Kit) and verified by DNA sequencing. Digoxigenin (DIG) labelled cRNA probes were synthesized using a 10x DIG RNA labelling kit (Roche) according to the manufacturer's instruction. Preparation of tissue sections

and ISH were performed as previously described [204]. Slides were imaged by an Aperio slide scanner and analyzed using the Image Scope software.

**Table 34. cDNA templates Sequence of primers used to generate ISH *Trpm6* probes.**

Name	Sequence
Probe1 forward	5'-aattaaccctcactaaagggGAGAGGAGGCCACAGTCAAG-3'
Probe1 reverse	5'-taatacgactcactatagggGCTCAAAGACGATGTCACGA-3'
Probe2 forward	5'-aattaaccctcactaaagggCCTGTCAAAGAAGAAGAGGAA-3'
Probe2 reverse	5'-taatacgactcactatagggAGAAAAGACTTCACAATG-3'

#### **4.10. Isolation and culture of primary AT2 cells and cell culture of A549 cell line**

Alveolar epithelial type 2 (AT2) cells were isolated from mouse lungs by intratracheal instillation of dispase and agarose as reported earlier [205].

Mice were tracheotomized and cannulated with a 20-gauge intravenous intubation cannula. To remove blood from the respiratory vessels and immune cells from the alveolar space, inferior vena cava and aorta near the kidneys were cut followed by perfusion of the lungs with 20 ml of 0.9 % NaCl via endobronchial lavage. Next, the lung was inflated with 1.5 ml of dispase solution (BD Biosciences). Without allowing the lungs to completely deflate, warmed low-melting-point agarose solution (1%) was quickly instilled into the trachea (0.3 mL). The trachea was removed at the hilus and the lung was incubated in 5 ml of dispase solution for 45 min at RT. The lung was separated into the lobes and treated by DNase (0.001%) containing DMEM medium. The tissue slurry was passed through sequential nylon meshes (100  $\mu$ m, 20  $\mu$ m, and 10  $\mu$ m) and the filtrate was centrifuged. The cell pellet was resuspended in minus medium (Table 9) and poured on antibody-treated (anti-CD45 and anti-CD16/32, BD biosciences) Petri dishes for 30 min at 37°C and 5% CO<sub>2</sub>. Nonadherent cells were collected, resuspended in the plus medium (Table 9) and placed in a fresh Petri dish for 30 min for negative selection of fibroblasts. Nonadherent AT2 cells were gently collected and centrifuged for 10 min at 1.340

rpm (Heraeus Biofuge Stratos centrifuge) at 15°C. The resulting cell pellet was resuspended in DMEM with 10% FBS, 100 µg/ml streptomycin, 100 U/ml penicillin. 24 h after isolation, the cell culture medium was exchanged.

Human adenocarcinoma A549 cells were cultured in Ham's F-12K (Kaighn's) Medium (F12K Nut Mix) supplemented with 10% FBS, 100 µg/ml streptomycin, 100 U/ml penicillin.

#### 4.11. Staining of cultured cells

Primary isolated AT2 cells were seeded on glass coverslips, fixed with 3.7% PFA in PBS. After washing 2x with PBS, cells were permeabilized using 0.5% Triton X-100 in PBS, blocked for 1 h at RT in PBS containing 4% normal goat serum and 4% BSA. The cells were incubated with primary antibodies (Table 35) diluted in PBS with 2% BSA for 2 h at RT and washed 6x with PBS containing 0.1% BSA. Next, cells were incubated in the presence of 1 µg/ml of the secondary antibodies (Table 35) for 1 h. After washing 3x with PBS containing 0.1% BSA, cells were incubated 10 min in Hoechst staining solution, washed 6x with PBS and covered with Mounting Medium (Dako Cytomation).

**Table 35. Antibodies and dyes used for IF staining of cells.**

Name	Type	Dilution	Supplier
Anti-ATP-binding cassette sub-family A member 3 (ABCa3)	Primary antibody	1:300	Abcam, # ab24751
Alexa Fluor 488 goat anti-mouse IgG (H+L)	Secondary antibody	1:400	Invitrogen, # A11029
Alexa Fluor 633 goat anti-mouse IgG (H+L)	Secondary antibody	1:400	Invitrogen, # A21050
Bodipy FL-ATP	Dye	1:500	Thermo Fisher Scientific, # A12410
LysoTracker Red	Dye	1:100	Invitrogen, # L7528
Quinacrine	Dye	1:50	Sigma-Aldrich, # Q3251

Cells from the A549 cell line and primary AT2 cells were stained by LysoTracker-Red (Invitrogen), Bodipy FL-ATP (Thermo Fisher Scientific) and Quinacrine (Sigma-Aldrich) according to manufacturer's instructions. The stained cells were examined on a confocal laser-scanning microscope LSM 880 (Zeiss) (C-Apochromat 63x/1.2 W objective, 410–501 nm and 493–630 nm filters; 488 nm and 633 nm laser excitation wavelengths). Obtained images were further processed using ZEN software.

#### **4.12. EM (Electron Microscopy) analysis of cells and lung tissue sections**

EM imaging of fixed cells and tissue sections was performed in collaboration with Prof. Gabriela Krasteva-Christ (Homburg University, Germany). 12-weeks old male mice were examined at the University of Homburg, Germany, as reported previously [206].

The animals were exsanguinated by cutting the caudal vena cava. A small cannula was inserted in the sublaryngeal part and fixed with a ligature. The fixative solution containing 1.5% of paraformaldehyde and 1.5% of glutaraldehyde in 0.15 M phosphate buffer was applied via the cannula by gravity. Afterwards, the lung was post-fixed over-night at RT. Next, the tissue was washed 5x in 0.1 M sodium cacodylate buffer (pH 7.35) for 5 min and incubated in 1% osmium tetroxide in 0.1 M sodium cacodylate buffer for 2 h at RT. The lung was rinsed 5x for 5 min with 0.1 M sodium cacodylate buffer followed by 2x for 5 min in ddH<sub>2</sub>O.

Finally, samples were stained en bloc over night at 4° C with half-saturated uranyl acetate. After an additional washing step (5 x for 5 min) dehydration was conducted using ascending ethanol series (30%, 50%, 70%, 90%, 96%, 2x 100%) followed by incubation with 100% ethanol for 15 min at RT. Samples were then incubated in propylene oxide followed by embedding in Epon (Serva, Heidelberg, Germany). Ultrathin sections (60 nm) (Ultracut-Schneidegerät E; Reichert-Jung, Nußloch) were counterstained with uranyl acetate (Serva, Heidelberg) and lead citrate (agar scientific, Stansted Essex). Transmission electron microscopy was performed using a LEO912 AB microscope (Zeiss, Oberkochen, Germany) including a digital camera (TRS, Tröndle, Munich, Germany).

Primary AT2 cells were isolated as reported in Section 4.10, placed on square glass coverslips (Roth, 20x20 mm) in 3 cm dishes directly on the day 0 and cultured for 12h. Afterwards, cells were fixed overnight at 4°C using 2.5% glutaraldehyde and 2% PFA in PBS. The next day,

cells were washed with PBS and maintained in PBS in 50 ml plastic tubes (Falcon) prior to EM analysis as described above.

#### **4.13. Determination of elementary Mg, Ca and Zn using inductively coupled plasma mass spectrometry (ICP-MS) and atomic absorption spectroscopy (AAS)**

Elementary Mg, Ca and Zn levels in serum and lavage samples were analyzed by inductively coupled plasma mass spectrometry (ICP-MS) performed at ALS Scandinavia (Sweden) as reported earlier [36].

In some experiments, the elemental analysis was performed using a Perkin Elmer PinAAcle 500 atomic absorption spectrophotometer and the Syngistik Touch Software. The spectrophotometer was calibrated using several standard concentrations of Ca<sup>2+</sup>, Mg<sup>2+</sup> and Zn<sup>2+</sup> ions prepared by serial dilutions of corresponding stock solutions.

The volume of alveolar lining fluid (ALF) recovered from BAL was estimated by measuring urea levels in the BAL and the serum [94]. Urea contents of plasma and lavage samples were determined by the Urea assay kit (Sigma MAK006) according to the manufacturer's instructions. The amount of Urea present in the sample is determined from the standard curve using the following formula:

$$C_s = S_a / S_v$$

where  $S_a$  = amount of urea in the sample (nmole) from standard curve,  $S_v$  = sample volume (ml) added into the wells,  $C$  = concentration of urea in sample (ng/ $\mu$ l)

With the amount of urea in the BAL and serum samples and recovered volume of BAL, actual volume of ALF is calculated:

$$[u]_{BAL} = S_{a(BAL)} * V_{(BAL)}$$

$$V_{ALF} = [u]_{BAL} / S_{a(serum)}$$

where  $[u]_{BAL}$  = the total amount of urea in the BAL (mg),  $S_{a(BAL)}$  = amount of urea in BAL (mg/l),  $V_{(BAL)}$  = volume of recovered BAL (ml),  $V_{ALF}$  = actual volume of ALF ( $\mu$ l),  $S_{a(serum)}$  = amount of urea in serum (mg/l).

#### **4.14. Statistical analysis**

Statistical evaluation of the data was performed by the GraphPad Prism Version 8.3.1 and Excel 2016 software (Microsoft). Unless otherwise specified, data are shown as mean values (MW)  $\pm$  standard error of the mean values (SEM). The two-sided student t-test was used to test for significant differences and compare two groups. A One-way ANOVA test was used for studies with more than two groups. P-values  $\leq 0.05$  (marked with \*), 0.01 (\*\*), 0.001 (\*\*\*) and 0.0001 (\*\*\*\*) were considered to be significantly different.

## 5. Results

### 5.1. Expression pattern of *Trpm6* in the mouse lung

In a pioneering study, Northern blot-based examination of multiple tissues revealed that *Trpm6* mRNA is highly expressed in the kidney, intestine and testis and modestly expressed in the lung [21]. While the role of TRPM6 in the kidney and intestine is relatively well studied [36], a functional role of *Trpm6* in the respiratory system remained unknown. Therefore, we attempted to use a set of our previously generated TRPM6-specific antibodies [36] in order to elucidate the expression pattern of TRPM6 in the mouse lung tissues. However, our systematic efforts to detect TRPM6 immuno-reactivity were unsuccessful, presumably because of the low expression levels of TRPM6 protein. Therefore, we relied on an alternative approach. In collaboration with Prof. Ulrich Böhm (University of Saarland, Germany), we generated a new mouse strain carrying a *Trpm6*<sup>Cre</sup> allele (Method section 4.1.3) for visualization of TRPM6 expressing cells because the stop-codon in the open reading frame of *Trpm6* was replaced by an internal ribosome entry site (IRES) followed by the coding sequence for the Cre recombinase (*Cre*). IRES enables translation of the WT TRPM6 and Cre proteins from such bicistronic mRNA. Next, we crossed *Trpm6*<sup>Cre/Cre</sup> animals with transgenic mice containing a *floxed-stop-τGFP* sequence in the *Rosa26* locus (*Rosa26*<sup>τGFP</sup> mice). Importantly, τGFP protein is not expressed from the *Rosa26* *floxed-stop-τGFP* locus in the absence of Cre. However, expression of Cre from *Trpm6*<sup>Cre</sup> will delete the Stop-codon from *Rosa26*<sup>τGFP</sup> and trigger expression of τGFP protein specifically in cells expressing TRPM6. Consequently, imaging of τGFP-positive cell in tissue sections will likely reflect the presence of TRPM6 mRNA.

In order to investigate the expression of *Trpm6* in the lung, we used immunofluorescence staining of cryosections of the lungs from *Trpm6*<sup>Cre/+</sup>; *Rosa26*<sup>τGFP/+</sup> mice (Figure 9). We observed that τGFP was explicitly present in the layer of bronchial epithelial cells and presumably in AT2 cells of the parenchyma. In contrast, τGFP was not detectable in tissue sections of *Rosa26*<sup>τGFP</sup> mice (Figure 10).

To verify these results, we stained tissue sections from *Trpm6*<sup>Cre/+</sup>; *Rosa26*<sup>τGFP/+</sup> and control (*Rosa26*<sup>+/+</sup>) mice with anti-ABCa3/anti-mouse antibodies labelled with the fluorescent marker AlexaFluor633. Of note, ATP-binding cassette sub family A member 3 (ABCa3) protein is enriched in AT2 cells, expressed on plasma membrane of lamellar bodies and broadly used as a marker of AT2 cells [207-209]. We found that τGFP was present in epithelial cells of

bronchi and a subset of cells in the parenchyma, which were also positive for ABCa3 (Figure 10). However,  $\tau$ GFP was not detectable in tissues of control mice. To quantify these results, we examined 45 randomly selected regions in two tissue sections from two independent *Trpm6*<sup>Cre/+</sup>; *Rosa26* <sup>$\tau$ GFP/+</sup> mice. We observed that all 338  $\tau$ GFP-positive cells in parenchyma also expressed ABCa3 (100% co-localization) (Figure 10). We also found that among 383 ABCa3-positive cells, 338 cells (88%) also harboured a  $\tau$ GFP signal. These results suggest that in the lung parenchyma TRPM6 is expressed explicitly in AT2 cells.

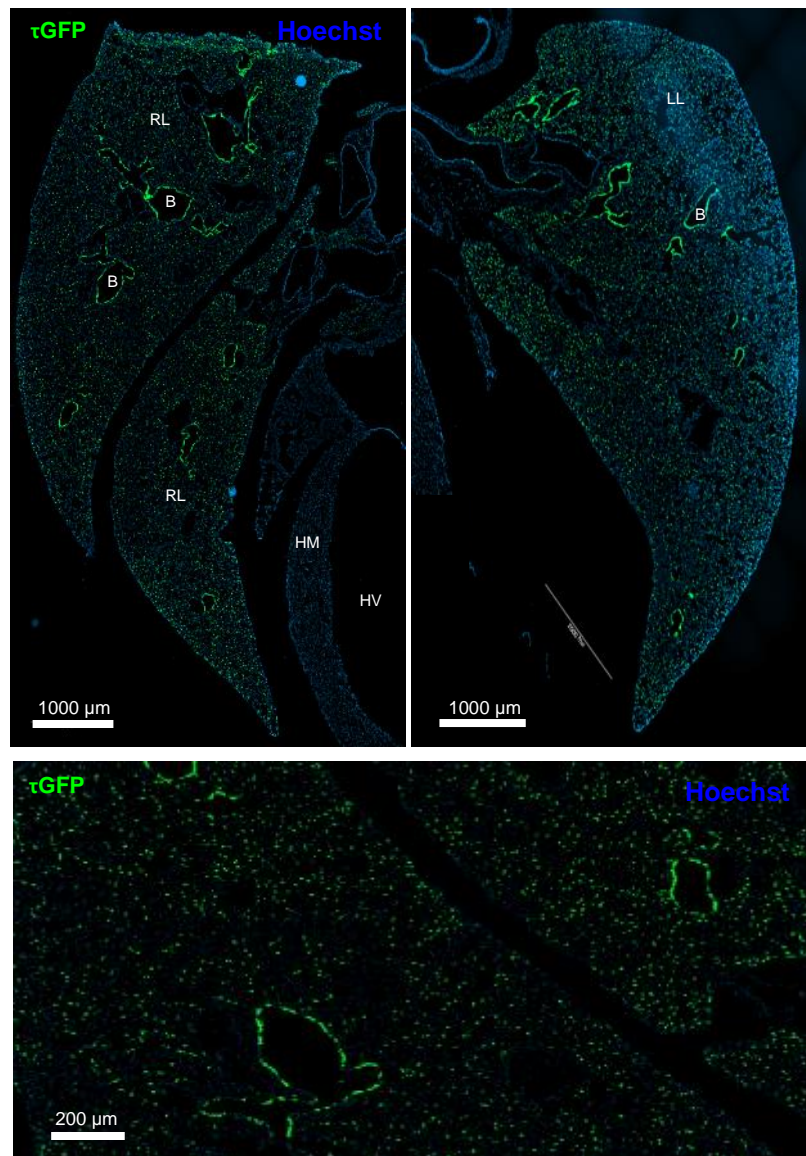


**Figure 9. Expression of  $\tau$ GFP in the lung of *Trpm6*<sup>Cre/+</sup>; *Rosa26* <sup>$\tau$ GFP/+</sup> mouse lungs.**  $\tau$ GFP (green) and Hoechst (blue) signals were imaged in tissue cryosections of 8-weeks old *Trpm6*<sup>Cre/+</sup>; *Rosa26* <sup>$\tau$ GFP/+</sup> mice. Representative results are shown from examinations of two sections from two mice. The magnified image from alveolar region is shown in the lower panel. RL= right lung, LL= left lung, HM = heart muscle, HV = heart ventricle, B = bronchiole.

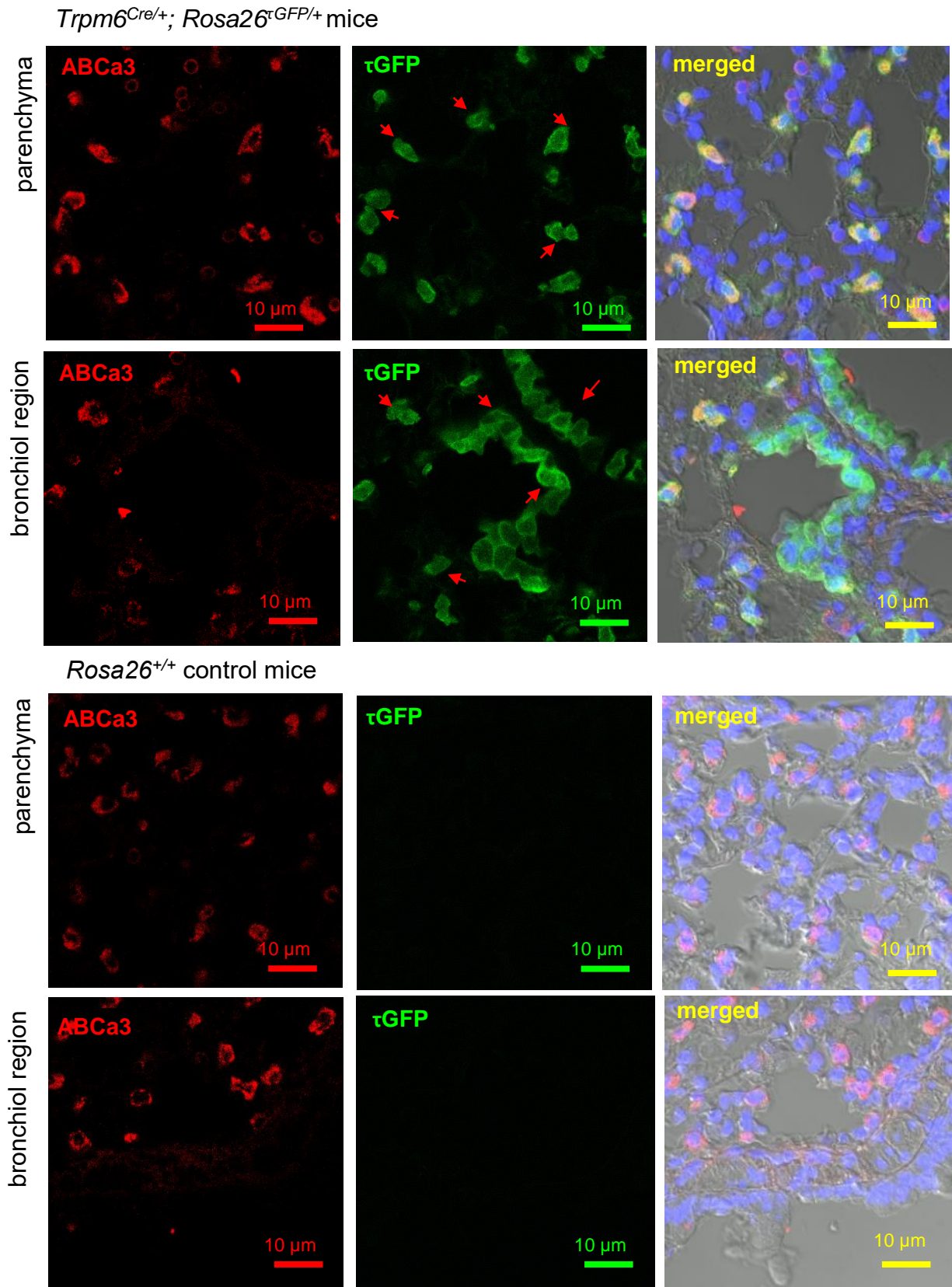


**Figure 10. Co-localization of  $\tau$ GFP and ABCa3 in lung tissue sections of *Trpm6<sup>Cre/+</sup>; Rosa26<sup>τGFP/+</sup>* mice.** Tissue cryosections were obtained from 8-weeks old *Trpm6<sup>Cre/+</sup>; Rosa26<sup>τGFP/+</sup>* and *Rosa26<sup>+/+</sup>* mice. Signals from ABCa3 antibodies labelled with the fluorescent marker AlexaFluor633 (red),  $\tau$ GFP (green), and Hoechst dye (blue) were merged to DIC images.

Since the expression of  $\tau$ GFP can potentially reflect the 'historical' expression of *Trpm6* in respiratory cells rather than the actual presence of *Trpm6* mRNA [203], we re-examined lung tissue sections from control mice using an *in situ* hybridization (ISH) approach [36]. As expected, an antisense *Trpm6* probe labelled a population of parenchyma cells resembling AT2 cells and bronchial epithelial cells (Figure 11). In contrast, a sense probe showed no staining of tissue sections, reinforcing the notion that *Trpm6* expression is restricted to AT2 cells and bronchial epithelial cells.

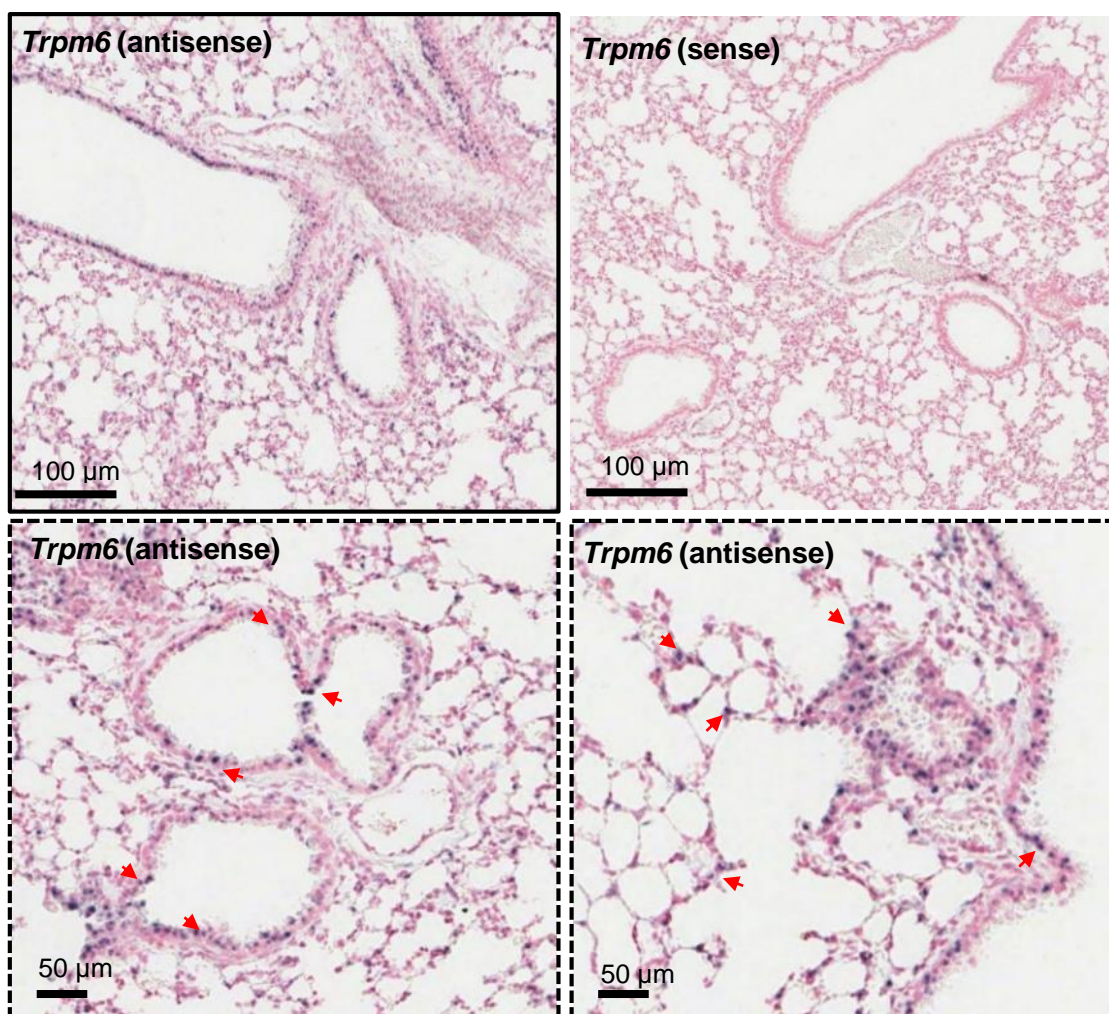


**Figure 11. In situ hybridization (ISH) of *Trpm6*<sup>fl/+</sup> (Control) lungs with *Trpm6* sense and antisense probes.** Expression of *Trpm6* mRNA was examined on serial paraffin sections obtained from 8-weeks old *Trpm6*<sup>fl/+</sup> (Control) mice using antisense (left) and sense (right) probes for *Trpm6*. Expression of *Trpm6* was detected presumably in AT2 cells of the parenchyma and bronchial epithelial cells (indicated by red arrows in the magnified images, lower panels). The dotted squares indicate the magnified images of *Trpm6* antisense probes. Representative images are shown from sections obtained from two mice.

## 5.2. Morphological and functional alterations in the lung of *Trpm6*-deficient mice

Previously, our group developed a new genetic approach to produce *Trpm6*-deficient (*Trpm6*<sup>Δ17/Δ17</sup>;*Sox2-Cre*) adult mice, which do not express functional TRPM6 channels (Methods section 4.1.1, [36]). Among other changes, these *Trpm6*-deficient mice displayed morphological alterations in many internal organs, including the lung. In the present study, we thought to use this genetic animal model to investigate the role of TRPM6 in the respiratory system. First, we studied whether *Sox2-cre* driven deletion of exon 17 in the *Trpm6* locus was achieved in the lung using qPCR approach. We extracted RNA from whole lungs of control and *Trpm6*-deficient littermates and examined relative levels of *Trpm6* mRNA using qRT-PCR. As expected, we found that mRNA of *Trpm6* was almost not detectable in the lung of *Trpm6*-deficient mice (Figure 12).

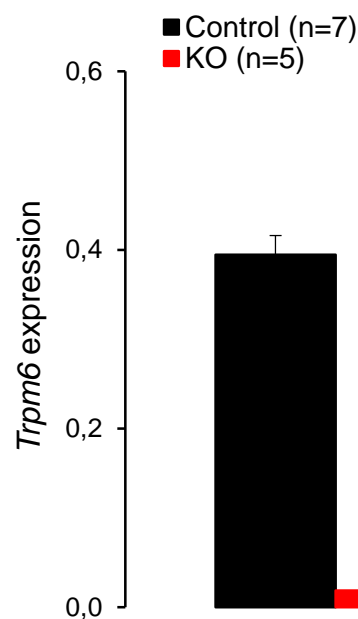


**Figure 12.** Relative *Trpm6* mRNA levels in whole lungs of *Trpm6*<sup>fl/+</sup> (Control) and *Trpm6*<sup>Δ17/Δ17</sup>;*Sox2-Cre* (KO) mice analyzed by qRT-PCR. HPRT was used as a reference transcript. Values are shown as mean ± SEM; \*\*\*\* - P≤0.0001 (Student's t-test); n - number of mice.

Next, we asked whether *Trpm6*-deficient adult mice develop morphological changes in lung tissues. HE staining of lung tissue sections of 4-weeks old *Trpm6*-deficient mice did not reveal remarkable histological alterations compared to control littermates. However, the tissues from 8- and 12-weeks old mice displayed significant airspace enlargements as compared to control littermates (Figure 13). Subsequently, we conducted quantitative morphometry to determine mean chord lengths ( $L_m$ ) in lung sections.  $L_m$  values were not different in tissues from 4-weeks old control and *Trpm6*-deficient mice. In contrast,  $L_m$  values were gradually increased in 8- and 12-weeks old *Trpm6*-deficient mice (Figure 14).

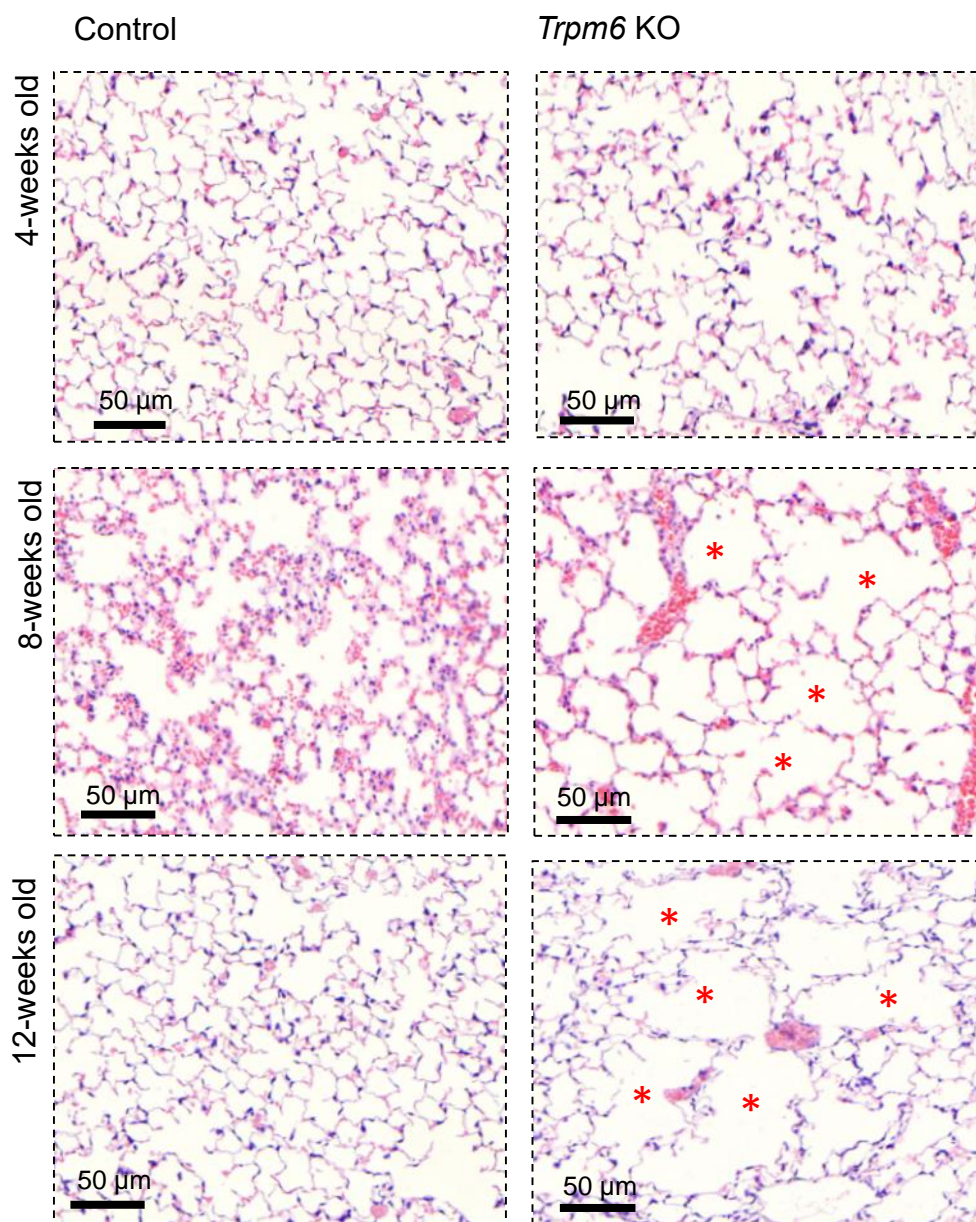


**Figure 13. Histological examination of lungs of *Trpm6*<sup>fl/+</sup> (Control) and *Trpm6*<sup>Δ17/Δ17</sup>; *Sox2-Cre* (KO) mice.** Hematoxylin and eosin (H&E) staining of paraffin-embedded lung tissue sections from 4-, 8- and 12-weeks old control (Control) and *Trpm6*-deficient (KO) littermates (n=6-12 mice per genotype).

Hence, we concluded that weaned *Trpm6*-deficient mice develop enlargement of alveolar air spaces in the lung parenchyma. We noted that such results resemble histological alterations of emphysema in lungs of human patients and mouse models of emphysema [65, 210-212].

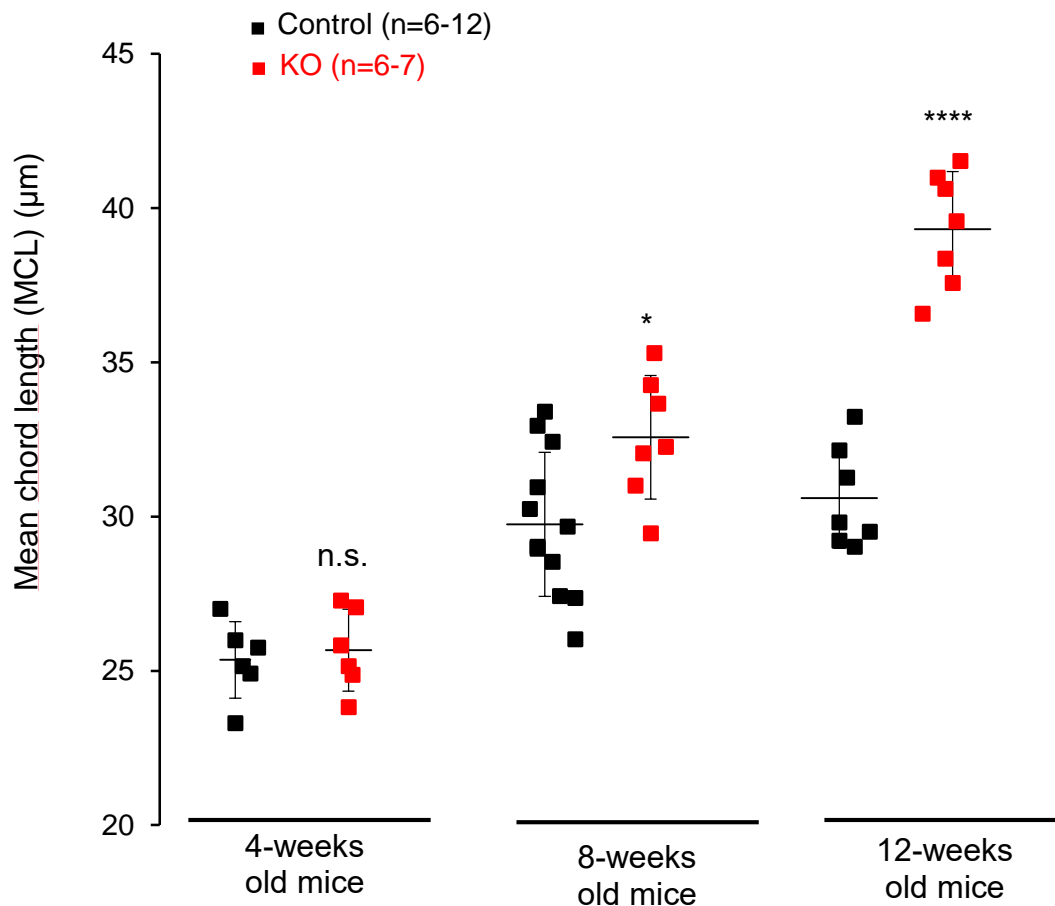


**Figure 14. Mean chord length analysis of morphological lung sections of 4-, 8- and 12-weeks old *Trpm6*<sup>fl/+</sup> (Control) and *Trpm6*<sup>Δ17/Δ17</sup>;*Sox2-Cre* (KO) mice.** The results are shown as mean ± SEM; \*\*\*\* -  $P \leq 0.0001$ , \* -  $P \leq 0.05$ , n.s. - not significantly different (Student's t-test); n - number of mice.

Respiratory emphysema is primarily defined by a declined ability of the lung for gas exchange [213]. To investigate whether enlarged airspace in the tissues of *Trpm6*-deficient mice is associated with a reduced pulmonary function, we used the FlexiVent system to examine airway resistance and compliance in living 8- and 12-weeks old mice. In line with our histological experiments, we observed that 8-weeks old *Trpm6*-deficient mice had an increased airway compliance and resistance as compared to control littermates and that such

phenotype was more pronounced in 12-weeks old mice (Figure 15). Both parameters are similarly affected in human subjects with emphysema [214] as well as in the corresponding mouse models of this disease [65, 213], reinforcing the notion that *Trpm6*-deficient mice developed respiratory emphysema.

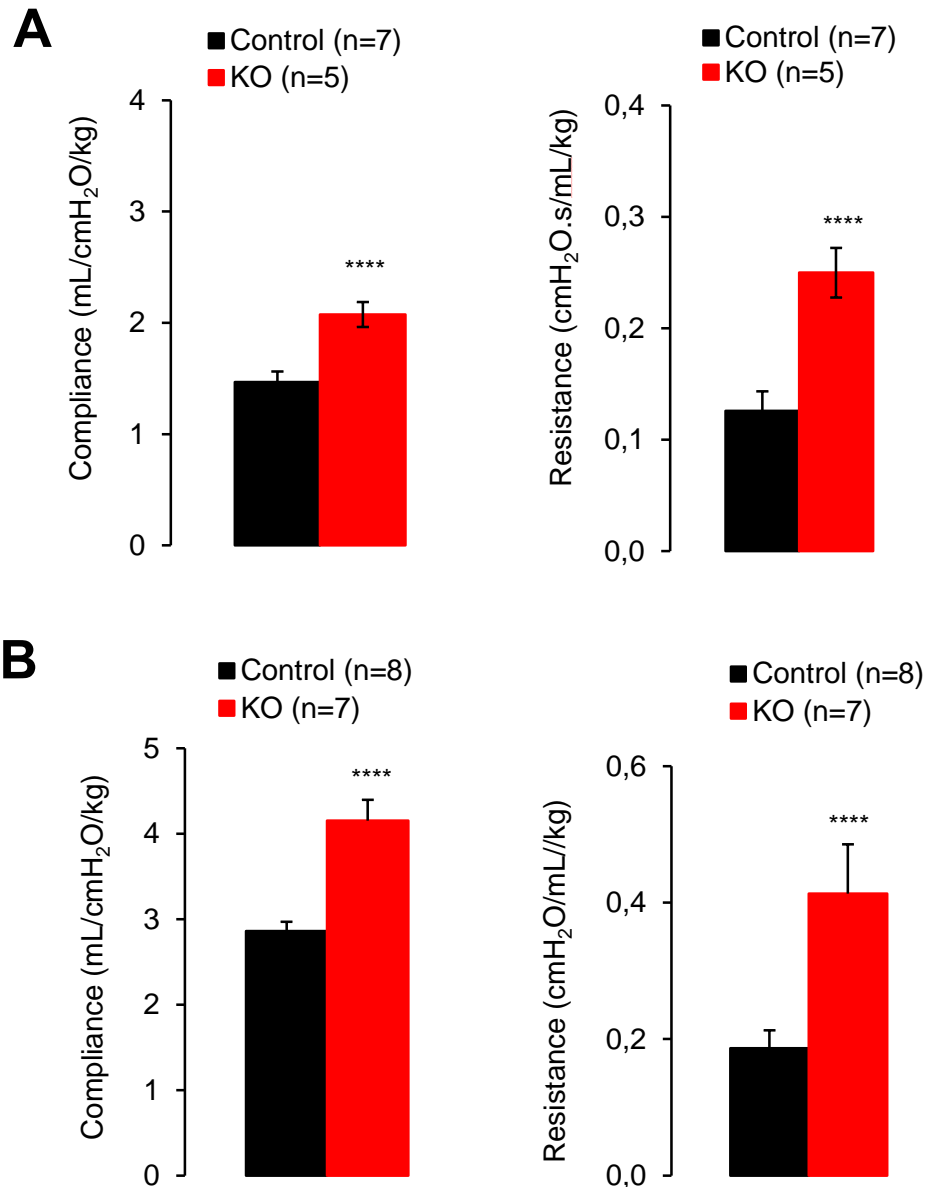


**Figure 15. Lung function parameters performed with *Trpm6*<sup>fl/+</sup> (Control) and *Trpm6*<sup>A17Δ17</sup>;*Sox2-Cre* (KO) mice.** Compliance (C) and resistance (R) of (A) 8-weeks old and (B) 12-weeks old *Trpm6*<sup>fl/+</sup> (Control) and *Trpm6*<sup>A17Δ17</sup>;*Sox2-Cre* (KO) mice were measured using FlexiVent system. Values are shown as mean ± SEM; \*\*\*\* - P≤0.0001 (Student's t-test); n - number of mice.

### 5.3. Effect of Mg<sup>2+</sup> supplementation on the respiratory phenotype of *Trpm6*-deficient mice

Previously our group has shown that TRPM6 channels control uptake of Mg<sup>2+</sup> in epithelial cells of the intestine and that genetic ablation of this mechanism can be compensated by dietary Mg<sup>2+</sup> supplementation [36]. Therefore, we asked whether dietary Mg<sup>2+</sup> supplementation can ameliorate the respiratory phenotype of *Trpm6*-deficient mice.

To this end, we maintained 4-weeks old offspring on a chow with 0.50% Mg<sup>2+</sup> (versus 0.22% in the normal diet) and compared the morphological and functional characteristics of the lung of 8- and 12-weeks old control and *Trpm6*-deficient littermates. Remarkably, none of the *Trpm6*-deficient mice displayed histological (Figures 16-17) or functional (Figure 18) signs of emphysema. These findings suggest that Mg<sup>2+</sup> supplementation was beneficial for maintaining lung morphology (Figures 16-17), suggesting that respiratory deficiency of *Trpm6*-deficient mice was triggered by Mg<sup>2+</sup> deficiency.

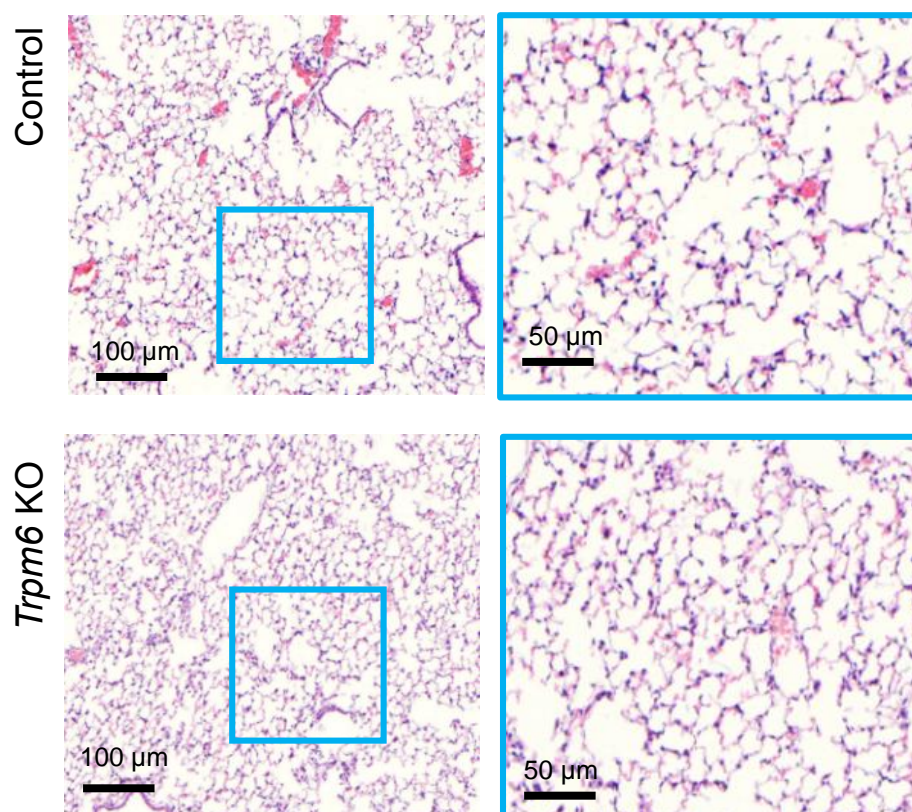


**Figure 16.** Histological examination of lungs from *Trpm6*<sup>fl/+</sup> (Control) and *Trpm6*<sup>Δ17/Δ17</sup>; *Sox2-Cre* (KO) mice fed with a high Mg<sup>2+</sup> diet. Representative images of hematoxylin and eosin (H&E) staining of paraffin-embedded lung tissue sections of 8-weeks old *Trpm6*<sup>fl/+</sup> (Control) and *Trpm6*<sup>Δ17/Δ17</sup>; *Sox2-Cre* (KO) littermates (n=7-9). The blue squares indicate the magnified images acquired from each tissue.

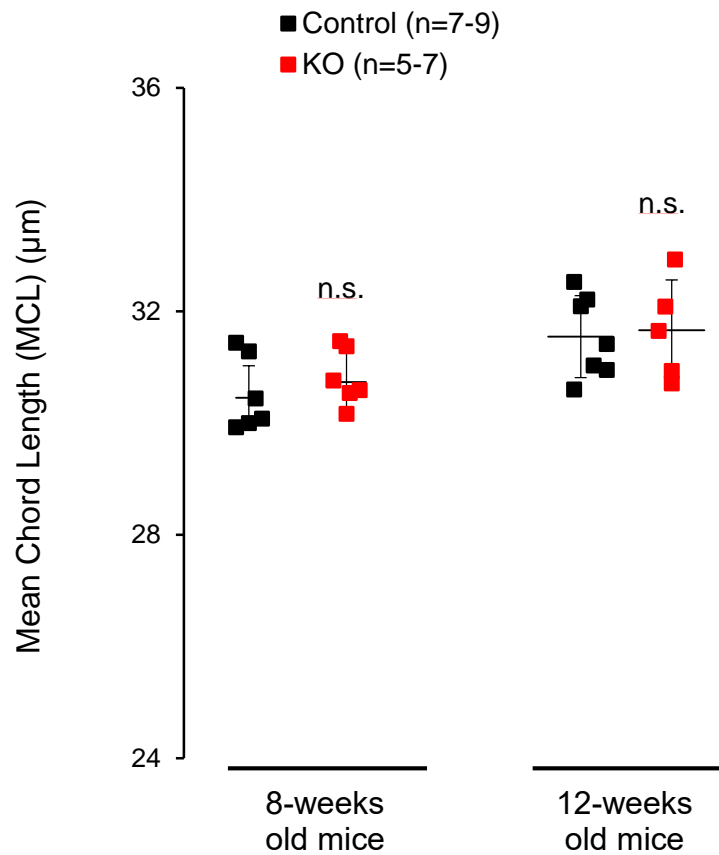


**Figure 17. Mean chord length analysis of morphological lung sections of *Trpm6*<sup>f/+</sup> (Control) and *Trpm6*<sup>Δ17/Δ17</sup>; *Sox2-Cre* (KO) mice fed with a high Mg<sup>2+</sup> diet.** H&E stained lung sections of 8- and 12-weeks old mice were assessed by quantitative morphometry method. The results are shown as mean ± SEM; n.s. - not significantly different (Student's t-test); n - number of mice.

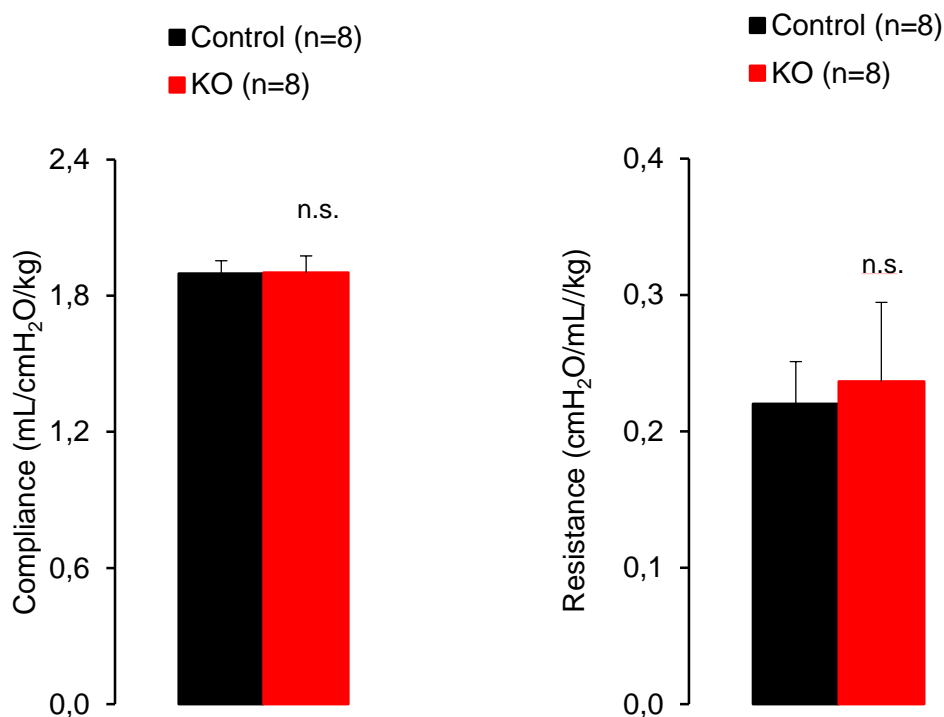


**Figure 18.** Lung function parameters performed with *Trpm6*<sup>fl/+</sup> (Control) and *Trpm6*<sup>Δ17/Δ17</sup>;*Sox2-Cre* (KO) mice fed with a high Mg<sup>2+</sup> diet. Compliance (C) and resistance (R) of 12-weeks old *Trpm6*<sup>fl/+</sup> (Control) and *Trpm6*<sup>Δ17/Δ17</sup>;*Sox2-Cre* (KO) mice fed with a high Mg<sup>2+</sup> diet were measured using FlexiVent system. Values are shown as mean ± SEM; n.s. - not significantly different (Student's t-test); n - number of mice.

#### 5.4. Electron microscopy (EM) assessment of the lung tissues from *Trpm6*-deficient mice

To get mechanistic insights on the respiratory phenotype of *Trpm6*-deficient mice, we performed EM of the lung tissue sections obtained from 12-weeks old control and *Trpm6*-deficient mice (Figure 19). We observed tubular myelin (TM) in the alveolar air space in the control tissues (Figure 19). However, the content of TM in alveolar spaces of *Trpm6*-deficient mice was significantly reduced (Figure 19). Furthermore, we detected extensive accumulation of lamellar bodies (LB) in AT2 cells in samples from *Trpm6*-deficient mice, suggesting that exocytosis of lung surfactants was affected (Figure 19).

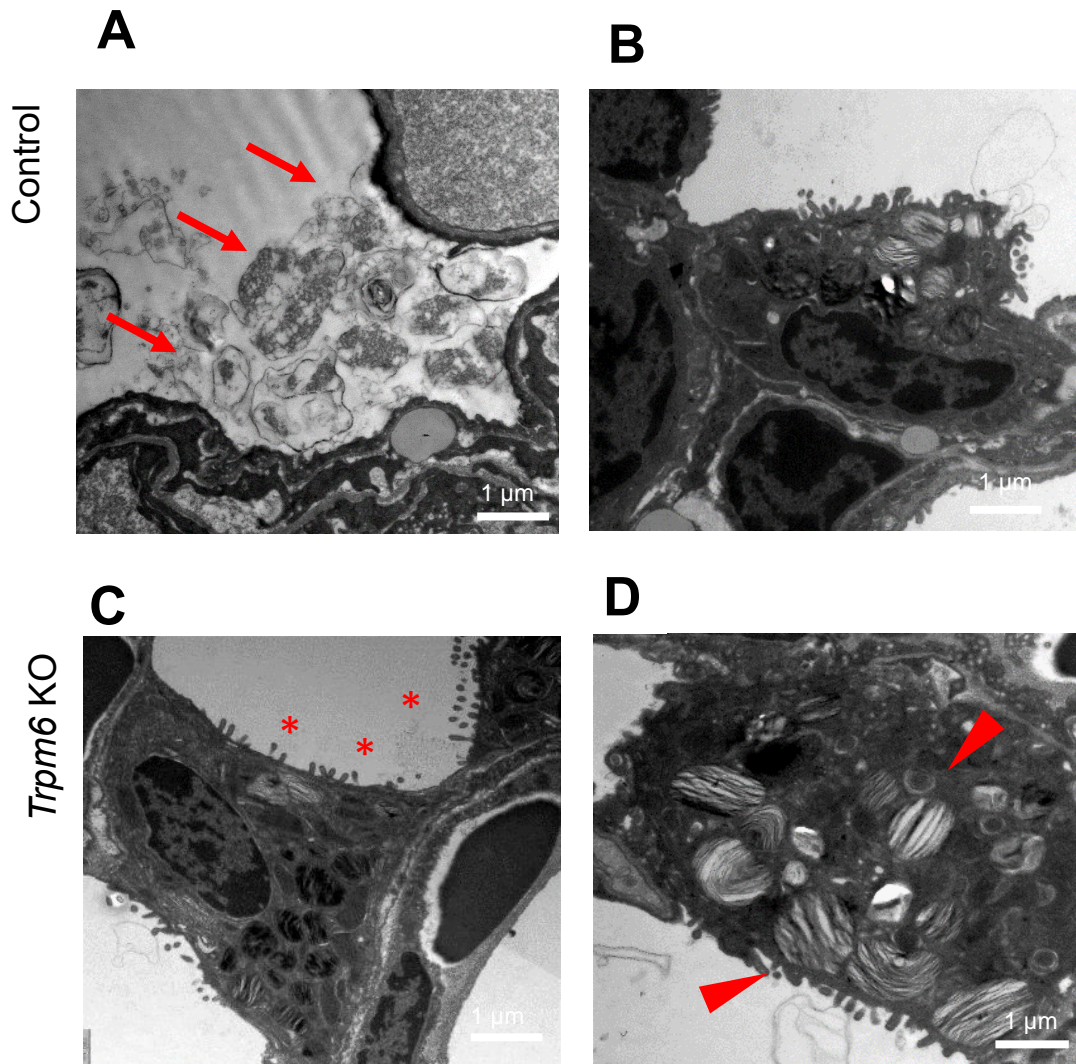


**Figure 19. Electron microscopic (EM) analysis of alveolar regions from lungs of *Trpm6<sup>fl/+</sup>* (Control) and *Trpm6<sup>A17/Δ17</sup>; Sox2-Cre* (KO) mice.** Lung tissues from adult 12-weeks old adult *Trpm6<sup>fl/+</sup>* (Control) (A, B) and *Trpm6<sup>A17/Δ17</sup>; Sox2-Cre* (KO) (C, D) mice were examined (n=3 mice per genotype). Red arrows in (A) point to tubular myelin abundantly present in the tissue of control mice. Stars in the tissue of *Trpm6<sup>A17/Δ17</sup>; Sox2-Cre* (KO) mice (C) indicate the alveolar airspace deficient in tubular myelin. Triangles in (D) indicate the accumulation of LBs. Representative images are shown.

## 5.5. Assessment of surfactant proteins in bronchoalveolar lavage (BAL) of *Trpm6*-deficient mice

Our previous results indicate that *Trpm6* is expressed in AT2 cells and that production of respiratory surfactants is likely abnormal in the tissues of *Trpm6*-deficient mice. To verify these findings, we collected bronchoalveolar lavage (BAL) from 12-weeks old control and *Trpm6*-deficient littermates maintained on the regular or Mg<sup>2+</sup>- rich diets and determined the levels of surfactant proteins (SPs) using Western-blot and a set of antibodies specific for SP-A, SP-B, SP-C and SP-D. We found that the content of all isoforms of surfactant proteins were very low in BAL obtained from *Trpm6*-deficient mice maintained on the regular diet. Strikingly, the levels of SP-A, SP-B, SP-C and SP-D were fully normalized in lungs of the group of Mg<sup>2+</sup> supplemented *Trpm6*-deficient mice (Figures 20-22), indicating that the abnormal contents of respiratory surfactant in the alveolar air space of *Trpm6*-deficient mice was triggered by Mg<sup>2+</sup> deficiency.

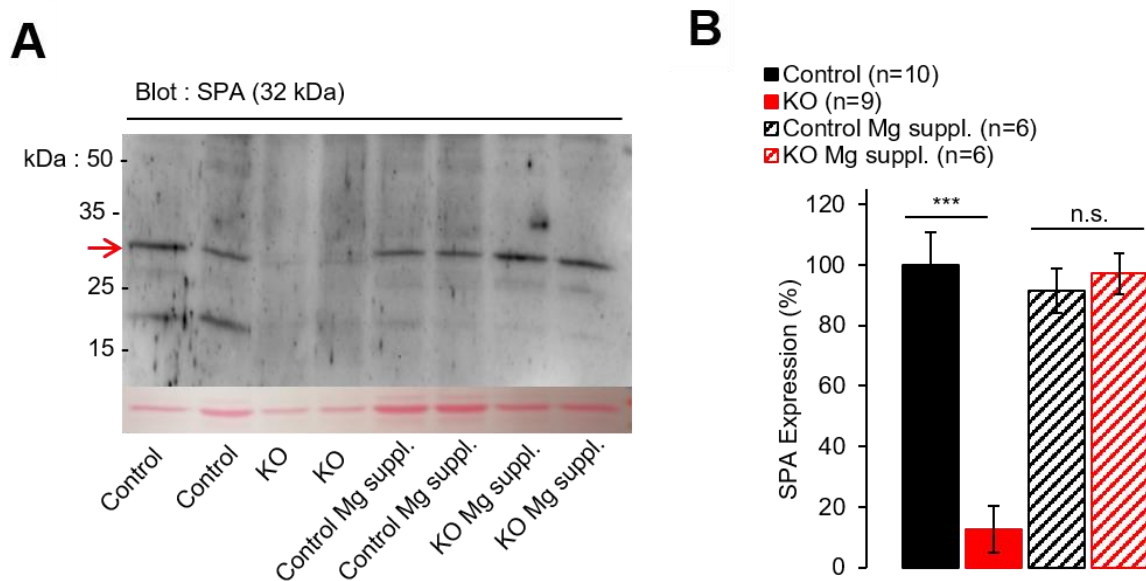


**Figure 20. Surfactant protein A (SP-A) levels in bronchoalveolar alveolar lavage (BAL) of *Trpm6*<sup>fl/+</sup> (Control) and *Trpm6*<sup>Δ17/Δ17</sup>; *Sox2-Cre* (KO) mice.** (A) BAL samples were collected from 12-weeks old mice and analyzed by Western blot using the anti-SP-A antibody. Upper panel: Representative Western blot is shown for BAL samples isolated from the mice maintained on the regular or Mg<sup>2+</sup>- supplemented diets (n = 2 mice per genotype). Red arrows indicate the position of the expected SP-A band (~32 kDa). Lower panel: Ponceau Red staining of the blot was used to control protein loading. (B) Quantification of SP-A levels in Western blots illustrated in (A). SP-A signal in BAL samples from the control mice maintained on the regular diet was estimated as 100%. Values are shown as mean ± SEM; \*\*\* - P≤0.001, n.s. – not significantly different (Student's t-test); n - number of mice.

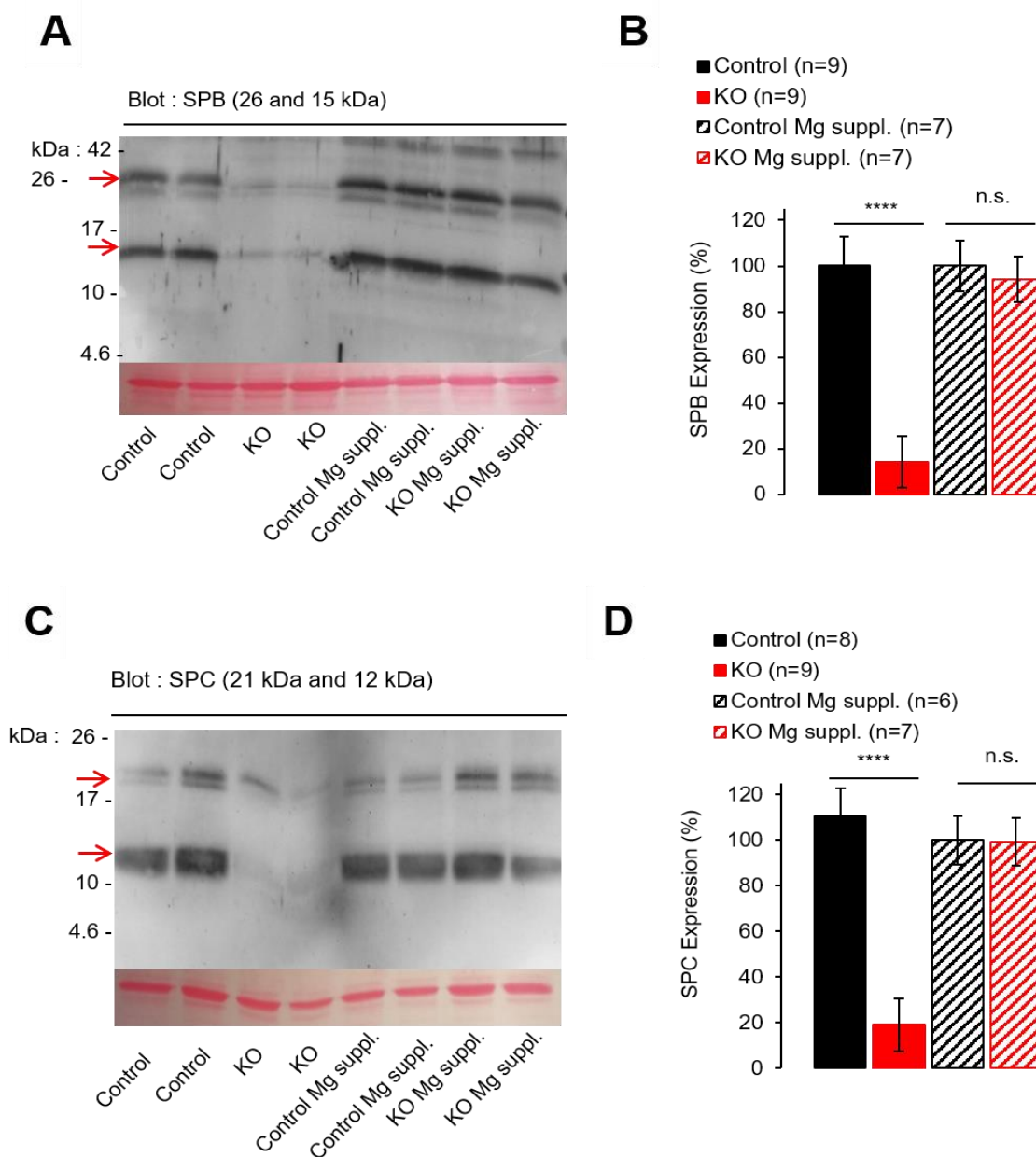


**Figure 21. Surfactant protein B (SP-B) and C (SP-C) levels in bronchoalveolar lavage (BAL) of *Trpm6<sup>fl/+</sup>* (Control) and *Trpm6<sup>Δ17/Δ17</sup>;Sox2-Cre* (KO) mice.** BAL samples were collected from 12-weeks old mice and analyzed by Western blot using the anti-SP-B antibody (A) and anti-SP-C antibody (C). Upper panel: Representative Western blot is shown for BAL samples isolated from the mice maintained on the regular or Mg<sup>2+</sup>- supplemented diets (n = 2 mice per genotype). Red arrows indicate the position of the expected SP-B bands (~26 and 15 kDa) and SP-C bands (~21 and 12 kDa). Lower panel: Ponceau Red staining of the blot was used to control protein loading. (B) Quantification of SP-B levels in Western blots illustrated in (A). SP-B signal in BAL samples from the control mice maintained on the regular diet was estimated as 100%. (D) Quantification of SP-B levels in Western blots illustrated in (C). SP-C signal in BAL samples from the control mice maintained on the regular diet was estimated as 100%. Values are shown as mean ± SEM; \*\*\*\* - P<0. 0001, n.s. – not significantly different (Student's t-test); n - number of mice.

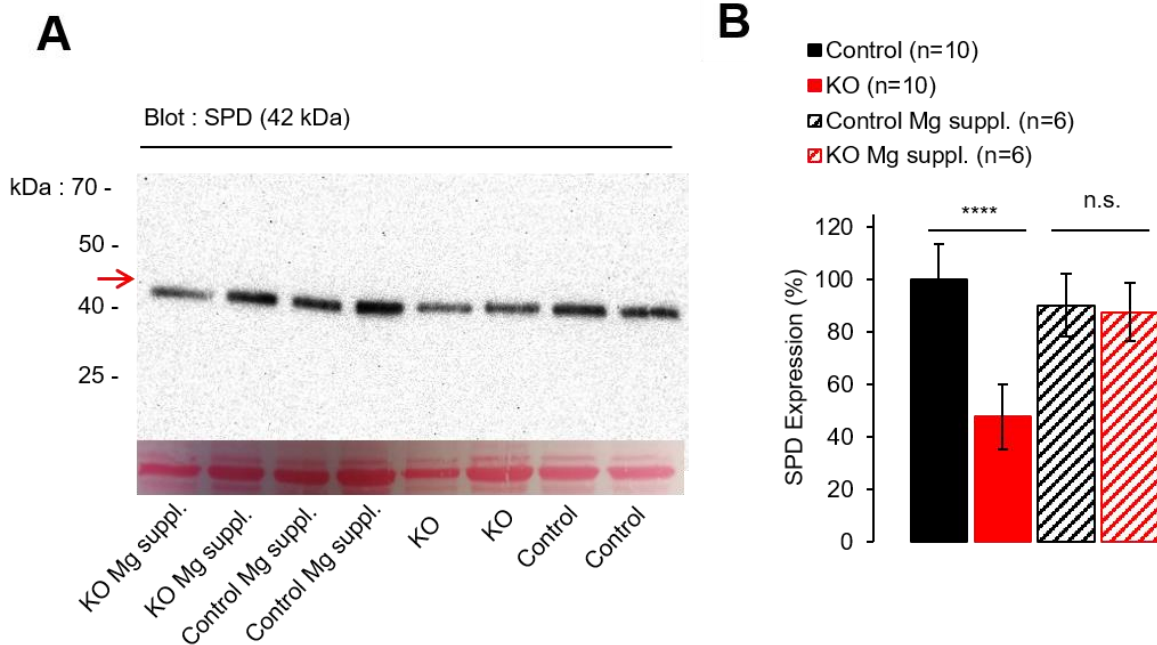


**Figure 22. Surfactant protein D (SP-D) levels in bronchoalveolar alveolar lavage (BAL) of *Trpm6*<sup>fl/+</sup> (Control) and *Trpm6* <sup>$\Delta 17/\Delta 17$</sup> ; *Sox2-Cre* (KO) mice. (A) BAL samples were collected from 12-weeks old mice and analyzed by Western blot using the anti-SP-D antibody. Upper panel: Representative Western blot is shown for BAL samples isolated from the mice maintained on the regular or Mg<sup>2+</sup>-supplemented diets (n = 2 mice per genotype). Red arrows indicate the position of the expected SP-D band (~42 kDa). Lower panel: Ponceau Red staining of the blot was used to control protein loading. (B) Quantification of SP-D levels in Western blots illustrated in (A). SP-D signal in BAL samples from the control mice maintained on the regular diet was estimated as 100%. Values are shown as mean  $\pm$  SEM; \*\*\*\* - P $\leq$ 0.0001, n.s. – not significantly different (Student's t-test); n - number of mice.**

## 5.6. Assessment of AT2 cells in the lungs of *Trpm6*-deficient mice

Since *Trpm6* is expressed in AT2 cells, and because *Trpm6*-deficient mice develop emphysema associated with reduced production of lung surfactants, we asked whether the ablation of TRPM6 could affect the viability and survival of AT2 cells. Using anti-ABCa3 antibody labelled with the fluorescent marker AlexaFluor633, we stained AT2 cells in lung tissue sections, while Hoechst dye was applied to estimate nuclei of all parenchyma cells. Randomly selected regions in the lung parenchyma were used to determine the fraction of AT2 cells. Such analysis revealed that lung tissues from 4-weeks old control mice contained 22% of AT2 cells and that the density of these cells were not affected in *Trpm6*-deficient littermates (Figure 23). However, evaluation of 8-10 weeks old mice uncovered modestly but significantly reduced abundance of AT2 cells in the *Trpm6*-deficient mice (19% in control tissues versus 16% in KO samples) (Figure 24).

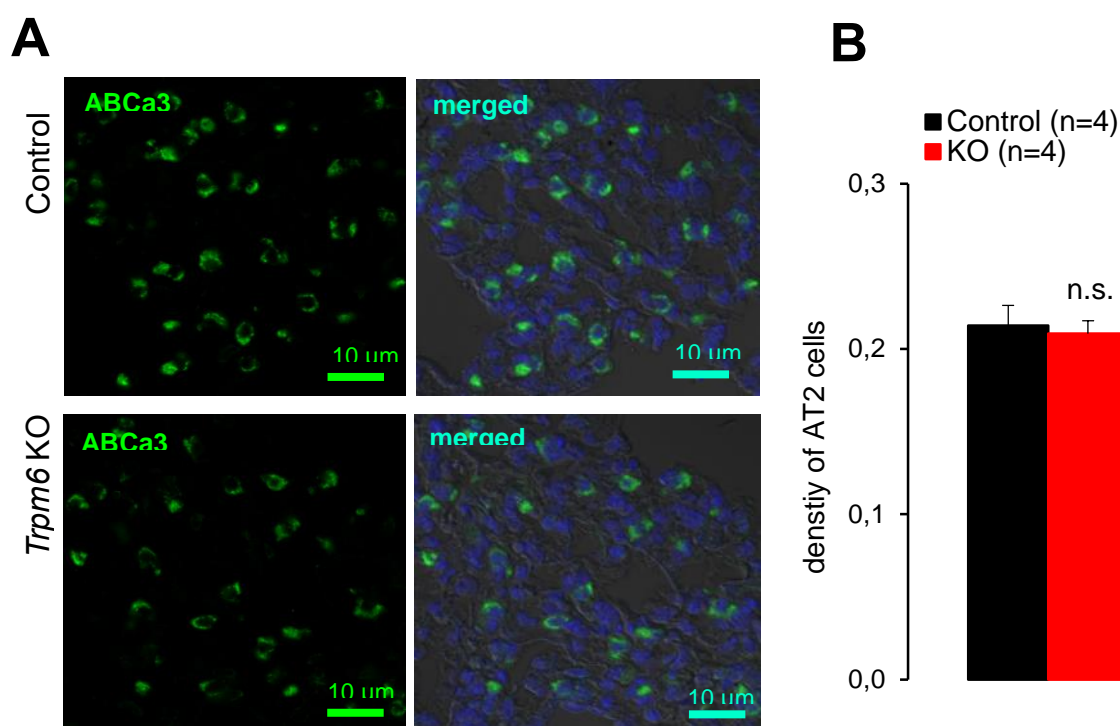


**Figure 23. Quantification of AT2 cells in the lung parenchyma of 4-weeks old *Trpm6*<sup>fl/+</sup> (Control) and *Trpm6*<sup>A17/A17</sup>; *Sox2-Cre* (KO) mice.** Tissue sections were stained with anti-ABCa3 antibody labelled with the fluorescent marker AlexaFluor633 (green) and Hoechst dye (blue). The fraction of ABCa3-positive cells was counted. (A) Representative images obtained from the stained tissue sections from *Trpm6*<sup>fl/+</sup> (Control) and *Trpm6*<sup>A17/A17</sup>; *Sox2-Cre* (KO) mice. (B) Frequency of AT2 cells in the tissue sections shown in (A). Hoechst signal was used to estimate the fraction of ABCa3-positive cells number. Values are shown as mean ± SEM; n – number of mice examined with 6 randomly selected images per mouse. n.s. – not significantly different (Student's t-test).

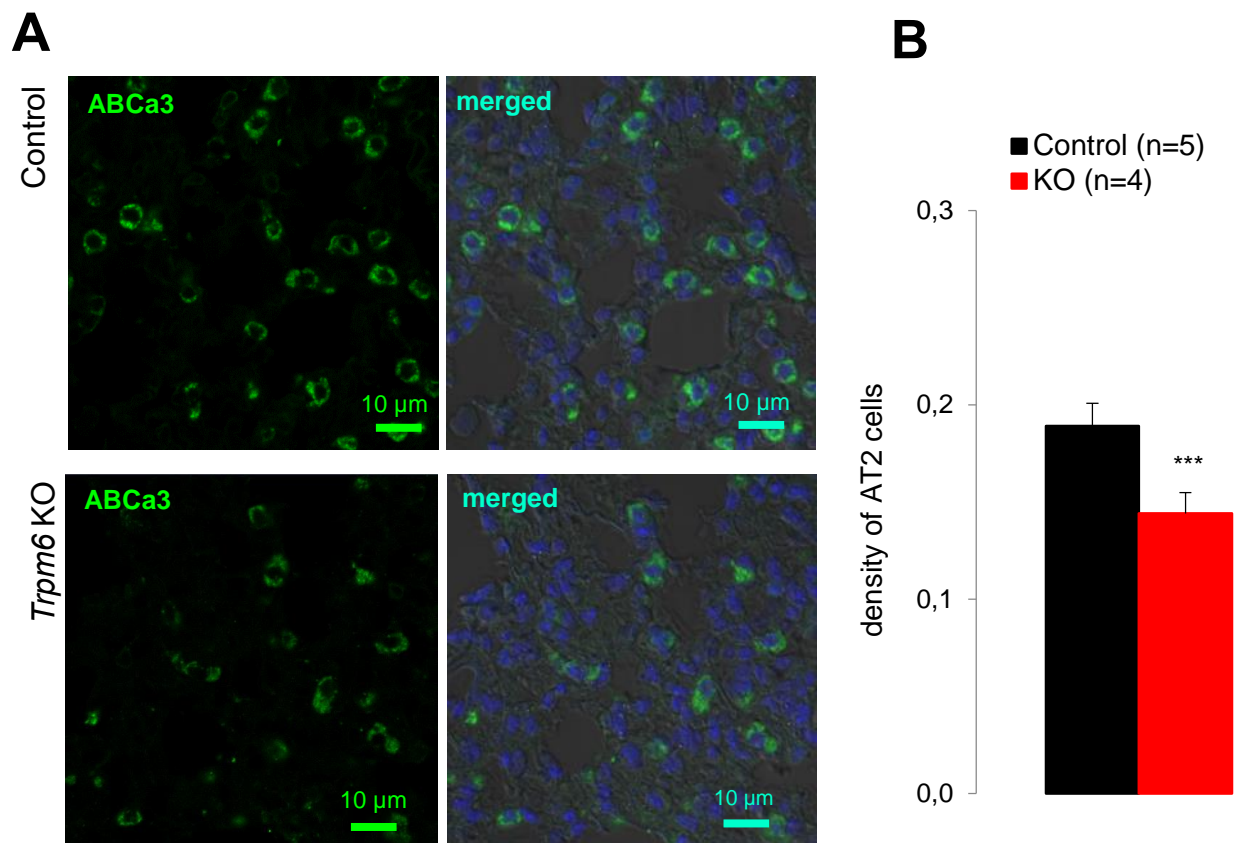


**Figure 24. Quantification of AT2 cells in the lung parenchyma of 8-weeks old *Trpm6*<sup>fl/+</sup> (Control) and *Trpm6* <sup>$\Delta$ 17/ $\Delta$ 17</sup>;Sox2-Cre (KO) mice.** Tissue sections were stained with anti-ABCa3 antibody labelled with the fluorescent marker AlexaFluor633 (green) and Hoechst dye (blue). The fraction of ABCa3-positive cells was counted. (A) Representative images obtained from the stained tissue sections from *Trpm6*<sup>fl/+</sup> (Control) and *Trpm6* <sup>$\Delta$ 17/ $\Delta$ 17</sup>;Sox2-Cre (KO) mice. (B) Frequency of AT2 cells in the tissue sections shown in (A). Hoechst signal was used to estimate the fraction of ABCa3-positive cells number. Values are shown as mean  $\pm$  SEM; n – number of mice examined with 6 randomly selected images per mouse. n.s. – not significantly different (Student's t-test).

## 5.7. Determination of elementary levels of divalent cations in serum and alveolar lining fluid (ALF) of *Trpm6*-deficient mice

As TRPM6 channels are essential for  $Mg^{2+}$  homeostasis in the body, we quantified  $Mg^{2+}$  and other divalent cations such as  $Ca^{2+}$  and  $Zn^{2+}$  in the blood serum and alveolar lining fluid (ALF) in 12-weeks old control and *Trpm6*-deficient mice.

In particular, we employed atomic absorption spectroscopy (AAS established in our laboratory in this project) and inductively-coupled plasma mass spectroscopy (ICP-MS by ALS Scandinavia, Sweden, as reported previously [36]). Both methods revealed  $Mg^{2+}$  concentrations in the serum of *Trpm6*-deficient mice of only 30% (according to AAS) compared with control littermates, while the amount of  $Ca^{2+}$  and  $Zn^{2+}$  ions were not changed (Figure 25), recapitulating our previous observations with 8-weeks old *Trpm6*-deficient mice [36].

Accordingly, we collected BAL using divalent cations-free phosphate buffered saline solution (PBS) followed by determination of urea levels in serum and BAL. Since urea freely diffuses between blood and ALF [94], this metabolite is broadly used to calculate the volume of ALF and estimate the absolute concentrations of other components in ALF [94]. We found that  $Mg^{2+}$  and  $Ca^{2+}$  concentrations were 3.1 and 2.0 folds higher in ALF of *Trpm6*-deficient mice respectively, while amounts of  $Zn^{2+}$  ions were not altered (Figure 26). Consequently, we asked whether the dietary  $Mg^{2+}$  supplementation could reverse these changes. As illustrated in Figure 27, such dietary treatment caused an elevation of  $Mg^{2+}$  concentrations in serum of *Trpm6*-deficient mice to the range observed in control mice maintained on the regular chow. Moreover,  $Mg^{2+}$  supplementation fully normalized concentrations of  $Mg^{2+}$  and  $Ca^{2+}$  in ALF. In summary, these results suggest that *Trpm6*-deficient mice displayed an abnormal balance of divalent cations in ALF, which is primarily driven by  $Mg^{2+}$  deficiency.

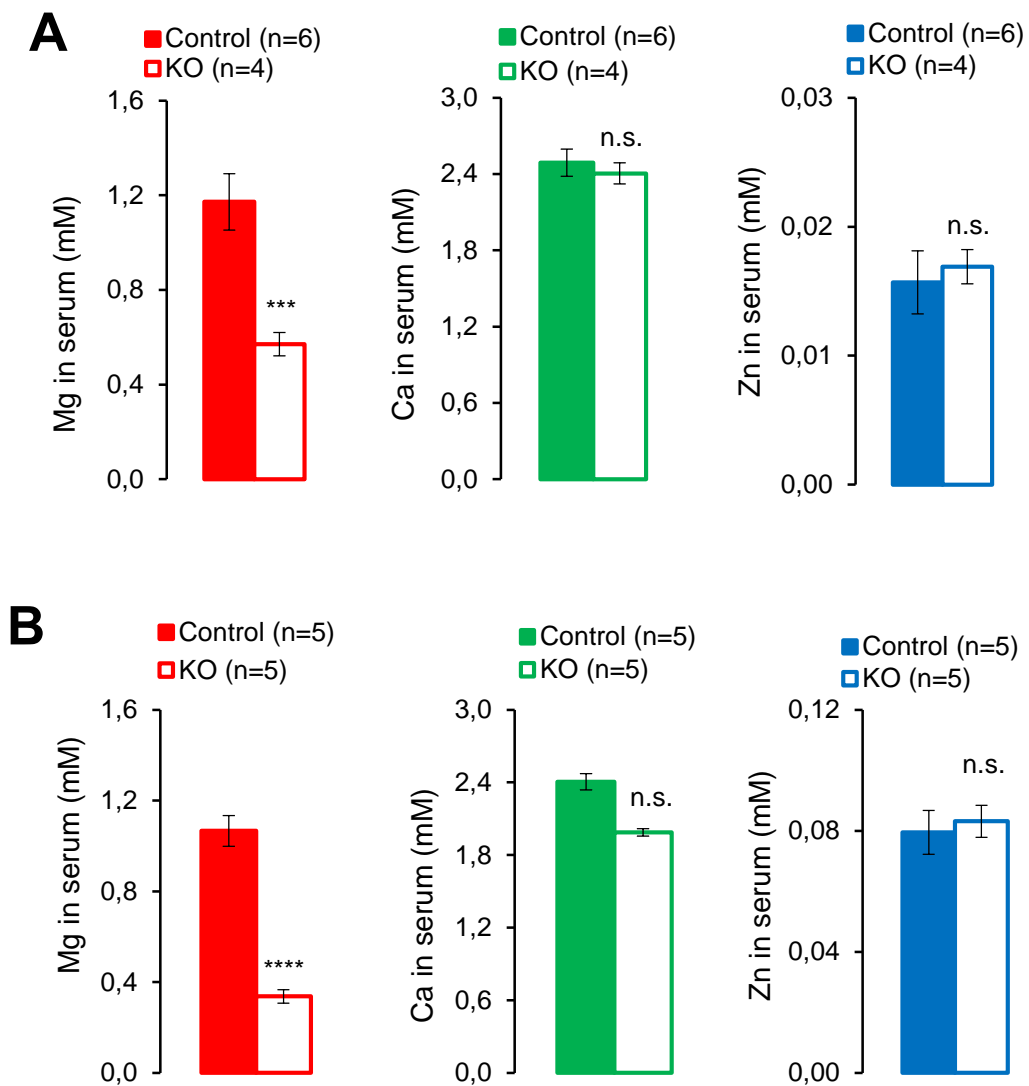


**Figure 25. Analysis of divalent cations in blood serum samples collected from *Trpm6<sup>fl/+</sup>* (Control) and *Trpm6<sup>Δ17/Δ17</sup>;Sox2-Cre* (KO) mice.** Levels of Mg (left panels), Ca (middle panels) and Zn (right panels) in the serum, obtained from 12-weeks old mice, were measured by (A) ICP-MS and (B) AAS techniques. Results are shown as mean  $\pm$  SEM; \*\*\*\* -  $P \leq 0.0001$ , \*\*\* -  $P \leq 0.001$ , n.s. – not significantly different (Student's t-test); n – number of mice.

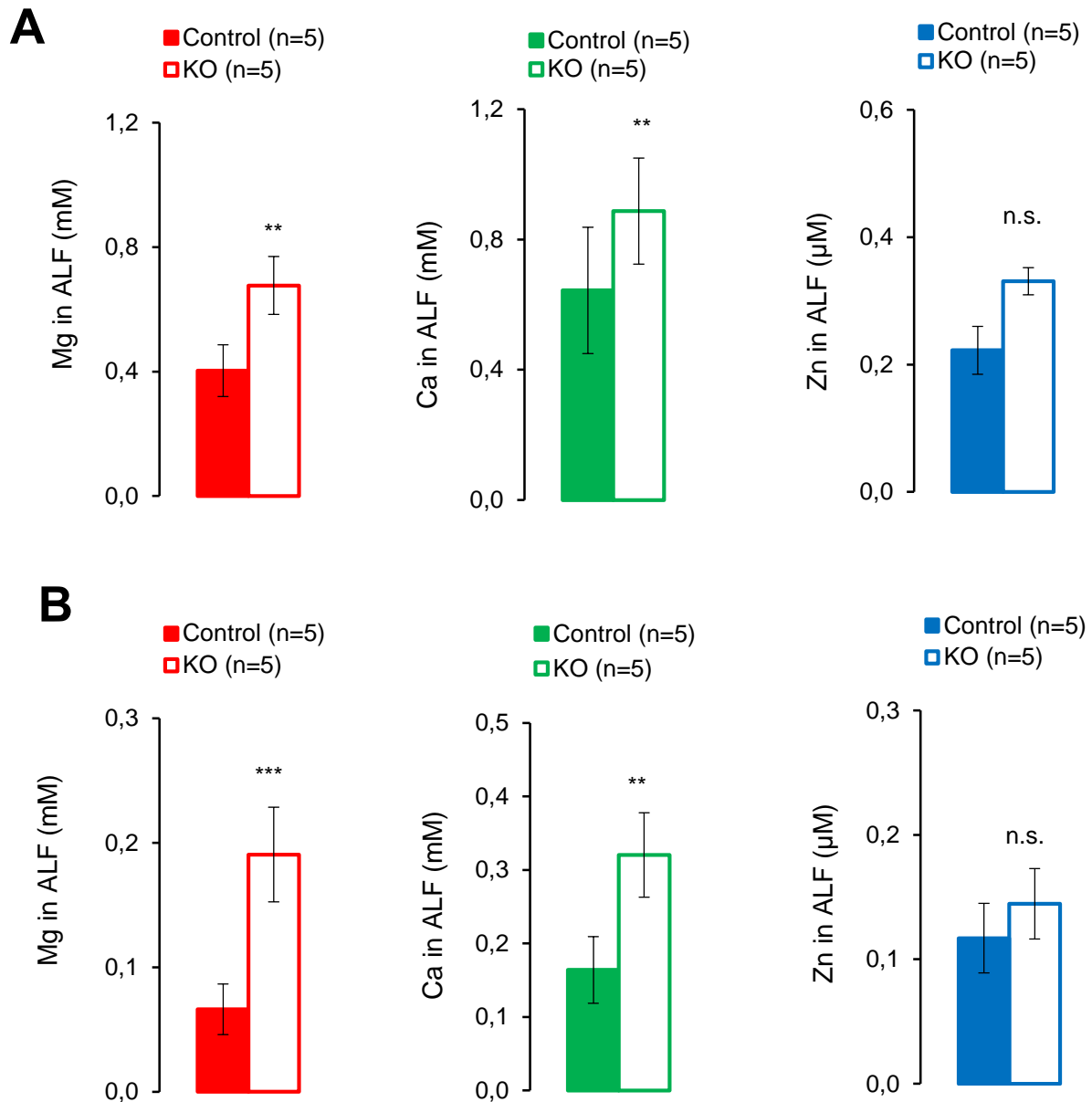


**Figure 26. Analysis of divalent cations in ALF samples collected from *Trpm6<sup>fl/+</sup>* (Control) and *Trpm6<sup>A17Δ17</sup>;Sox2-Cre* (KO) mice.** Elementary levels of Mg (left panels), Ca (middle panels) and Zn (right panels) in ALF, obtained from 12-weeks old mice, were measured by (A) ICP-MS and (B) AAS techniques. Results are shown as mean  $\pm$  SEM; \*\*\* -  $P \leq 0.001$ , \*\* -  $P \leq 0.01$ , n.s. – not significantly different (Student's t-test); n – number of mice.

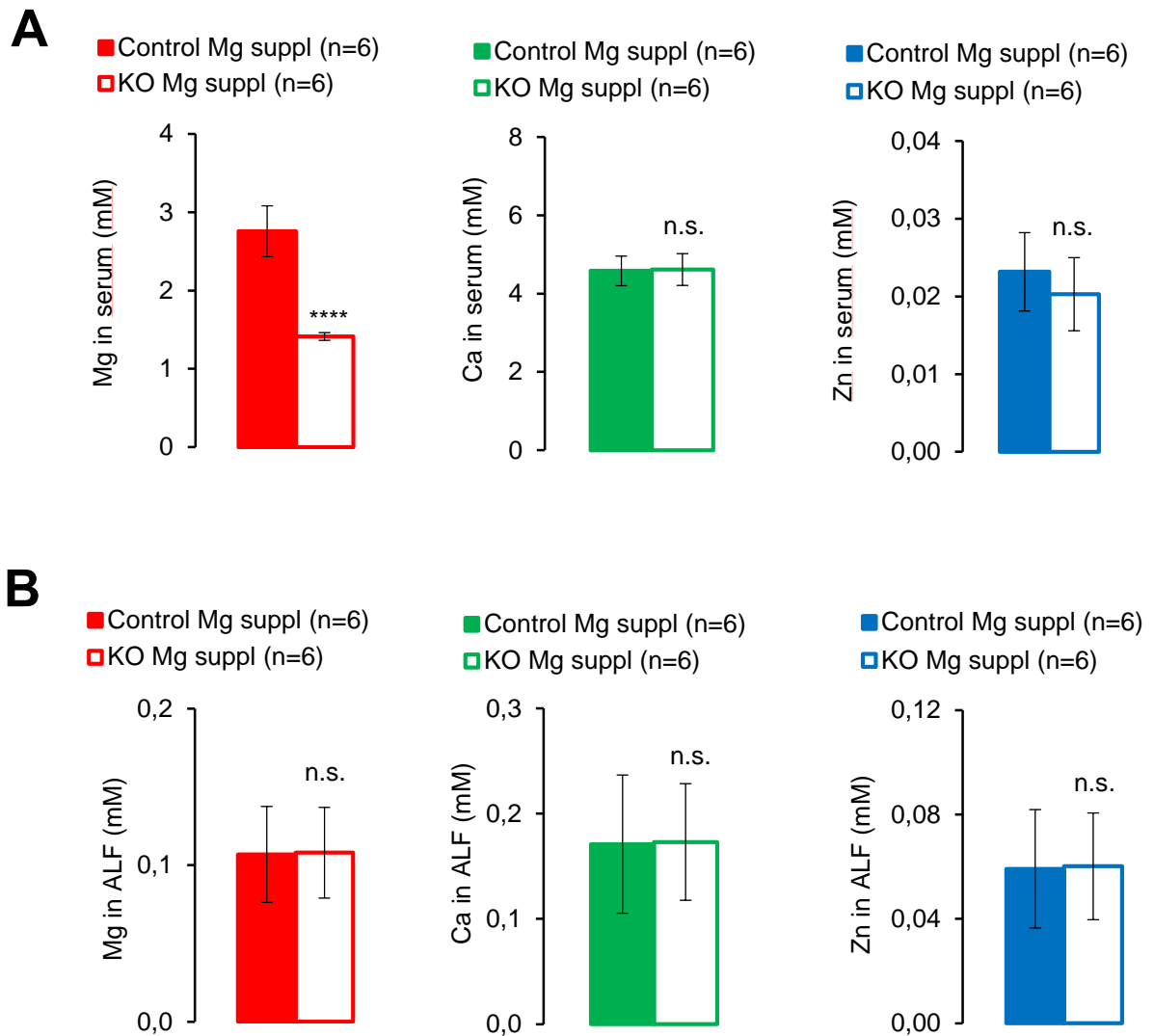


**Figure 27. Analysis of divalent cations in blood serum and ALF samples collected from *Trpm6<sup>fl/+</sup>* (Control) and *Trpm6<sup>A17Δ17</sup>;Sox2-Cre* (KO) mice fed with a high  $Mg^{2+}$  diet.** Elementary levels of Mg (left panels), Ca (middle panels) and Zn (right panels) in the (A) serum and (B) ALF obtained from 12-weeks old mice were measured by AAS technique. BAL samples were urea normalized. Results are shown as mean  $\pm$  SEM; \*\*\*\* -  $P \leq 0.0001$ , n.s. – not significantly different (Student's t-test); n – number of mice.

We noted that  $Mg^{2+}$  and  $Ca^{2+}$  levels in ALF of control mice were substantially lower than that in the blood. Such findings are in line with data from the literature [123, 124] and reinforced the idea that a putative active transcellular transport of  $Mg^{2+}$  and  $Ca^{2+}$  maintains such differences, somewhat recapitulating the processes driving absorption of divalent cations in the intestine and renal reabsorption of minerals. To this end, we calculated the serum/ALF  $Mg^{2+}$  ratios in individual control and *Trpm6*-deficient littermates (Figure 28). Such analysis revealed that serum levels of  $Mg^{2+}$  was ~17 fold higher in control mice maintained on the regular diet and that this parameter was further increased in the  $Mg^{2+}$  supplemented group. In contrast, the difference between  $Mg^{2+}$  concentrations in serum and ALF was very low in *Trpm6*-deficient mice (1.7 fold), but it was elevated to the normal range in *Trpm6*-deficient mice fed with  $Mg^{2+}$  enriched diet (Figure 28).

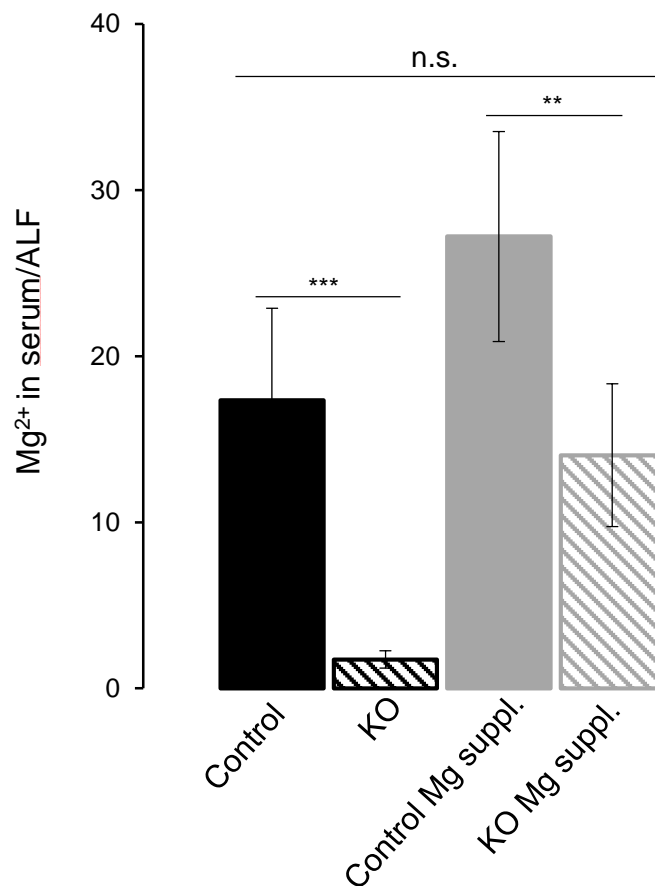


**Figure 28. Ratios of  $Mg^{2+}$  concentrations in the serum to ALF of *Trpm6*<sup>fl/+</sup> (Control) and *Trpm6*<sup>A17/A17</sup>;Sox2-Cre (KO) mice.** Elementary levels of  $Mg^{2+}$  in serum and ALF of 12-weeks old mice with and without dietary  $Mg^{2+}$  supplementation were proportioned. Urea normalized lavage samples were used for calculations. Results are shown as mean  $\pm$  SEM; \*\*\* -  $P \leq 0.001$ , \*\* -  $P \leq 0.01$ , n.s. – not significantly different (One-Way ANOVA); n – number of mice.

## 5.8. Generation and phenotypic evaluation of a kinase-dead *Trpm6* mice

Since the TRPM6 protein comprises both a channel and a kinase moiety, we asked whether the lack of kinase activity contributed to the *Trpm6* KO phenotype. Previously, we reported that, in analogy to the K1646R mutation in TRPM7 channels [55], a K1810R mutation in TRPM6 protein inactivates its kinase activity. This effect was demonstrated by comparative Western blot analysis of WT and mutant murine TRPM6 protein with the help of an antibody explicitly detecting the phosphorylated autophosphorylation site at T1370 [34]. Accordingly, our targeting strategy was based on the generation of a new mice strain with a 'kinase-dead' point mutation in the *Trpm6* locus (Figure 6). As the *Trpm6* null mutations interfered with early embryonic development [37], we relied on the Cre/LoxP technology for a conditional modification of the genomic region coding for the kinase domain of TRPM6 (Figure 6).

Specifically, we replaced exon 34 of *Trpm6* with a cDNA sequence encoding the whole kinase unit (exons 34-39) with the adjacent STOP codon flanked by LoxP sites followed by an additional sequence coding for exon 34 with the K1810R mutation (Figure 6). Consequently, we expected that the floxed (*fl*) allele would express the WT TRPM6. However, Cre-mediated deletion of the floxed sequence will introduce the K1810R mutation in *Trpm6* and the translated protein. This mutation was introduced by homologous recombination in embryonic stem (ES) cells at Taconic Biosciences GmbH (Köln, Germany). Next, the generated ES cells were used to produce chimeric mice, which were crossed with *Flp* deleter mice to remove the neomycin resistance cassette (*Neo*, not shown in Figure 6). Animals displaying germ-line transmission were selected to produce mice homozygous for the *fl* allele. We used mice with the *Sox2-Cre* transgene to generate mice heterozygous for the *Trpm6<sup>R</sup>* allele. Viable *Trpm6<sup>R/+</sup>* mice were verified by diagnostic PCR with primers spanning exon 34 followed by sequencing the amplified PCR product. Finally, we crossed *Trpm6<sup>R/+</sup>* males and females and obtained viable *Trpm6<sup>R/R</sup>* offspring as predicted by Mendel's rules of inheritance (Table 15). The presence of K1810R mutation in *Trpm6<sup>R/R</sup>* pups was confirmed by PCR analysis of DNA extracted from ear fragments (Figure 29) and mRNA isolated from the kidney, lung and intestine. As "kinase-dead" mutant mice were born at a normal Mendelian distribution, we concluded that early embryonic mortality of *Trpm6*-deficient mice was primarily due to the lack of channel activity of TRPM6.

Previously, our laboratory developed a genetic approach to produce *Trpm6*-deficient offspring, which normally developed during the first 4 weeks of postnatal life. However, soon after weaning, *Trpm6*-deficient mice stopped to grow and displayed a low survival rate with 100%

mortality among 16-weeks old mutants. Therefore, we asked if kinase-dead mice will show any changes in postnatal survival and growth. However, *Trpm6<sup>R/R</sup>* mice displayed an unchanged body weight compared to *Trpm6<sup>+/+</sup>* littermates (Figure 30). Moreover, *Trpm6<sup>R/R</sup>* mice showed no signs of reduced postnatal survival since 100% of individuals from the group of ten 12-weeks old *Trpm6<sup>R/R</sup>* were viable. We also observed that *Trpm6<sup>R/R</sup>* animals were fertile and did not display remarkable alterations in physical appearance and behaviour, arguing that the lack of the channel rather than the kinase activity of TRPM6 attributed to postnatal mortality and growth failure of *Trpm6*-deficient mice.

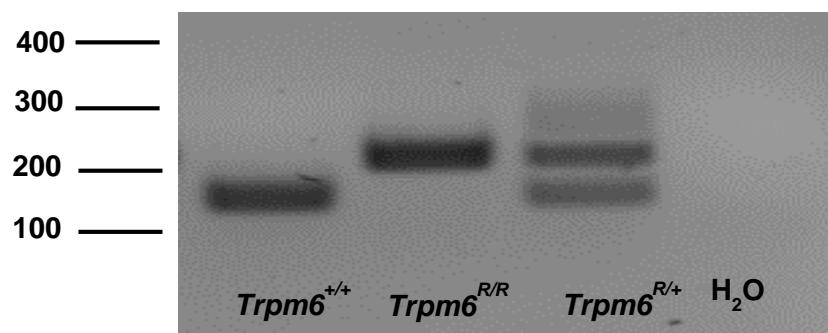


**Figure 29. Genotyping of *Trpm6<sup>R/R</sup>*, *Trpm6<sup>R/+</sup>* and *Trpm6<sup>+/+</sup>* mice.** Genomic DNA obtained from ear fragments of *Trpm6<sup>R/R</sup>*, *Trpm6<sup>R/+</sup>* and *Trpm6<sup>+/+</sup>* mice was analyzed by PCR using primers specific for the region carrying the point mutation. PCR amplicons (240 bp for *Trpm6<sup>R/R</sup>*; 153 bp for *Trpm6<sup>+/+</sup>*) were examined using agarose gel electrophoresis. To verify the specificity of PCR no genomic DNA was added to the control (H<sub>2</sub>O).

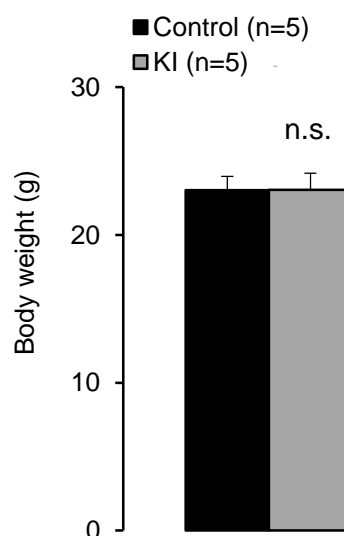


**Figure 30. Body weights of *Trpm6<sup>+/+</sup>* (Control) and *Trpm6<sup>R/R</sup>* (KI) mice.** Values are shown as mean  $\pm$  SEM; n.s. - not significantly different (Student's t-test); n - number of mice.

Next, we investigated whether *Trpm6*<sup>R/R</sup> mice develop a respiratory phenotype like the *Trpm6*-deficient mice (Figure 13). We performed a histological evaluation of lung tissue section in conjunction with a lung function test like in our previous experiments with the *Trpm6*-deficient mice. The morphology of tissues and mean cord lengths of 12-weeks old *Trpm6*<sup>R/R</sup> mice, however, were not changed as compared to control littermates (Figure 31). Furthermore, functional characteristics of the lung, like compliance and resistance, were not affected in *Trpm6*<sup>R/R</sup> mice (Figure 32). In accord with these findings, Mg<sup>2+</sup> levels in serum and ALF samples of *Trpm6*<sup>R/R</sup> mice were not distinguishable from control values (Figure 33). Taken together, we concluded that specific ablation of the TRPM6 kinase activity did not impact the biochemical, morphological and functional characteristics of the lung like in *Trpm6*-deficient mice.

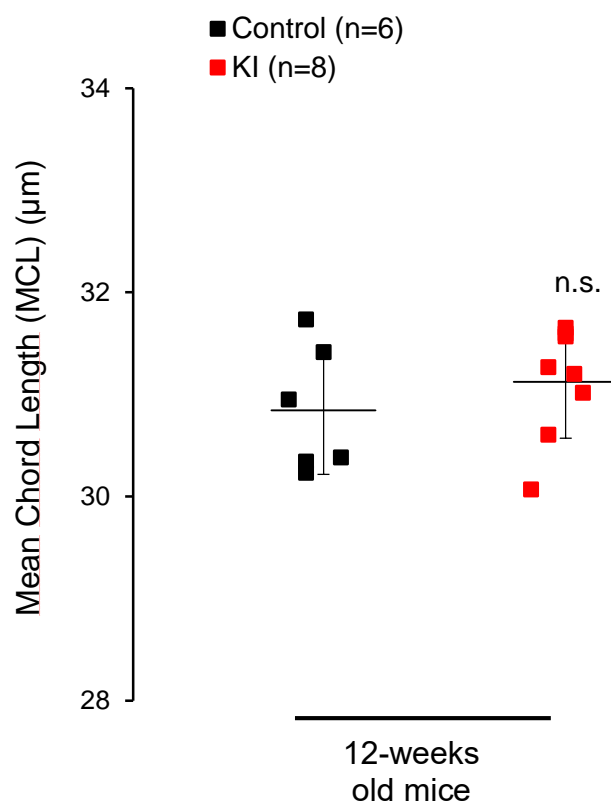


**Figure 31. Morphological analysis of lungs from *Trpm6*<sup>+/+</sup> (Control) and *Trpm6*<sup>R/R</sup> (KI) mice.** Mean chord lengths of 12-weeks old *Trpm6*<sup>R/R</sup> (KI) mice were compared to *Trpm6*<sup>+/+</sup> controls. The results are shown as mean ± SEM; n.s. - not significantly different (Student's t-test); n - number of mice.

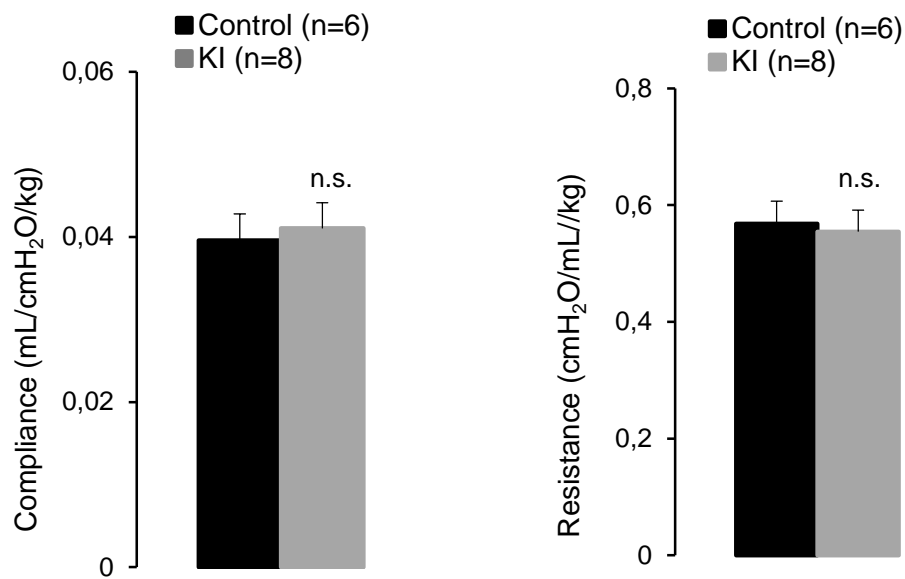


**Figure 32. Functional analysis of lungs from *Trpm6*<sup>+/+</sup> (Control) and *Trpm6*<sup>R/R</sup> (KI) mice.** Lung function parameters were analyzed in 12-weeks old mice of each genotype. Results are shown as mean  $\pm$  SEM; n.s. - not significantly different (Student's t-test); n - number of mice.

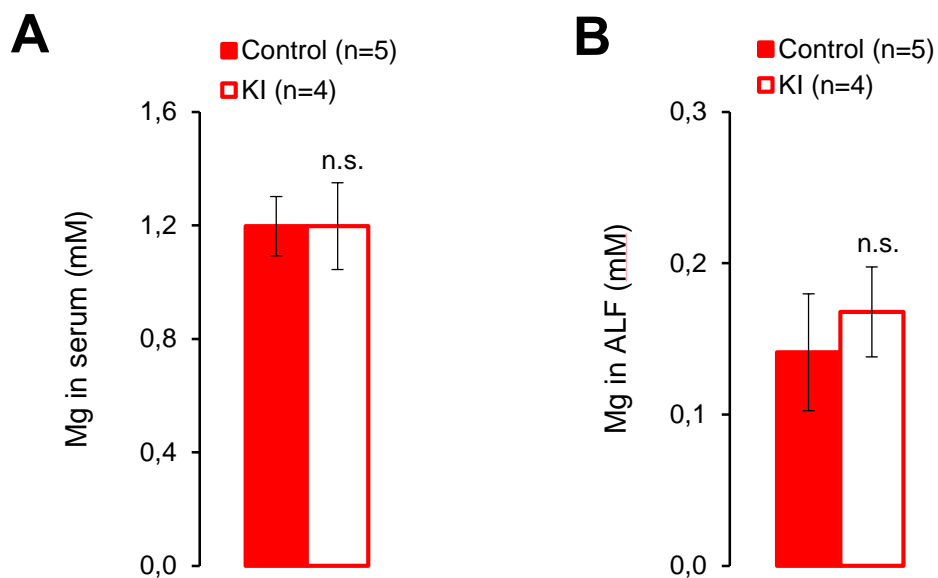


**Figure 33. Analysis of divalent cations in blood serum and ALF samples collected from *Trpm6*<sup>+/+</sup> (Control) and *Trpm6*<sup>R/R</sup> (KI) mice.** Levels of Mg in the (A) serum and (B) ALF obtained from 12-weeks old mice were measured by AAS technique. Results are shown as mean  $\pm$  SEM; n.s. – not significantly different (Student's t-test); n – number of mice.

## 5.9. Morphological changes in primary AT2 cells isolated from *Trpm6*-deficient mice

Our experiments with *Trpm6*<sup>Cre/+</sup>; *Rosa26*<sup>τGFP/+</sup> mice suggested that *Trpm6* is expressed in AT2 cells. To get further insights on the cellular role of TRPM6, we isolated AT2 cells from adult control and *Trpm6*-deficient mice to elucidate the impact of TRPM6 on the content and processing of respiratory surfactants.

As expected from data of the literature [215], primary isolated AT2 cells displayed epithelial-like flat shaped characteristic colonies, which could be observed on day 1 (24 h after isolation). The isolated cells proliferated and formed a cell monolayer on day 2–3 (Figure 34). In follow up experiments, we studied AT2 cells on day 3.

To examine the purity of our primary AT2 cells, we analyzed expression levels of *Aqp-5* (AT1 cells marker), *Sp-C* (AT2 cells marker),  $\alpha$ -*Sma* (fibroblasts marker) and *Trpm6* using an qRT-PCR approach. We found that the isolated cells represent AT2 cells since only *Sp-C* and *Trpm6* transcripts were abundantly present (Figure 35).

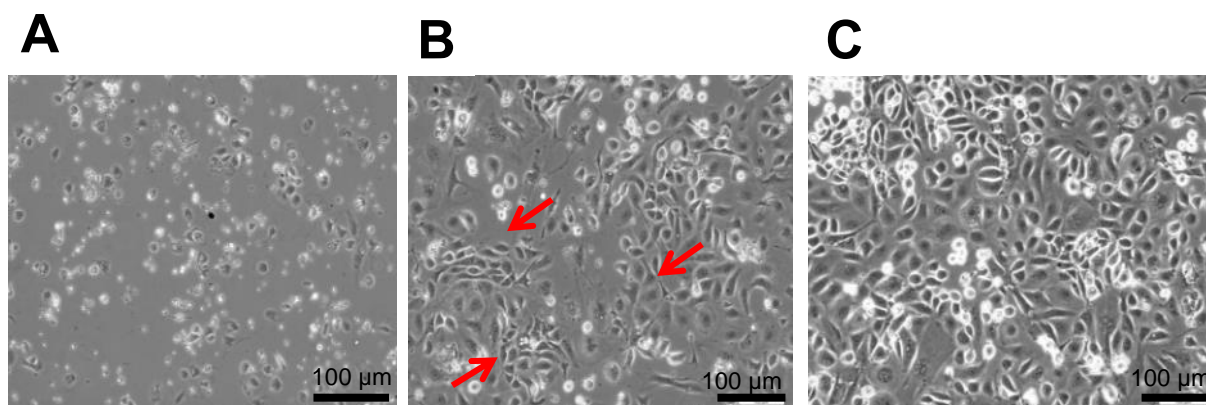


**Figure 34. Representative light microscopy images obtained from primary isolated murine alveolar type 2 (AT2) cells.** The morphological appearance of AT2 cells isolated from *Trpm6*<sup>fl/+</sup> (Control) mice on (A) day1, (B) day 2, (C) day 3 after isolation are shown. Starting from day 1, AT2 cells form colonies as indicated by arrows (A). Proliferated isolated cells form a cell monolayer on day 3 (C).

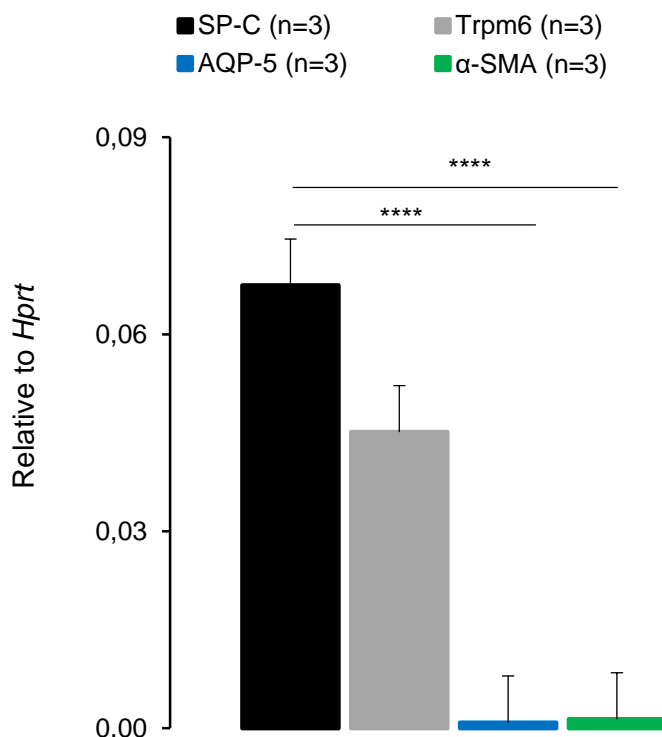


**Figure 35. Relative expression levels of *Sp-C*, *Trpm6*, *Aqp-5* and  $\alpha$ -*Sma* mRNA in *Trpm6<sup>fl/+</sup>* (Control) primary AT2 cells.** mRNA levels of *Sp-C*, *Trpm6*, *Aqp-5* and  $\alpha$ -*Sma* were examined using qRT-PCR and *Hprt* as a reference transcript. Values are shown as mean  $\pm$  SEM. \*\*\*\* -  $P \leq 0.0001$ , (One-Way ANOVA); n – number of measurements.

Next, we verified experimental conditions for the labelling of surfactant-containing intracellular compartments of AT2 cells by the fluorescent LysoTracker Red (LyTR) dye, the known probe for lamellar bodies (LB) in living cells [207, 216], and anti-ABCa3 antibody, the broadly used reagent to detect the LB-specific ABCa3 transporter [207-209]. In our settings, LyTR stained efficiently intracellular compartments in the cell line A549 from an adenocarcinoma of a human lung (Figure 36) as well as in  $\tau$ GFP-positive primary AT2 cells (Figure 37) isolated from the lung of *Trpm6<sup>Cre/+</sup>; Rosa26<sup>rGFP/+</sup>* transgenic mouse. Also, the Anti-ABCa3 antibody labelled with AlexaFluor633 also stained AT2 cells isolated either from control mice or from *Trpm6<sup>Cre/+</sup>; Rosa26<sup>rGFP/+</sup>* (Figure 38).

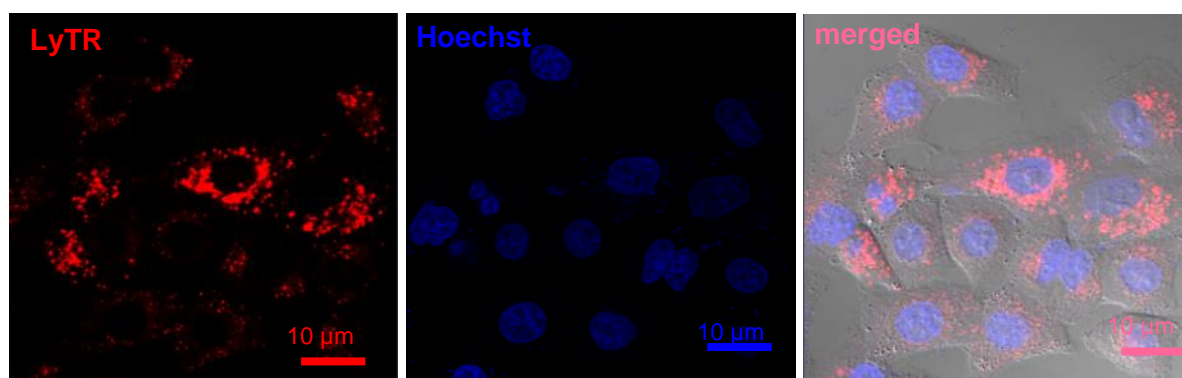


**Figure 36.** Imaging of living cells from the A549 cell line stained with the fluorescent LyTR and Hoechst dye. Representative images of LyTR (left), Hoechst (middle) and DIC merged with LyTR and Hoechst signals (right) are shown.

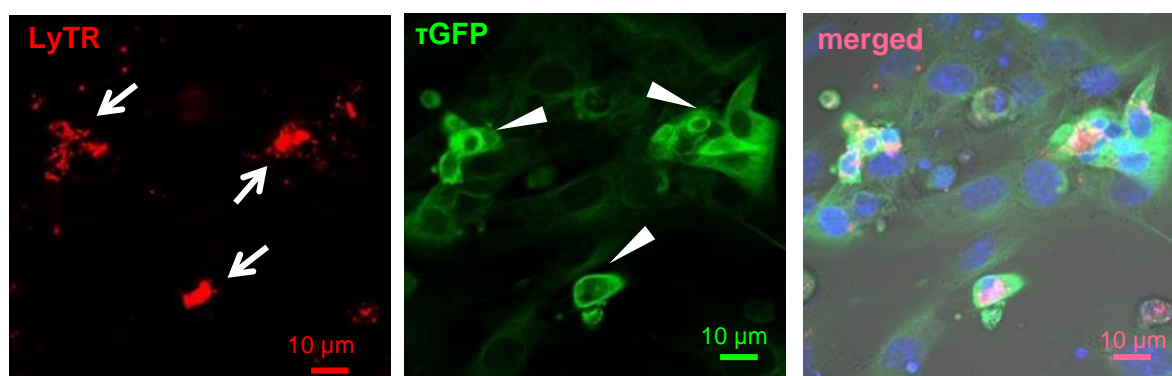


**Figure 37.** Imaging of living primary AT2 cells. Murine primary AT2 cells isolated from *Trpm6<sup>Cre/+</sup>;Rosa26<sup>τGFP/+</sup>* mice were examined. Representative images of LyTR (left),  $\tau$ GFP (middle) and DIC merged with LyTR, Hoechst, and  $\tau$ GFP are shown. Arrows in (A) indicate LyTR-positive LB. Triangles in (B) point out on colonies of  $\tau$ GFP-positive cells.

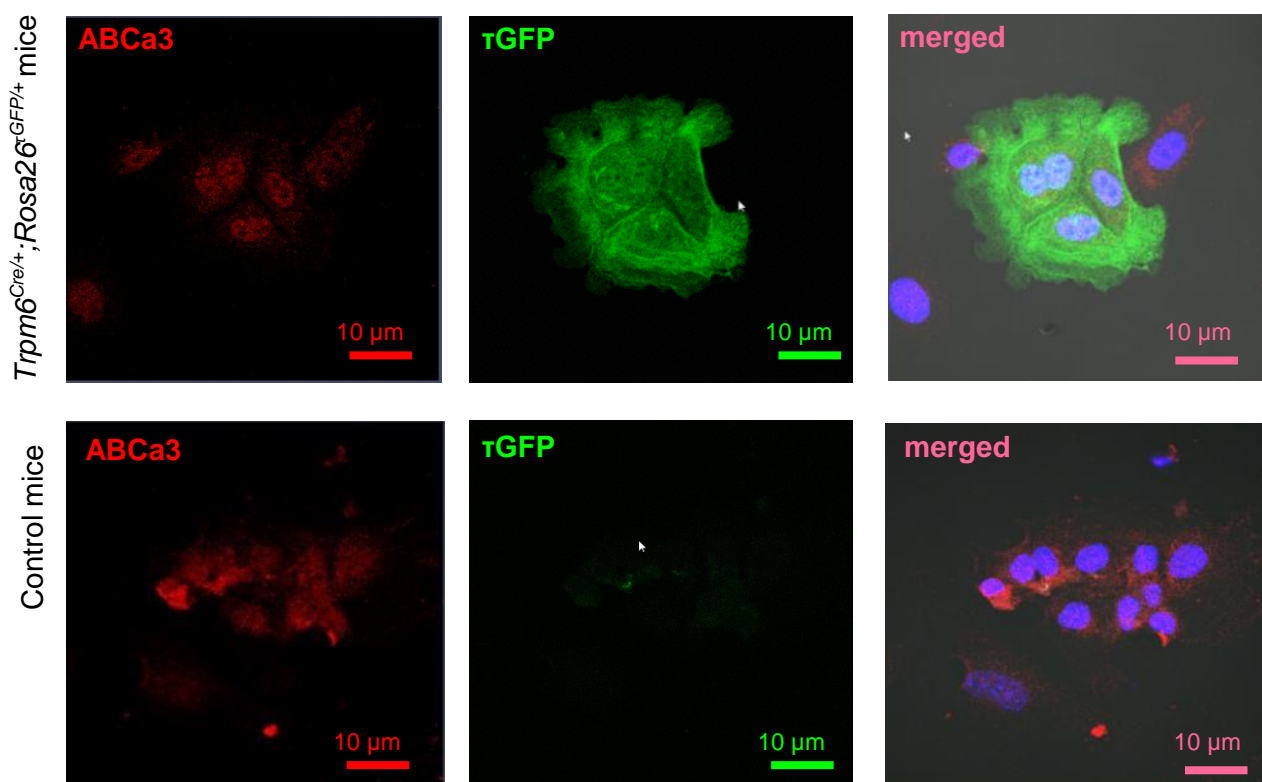


**Figure 38. Immunofluorescence staining of primary AT2 cells obtained from *Rosa26*<sup>+/+</sup> (Control) and *Trpm6*<sup>Cre/+</sup>; *Rosa26*<sup>τGFP/+</sup> mice.** Murine primary AT2 cells isolated from *Rosa26*<sup>+/+</sup> (Control) *Trpm6*<sup>Cre/+</sup>; *Rosa26*<sup>τGFP/+</sup> mice were examined. Representative images of ABCa3 labelled with AlexaFluor633 (left), τGFP (middle) and DIC merged with ABCa3, Hoechst, and τGFP are shown (n=3 mice per genotype).

Next, we asked whether primary AT2 cells isolated from *Trpm6*-deficient mice will display alterations in the processing of respiratory surfactants to recapitulate in vitro our results obtained from tissue sections (Figure 19). To this end we isolated AT2 cells from controls and *Trpm6*-deficient littermates and examined the cells after labeling with fluorescent LyTR dye (Figure 39) or anti-ABCa3 antibody coupled to AlexaFluor633 (Figure 40). Remarkably, both approaches revealed that *Trpm6*-deficient cells accumulated LyTR- and ABCa3-positive intracellular organelles (presumably LB), in clear contrast to control cells. These results reproduce our data obtained in the histological and EM analysis of tissue sections (Figure 19).

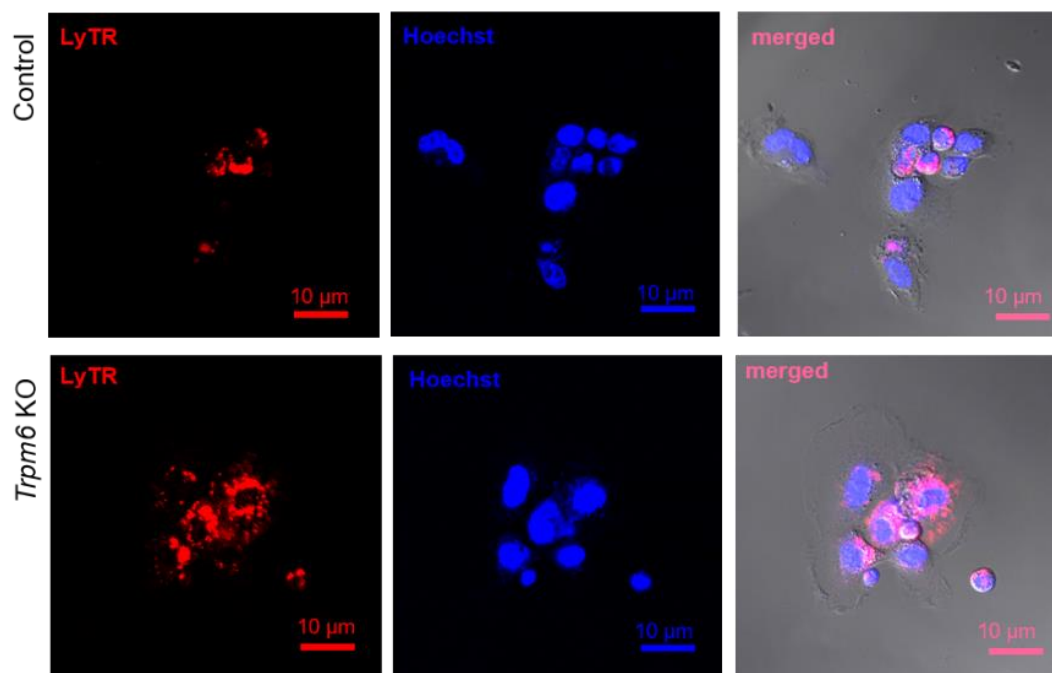


**Figure 39.** Imaging of living primary AT2 cells obtained from *Trpm6<sup>fl/+</sup>* (Control) and *Trpm6<sup>Δ17/Δ17</sup>;Sox2-Cre* (KO) mice stained with fluorescent LyTR dye *in vitro*. Representative images of LyTR (left), Hoechst (middle) and DIC merged with LyTR and Hoechst are shown (n=4 mice).

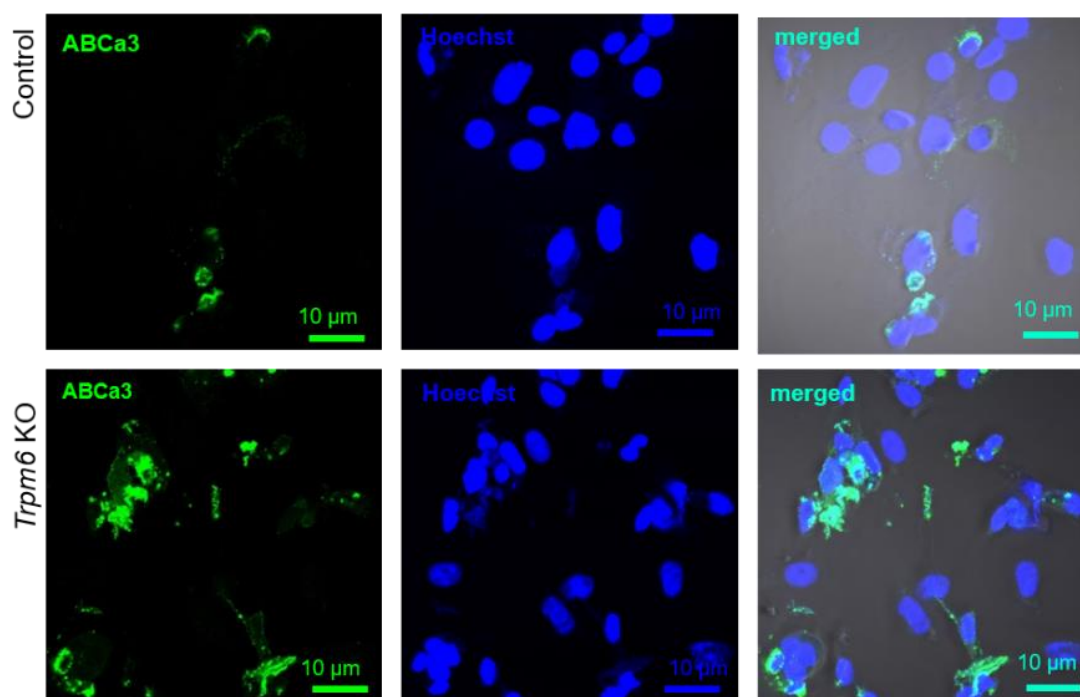


**Figure 40.** Immunofluorescence staining of primary AT2 cells obtained *Trpm6<sup>fl/+</sup>* (Control) and *Trpm6<sup>Δ17/Δ17</sup>;Sox2-Cre* (KO) mice. Murine primary AT2 cells isolated from *Trpm6<sup>fl/+</sup>* (Control) and *Trpm6<sup>Δ17/Δ17</sup>;Sox2-Cre* (KO) mice were examined. Representative images of ABCa3 labelled with AlexaFluor633 (left), Hoechst (middle) and DIC merged with ABCa3 and Hoechst are shown (n=4 mice per genotype).

To further verify these results, we performed electron microscopy of the primary AT2 cells obtained from 12-weeks of age control and *Trpm6*-deficient mice (Figure 41). *Trpm6*-deficient AT2 cells frequently contained very large LB, not observed in control cells (Figure 41). Moreover, in the extracellular space tubular myelin (TM) structures were absent in primary AT2 cells of *Trpm6*-deficient mice (Figure 41).

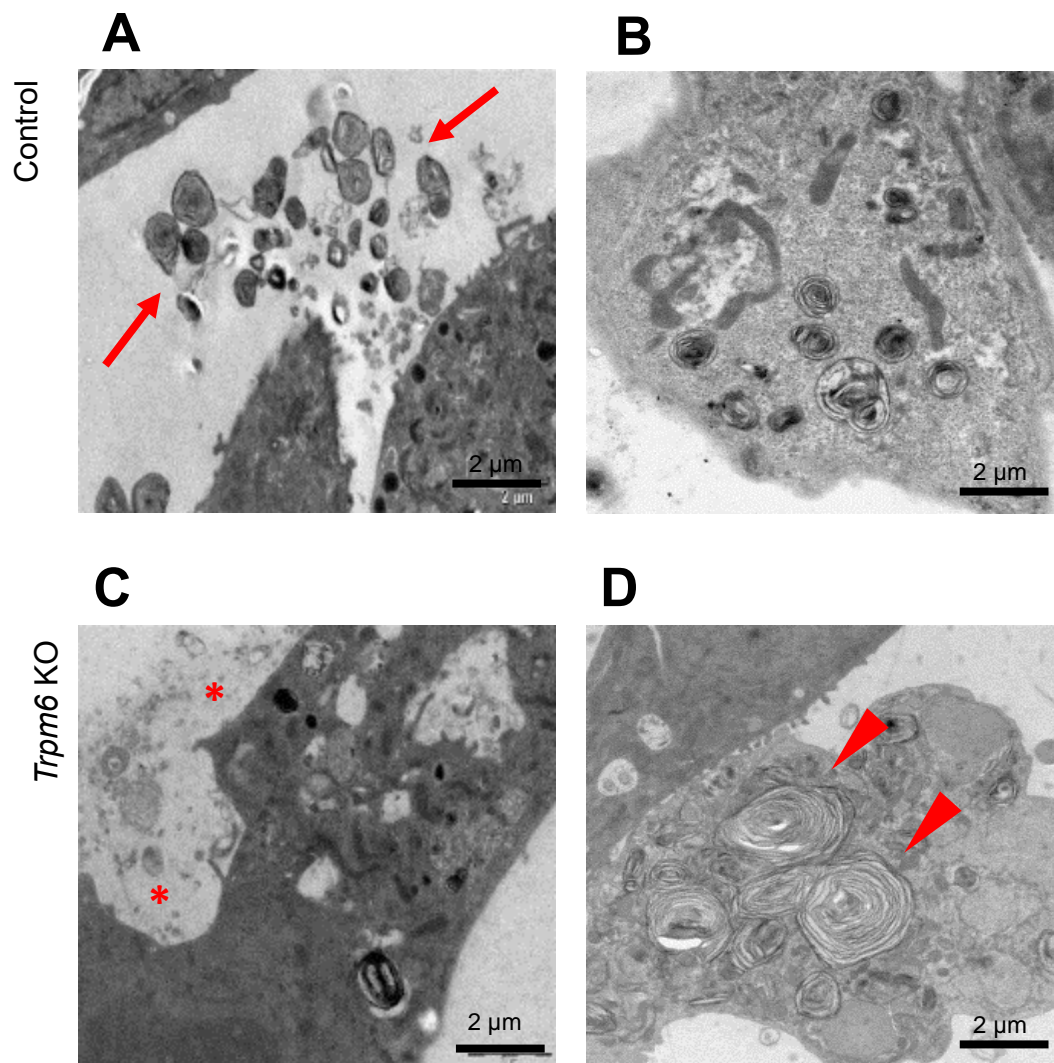


**Figure 41. Images obtained by electron microscopy (EM) of primary AT2 cells from *Trpm6*<sup>fl/+</sup> (Control) and *Trpm6*<sup>Δ17/Δ17</sup>;Sox2-Cre (KO) mice.** Ultrastructure of alveolar epithelial Type 2 (AT2) cells isolated from *Trpm6*<sup>fl/+</sup> (Control) (A, B) and *Trpm6*<sup>Δ17/Δ17</sup>;Sox2-Cre (KO) (C, D) mice. Tubular myelin is present in alveolar space of *Trpm6*<sup>fl/+</sup> (Control) mice (indicated by red arrows in A) but absent in *Trpm6*<sup>Δ17/Δ17</sup>;Sox2-Cre (KO) mice (indicated by red stars in C). In addition, large LBs (shown by red triangles in D) were observed in AT2 cells isolated from *Trpm6*<sup>Δ17/Δ17</sup>;Sox2-Cre (KO) mice. Representative images are shown (n=6 mice per genotype).

It is well documented in the literature that significant amount of ATP are stored in a variety of secretory vesicles, including lysosome-related organelles like LB [217-220]. Furthermore, it was shown that ATP regulates the release of surfactants from AT2 cells [221, 222]. Since ATP has a high apparent affinity to  $Mg^{2+}$ , it was estimated that ~90 ATP molecules are present in a cellular MgATP complex [223, 224].

Consequently, we hypothesized that  $Mg^{2+}$  deficiency observed in *Trpm6*-deficient mice, could affect total levels of MgATP and that such imbalance can be associated with the abnormal capability of *Trpm6*-deficient cells to release respiratory surfactants. In line with this idea, we observed that quinacrine, a dye known to be associated with ATP stores [207], including LB, was colocalized with LysoTracker signal in both cells from the A549 cell line and control primary AT2 cells (Figure 42). In addition, we tested the ATP-specific probe, BODIPY FL-ATP, which is also able to detect ATP in LB [207, 225]. As outlined in Figure 42, BODIPY FL-ATP labelled LB in control AT2 cells in our experimental settings. Finally, we examined AT2 cells from *Trpm6*-deficient mice using quinacrine and BODIPY FL-ATP, and found that the vesicular content of ATP was significantly increased, suggesting that ATP metabolism was affected in *Trpm6*-deficient cells (Figure 43).

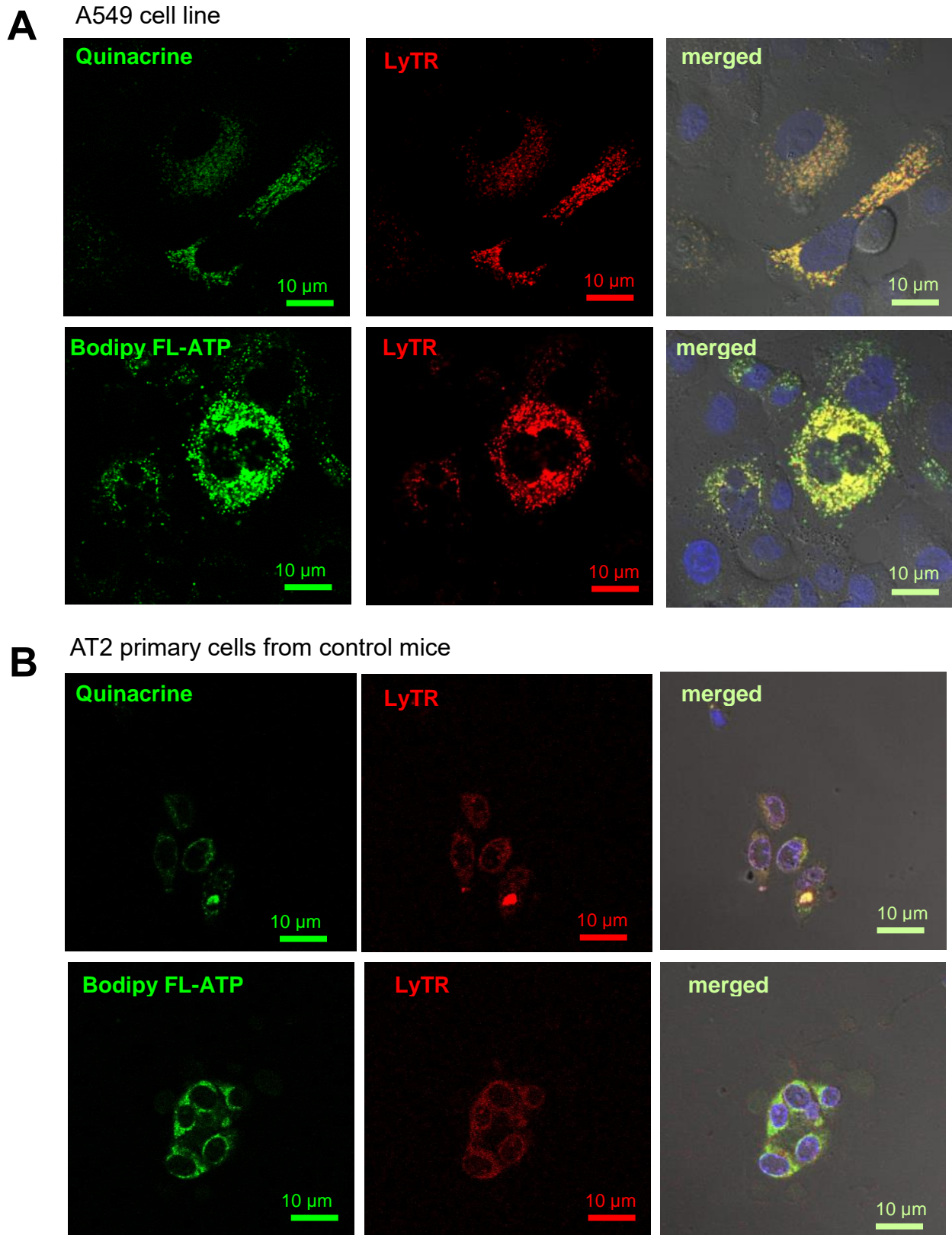


**Figure 42. Labelling of ATP stores in lamellar bodies (LB) of cells from A549 cell line and primary AT2 cells from *Trpm6*<sup>fl/+</sup> (Control) mice.** Staining of (A) A549 cell line and (B) primary AT2 cells obtained from *Trpm6*<sup>fl/+</sup> (Control) mice lung with quinacrine, LyTR (a marker of LBs) and BODIPY FL-ATP, indicating the presence of intravesicular ATP in LBs. Representative fluorescence and merged images of AT2 cells are shown.

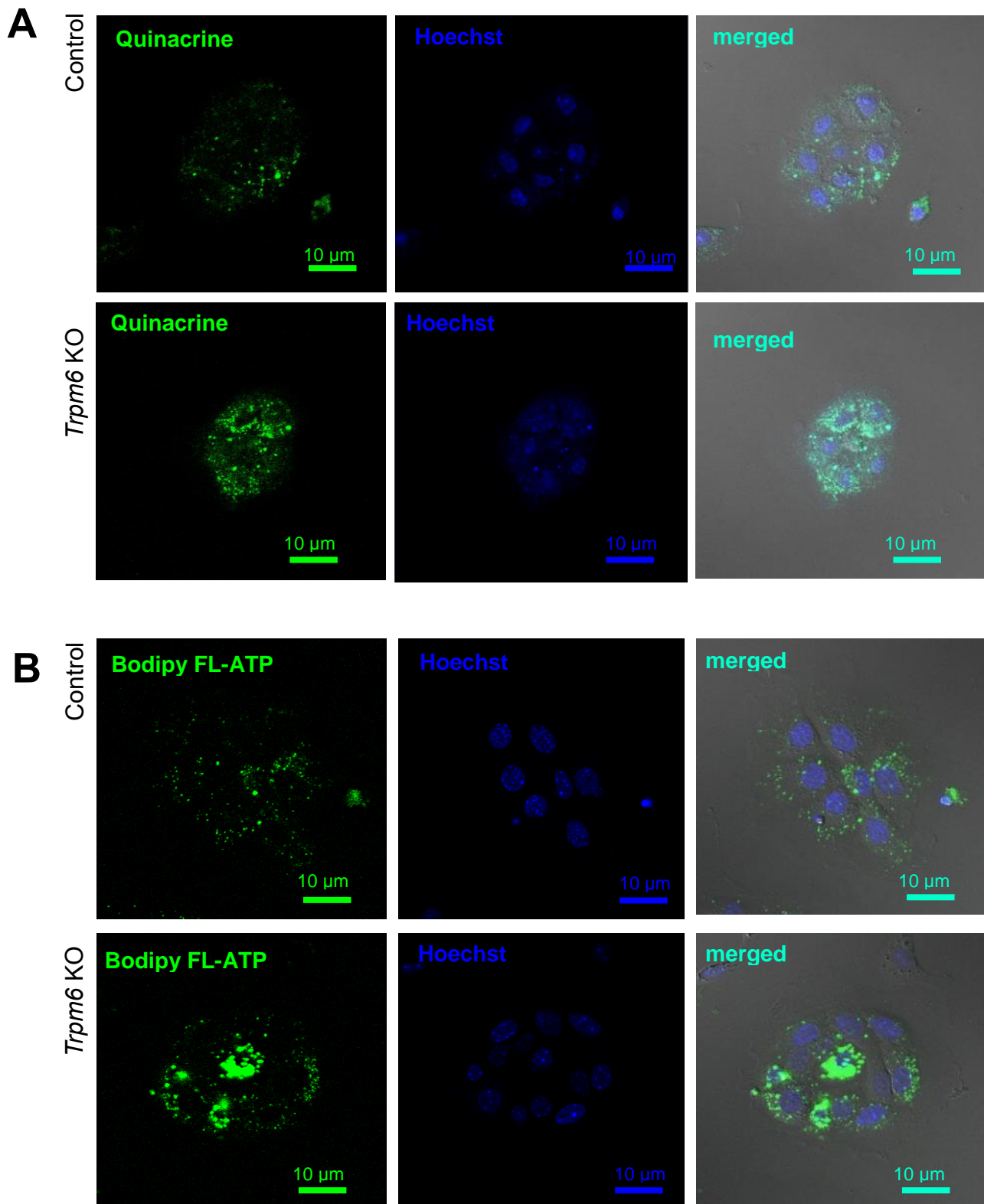


**Figure 43. Staining of primary AT2 cells isolated from *Trpm6*<sup>fl/+</sup> (Control) and *Trpm6*<sup>A17/Δ17</sup>;Sox2-Cre (KO) mice with fluorescent dyes.** Primary AT2 cells were stained with (A) quinacrine and (B) BODIPY FL-ATP, indicating the presence of intravesicular ATP in LBS. Cells were incubated with quinacrine dye for 15 min and with BODIPY ATP for 3 h. Representative fluorescence, Hoechst and merged images of primary AT2 cells are shown (n=5 mice per genotype).

## 6. Discussion

Previously, independent studies of several laboratories have established that the homologous channel-kinases TRPM6 and TRPM7 control the cellular uptake of divalent cations in epithelial cells, including  $\text{Ca}^{2+}$ ,  $\text{Mg}^{2+}$  and  $\text{Zn}^{2+}$  [31, 36]. The pathophysiological relevance of such TRPM6 function was demonstrated in clinical studies of Hypomagnesemia with secondary hypocalcemia (HSH) syndrome caused by loss-of-function mutations in the human *TRPM6* gene [20, 21]. Moreover, a detailed analysis of gene-modified mice showed that the channel-kinase TRPM6 is vital for the placental and intestinal  $\text{Mg}^{2+}$  supply of the organism [36]. In the present work, we identified a new role of TRPM6 in homeostatic control of  $\text{Mg}^{2+}$  in the respiratory system and delineated the pathophysiological importance of this process. Our results support the new concept (Figure 44) of TRPM6 operating in AT2 cells to regulate the ALF balance of  $\text{Mg}^{2+}$  a mechanism vital for maintaining the air-liquid interface in the alveoli. Our data suggest that the lack of in TRPM6 channel activity induced respiratory emphysema, implying that dietary  $\text{Mg}^{2+}$  supplementation may be also beneficial in the prevention or delay of emphysema in humans.

### 6.1. Expression patterns of TRPM6 in the lung

The current literature indicates that TRPM6 is most abundantly present on the apical surface (luminal side) of the transporting epithelia in the kidney (primarily in the DCT segment of the nephron), enterocytes of the colon and placental trophoblast to control transcellular transport of  $\text{Mg}^{2+}$  [22, 36]. Moreover, pioneering studies suggested that TRPM6 can be expressed in other organs, for instance, in testis, heart and the lung [21]. However, the presence of TRPM6 in particular respiratory cells and the corresponding function of TRPM6 have remained unknown.

Consequently, one of the aims of the present study was to investigate the expression pattern of *Trpm6* in the lung of mice.

In the first line of our experiments, we used a new mouse strain, *Trpm6*<sup>Cre/+</sup>;*Rosa26*<sup>τGFP/+</sup>, which allows tracing of cells expressing of τGFP under the control of *Trpm6* promoter [203]. Using such a strategy, we could perform localization of *Trpm6* by the identification of τGFP positive

cells in lung tissue. Furthermore, we colocalized the  $\tau$ GFP expression indicative for *Trpm6* mRNA in the alveolar epithelium by labelling the cryosections with an AT2 cells marker (anti ABCa3 labelled AlexaFluor633). In our studies, we could detect that all  $\tau$ GFP positive cells colocalized with the AT2 cells marker, ABCa3.

Our second approach relied on *in situ* hybridization (ISH) techniques. Previously, our group employed this method to show that *Trpm6* transcripts are abundantly present in placental trophoblasts, DCT cells of the kidney and intestinal enterocytes [36]. In the present study, we used the previously characterized *Trpm6* anti-sense probe [36]. In accord with our results obtained with *Trpm6*<sup>Cre/+</sup>; *Rosa26*<sup>GFP/+</sup> mice, we could show that *Trpm6* mRNA was abundantly present in bronchial epithelial cells and AT2 cells. To summarize, we showed the expression pattern of *Trpm6* in the lung with two independent methods.

Finally, we employed q-PCR technique to examine the levels of *Trpm6* transcripts in RNA extracted from lungs of control and *Trpm6*-deficient mice. Since we used PCR primers detecting the floxed exon 17 of *Trpm6*, *Trpm6* transcripts were readily detectable in control tissues and absent in lungs from *Trpm6*-deficient mice, reinforcing our previous conclusion that Sox2-Cre transgene enables to efficiently recombine the floxed *Trpm6* allele in the whole body [21, 28].

To summarize, our data indicate that *Trpm6* is explicitly expressed in bronchial epithelial cells and AT2 cells.

## 6.2. Pulmonary emphysema in *Trpm6*-deficient mice

In order to uncover the physiological role of TRPM6 in the lung, we conducted systematic phenotyping of mice with a global *Trpm6* null mutation using an array of functional, histological and biochemical techniques. Notably, these experiments collectively support the notion that genetic inactivation of *Trpm6* triggered severe pulmonary emphysema in mice. Thus, our histological examination of the lung sections demonstrated a significant enlargement of alveolar space, representing the key morphological indicator of parenchymal destruction during lung emphysema in human patients as well as in animal models [65, 210-212]. We also noted that this phenotype was not detectable in 4-weeks old mice but was present in all 8-weeks old *Trpm6*-deficient mice (100% penetrance), hence ruling out that destruction of lung parenchyma reflected a development defect of *Trpm6*-deficient mice. Furthermore, we recognized that the morphological changes were more pronounced in 12-weeks old *Trpm6*-

deficient individuals, suggesting that the severity of the respiratory phenotype in *Trpm6*-deficient mice was age-dependent. We were not able to conduct such experiments with older groups of mice since none of the *Trpm6*-deficient mice could survive after ~16 weeks of the postnatal life [36].

Emphysema in human patients is defined as a loss of elastic recoil within the lung [226, 227]. Parenchymal destruction in men is associated with increased lung resistance and compliance [165, 228-230]. Consequently, homologous changes in respiratory parameters are broadly used for diagnostic of emphysema in animal models [65, 213]. To this end, we examined whether lung function of 8- and 12-weeks old *Trpm6*-deficient mice were affected similarly. Our experiments used the FlexiVent system, which allows mechanical ventilation of the mouse lungs with a given pressure [228, 229, 231]. Forced oscillation technique (FOT) was applied [213] to measure pulmonary resistance (R) and dynamic compliance ( $C_{dyn}$ ) as parameters providing sufficient detailed insight into pulmonary mechanics. R reflects the parenchymal viscosity and narrowing of the conducting airways, whereas  $C_{dyn}$  corresponds to the elasticity of the lung parenchyma [232]. Remarkably, we observed that 8-weeks old *Trpm6*-deficient mice displayed increased the R and  $C_{dyn}$  values and that these alterations were more robust in 12-weeks old *Trpm6*-deficient mice.

Taken together, we concluded that *Trpm6*-deficient mice spontaneously develop pulmonary emphysema.

### **6.3. $Mg^{2+}$ dependency of the respiratory phenotype of *Trpm6*-deficient mice**

Recently, our group has demonstrated that global deletion of *Trpm6* in mice resulted in severe organismal  $Mg^{2+}$  deficiency [36]. In particular, 8-weeks old *Trpm6*-deficient mice displayed a significant reduction of  $Mg^{2+}$  levels in the blood serum and bones associated with abnormal intestinal absorption of  $Mg^{2+}$ . *Trpm6*-deficient mice showed normal development and physical appearance at the weaning stage (2-4-weeks old mice). However, soon after weaning, *Trpm6*-deficient individuals maintained on a standard animal chow contain 0.22%  $Mg^{2+}$  stopped to grow and displayed a high mortality rate. *Trpm6*-deficient mice were not viable after 16 weeks of postnatal life [36]. In many regards, the phenotype of *Trpm6*-deficient mice recapitulated the clinical presentation of HSH patients carrying loss-of-function mutations in *TRPM6* [20, 21, 36].

Interestingly, clinical symptoms of HSH patients were fully ameliorated by dietary  $Mg^{2+}$  supplementation, indicating that the HSH syndrome is primarily driven by systemic  $Mg^{2+}$  deficiency likely due to a defect in nutritional intake of  $Mg^{2+}$  [20, 21]. In line with this notion, weaned *Trpm6*-deficient mice maintained on an  $Mg^{2+}$ -enriched diet (0.75%  $Mg^{2+}$ ) rescued hypomagnesemia, growth failure and mortality of the *Trpm6*-deficient mice [36]. Accordingly, we asked whether  $Mg^{2+}$  supplementation enables to reverse the respiratory phenotype of *Trpm6*-deficient mice. To address this question, we generated a new group of 4-weeks old *Trpm6*-deficient and control littermates, which after weaning received  $Mg^{2+}$ -enriched chow. Remarkably, we found that such treatment fully normalized morphological and functional parameters of the lung of *Trpm6*-deficient mice.

Because lung function in *Trpm6*-deficient mice were affected by  $Mg^{2+}$  deficiency, we asked whether TRPM6 plays a role in the alveolar balance of  $Mg^{2+}$ . Of note, concentrations of  $Na^+$ ,  $K^+$  and  $Cl^-$  in ALF were found to be equal to blood serum levels [124], and it was suggested that such balance is maintained by active transcellular transport of these ions driven by apically localized  $Na^+$ ,  $K^+$  and  $Cl^-$  channels [78, 233, 234]. Accumulating evidence indicates that in the alveolar airspace, AT2 cells are primarily responsible for transcellular transport of  $Na^+$ ,  $K^+$  and  $Cl^-$  [78, 235, 236].

A similar mechanism was also anticipated for the upstream pulmonary epithelium of bronchi, but particular cellular and molecular entities remain to be discovered. Of note, a few available studies proposed that  $Ca^{2+}$  and  $Mg^{2+}$  concentrations in ALF are significantly lower than in the blood space [123, 124] implying that active transcellular transport of  $Ca^{2+}$  and  $Mg^{2+}$  from ALF to serum should exist.

It has been shown previously, that TRPM6 operates on the apical cell surface of the DCT cells of the kidney and intestinal enterocytes to mediate uptake of  $Mg^{2+}$  from the luminal side of transporting epithelia [22, 237]. Given the fact that TRPM6 is expressed in AT2 cells, we hypothesized that analogously to the situation in renal and intestinal cells, TRPM6 regulates the transport of  $Mg^{2+}$  from ALF to serum through AT2 cells. Accordingly, we assumed that the lack of TRPM6 could (i) reduce intracellular  $Mg^{2+}$  contents in AT2 cells leading to an abnormal function of these metabolically active cells and (ii) affecting extracellular (ALF) levels of  $Mg^{2+}$  which can negatively impact functions of other alveolar cells such as AT1 cells and alveolar macrophages.

To this end, we compared elementary levels of divalent cations in the serum and ALF in 12-weeks old control and *Trpm6*-deficient mice and found out that  $Mg^{2+}$  concentration in the serum of *Trpm6*-deficient mice was only 30% of that in the control littermates (Figure 25). These results are in line with our previous analysis of 8-weeks old *Trpm6*-deficient mice [36].

Moreover, we found that elementary  $Mg^{2+}$  concentrations were 3.1 folds higher in ALF of *Trpm6*-deficient mice (Figure 26). However, the dietary  $Mg^{2+}$  supplementation caused an elevation of  $Mg^{2+}$  levels in the blood serum to the normal range found in control mice maintained on a regular diet. Besides,  $Mg^{2+}$  supplementation fully normalized concentrations of  $Mg^{2+}$  in ALF. These results suggest that *Trpm6*-deficient mice displayed an abnormal balance of  $Mg^{2+}$  in ALF, supporting the idea that TRPM6 plays a critical role in  $Mg^{2+}$  uptake in AT2 cells from ALF.

Our findings also suggest that HSH patients may display not yet recognized symptoms of abnormal respiration. Furthermore, our study stresses that clinical symptoms of patients suffering from other inherited forms of  $Mg^{2+}$  deficiency, for instance Bartter syndrome type 3, Gitelman syndrome type 4, FHHNC type 1 [238], may also develop alterations in lung function.

#### **6.4. No involvement of TRPM6 kinase activity in the respiratory phenotype of *Trpm6*-deficient mice**

TRPM6 is a bifunctional protein consisting of a channel and a kinase unit [17, 18, 23]. The functional and physiological roles of the kinase domain of TRPM6 remains poorly understood. For instance, the physiological targets for phosphorylation by the TRPM6 kinase domain are unknown [23]. However, several Ser and Thr residues located in a 'substrate' segment of TRPM6 were found to be phosphorylated by the kinase domain [23, 239].

Recently, Ferioli *et al.* [34] reported that autophosphorylation levels of TRPM6 reliably reflects the kinase activity of TRPM6. Using a specific anti-p-TRPM6 antibody, Ferioli *et al.* [34] demonstrated that a 'kinase-dead' point mutation K1810R in mouse TRPM6 fully ablated autophosphorylation of T1730 in TRPM6 [34]. In analogy to TRPM7 [55], it was predicted that K1810 is located in the catalytic site of the TRPM6 kinase domain and that the K1810R mutation should cause 100% suppression of kinase activity. In line with such an idea, the anti-p-TRPM6 antibody was able to detect WT, but not the K1810R or T1730A variants of TRPM6 [34]. In addition, Ferioli *et al.* [34] observed that the 'kinase-dead' mutation in TRPM6 did not induce remarkable alterations in TRPM6 currents, reinforcing the idea [34] that 'kinase-dead' variants of TRPM6 and TRPM7 are very instrumental for specific ablation of the kinase activity without a significant impact on the channel units of these bi-functional proteins.

In order to investigate the physiological role of TRPM6 kinase, in particular, to elucidate its contribution to the respiratory phenotype of *Trpm6*-deficient mice, we generated a new mouse

strain carrying a constitutive kinase-dead K1810R mutation in *Trpm6* (*Trpm6<sup>R/R</sup>*). During early postnatal life and after weaning, kinase-dead TRPM6 mice developed normally and did not show signs of reduced survival or behavioural abnormalities. In particular, the mutants showed a normal gain of weight, fertility and overall physical appearance. In accord, *Trpm6<sup>R/R</sup>* mice displayed normal  $Mg^{2+}$  levels in the blood serum and ALF samples, and no changes in morphology and respiratory characteristics of the lung. Hence, our findings support the concept that phenotypes of *Trpm6*-deficient mice, i.e. systemic  $Mg^{2+}$  deficiency incompatible with the embryonic development and postnatal survival, are primarily driven by the lack of TRPM6 channel unit rather than by disruption of the TRPM6 kinase function. Furthermore, *Trpm6<sup>R/R</sup>* mice clearly showed that the kinase moiety of TRPM6 played no role in the development of emphysema in *Trpm6*-deficient mice.

## **6.5. Impaired production of respiratory surfactants in the lung of *Trpm6*-deficient mice**

A critical function of metabolically active AT2 cells is the production, exocytosis and recycling of respiratory surfactants. Interestingly, mouse strains carrying null mutations in the genes encoding major surfactant proteins (SP-A, SP-C and SP-D) develop lung emphysema spontaneously [112, 178, 180, 181, 183], resembling in many regards the respiratory phenotype of *Trpm6*-deficient mice. For instance, SP-D-deficient mice displayed emphysema-like changes recognized by an enlargement of alveolar air spaces, diminished number of AT2 cells, increased alveolar size and decreased alveolar surface area [112]. As expected, surfactant homeostasis is disturbed in SP-D deficient mice, which is indicated by the presence of giant lamellar bodies in AT2 cells [112, 184]. Besides, SP-C-deficient mice developed emphysema associated with accumulations of intracellular lipids in AT2 cells [183]. In accord, SP-C deficient mice demonstrated abnormal respiratory parameters typical for emphysema [183]. Mice lacking SP-A and SP-D revealed an increase in mean chord lengths indicating air space enlargement. The stereological analysis demonstrated that SPA-D deficient mice developed pulmonary emphysema [180].

Overall, these experiments indicate that a defect in the homeostasis of respiratory surfactants is sufficient for induction of lung emphysema. Accordingly, we hypothesized that TRPM6-dependent depletion of  $Mg^{2+}$  in AT2 cells could affect the metabolic capability of these cells, including production/recycling of surfactants. To test this hypothesis, we investigated the

contents of SP-A, SP-B, SP-C and SP-D proteins in BAL samples of *Trpm6*-deficient mice by electron microscopy (EM) of lung tissues. Both approaches revealed a severe decline in the content of respiratory surfactant in alveolar airspace. In accord with this notion, we observed accumulation of the LB inside of AT2 cells in tissue sections from *Trpm6*-deficient mice. However, SP-A, SP-B, SP-C and SP-D levels in BAL were normal in *Trpm6*-deficient mice maintained on a  $Mg^{2+}$ -enriched diet. Hence, we concluded that lung emphysema in *Trpm6*-deficient mice was caused by a severe defect in production and release of respiratory surfactants and that, in turn, this deficit was triggered by  $Mg^{2+}$  deprivation of AT2 cells. One possible explanation of such a phenomenon relies on a critical role of intracellular  $Mg^{2+}$  in energy metabolism [223] and protein synthesis [223].

Next, we asked whether abnormal metabolism of surfactants in AT2 cells can be recapitulated *in vitro* using primary isolated AT2 cells from *Trpm6*-deficient mice. To this end, we isolated AT2 cells from *Trpm6*<sup>Cre/+</sup>; *Rosa26*<sup>τGFP/+</sup> transgenic mice and controls. Cultured τGFP-positive cells morphologically resembled AT2 cells and expressed the LB markers (ABCa3, LyTR) as expected from our histological assessment of tissue sections from *Trpm6*<sup>Cre/+</sup>; *Rosa26*<sup>τGFP/+</sup>. The lack of TRPM6 is associated with a significantly increased content of LB, reproducing our findings by biochemical and EM analysis of lung tissue sections. Finally, using quinacrine and BODIPY FL-ATP, the fluorescent probe for ATP in LB [207, 225], we detected a significantly increased vesicular content of ATP in LB in cells lacking TRPM6, suggesting that ATP metabolism was abnormal in *Trpm6*-deficient mice (Figure 43). Of note, it was proposed [240] that during exocytosis the pool of ATP in LB is co-released with lung surfactants in the alveolar airspace and that such extracellular ATP modulates the activity of AT1 and AT2 cells [240]. Besides, extracellular ATP elicits a positive feedback effect on the production of surfactant proteins by AT2 cells [241]. Taken together, we anticipate that  $Mg^{2+}$  deprivation of AT2 cells can elicit multiple secondary pathophysiological changes in alveolar cells.

A possible explanation of the robust response of AT2 cells to  $Mg^{2+}$  deprivation relies on a critical role of intracellular  $Mg^{2+}$  in energy metabolism and protein synthesis [223, 242]. Under physiologic conditions, free cytosolic  $Mg^{2+}$  concentrations are in the range of 1-2 mM [242]. The total  $Mg^{2+}$  content varies between 10-20 mM [224, 242]. The concentration of ionised  $Mg^{2+}$  is 'buffered' by ATP, nucleic acids and proteins [242]. Thus, ATP binds with a  $K_d$  value of ~50  $\mu$ M [242]. Therefore,  $Mg^{2+}$  in the cytosol exists in a complex with ATP (MgATP) [224, 242, 243]. Because of its abundance (~5 mM), ATP represents the primary intracellular  $Mg^{2+}$  'buffer' [242]. MgATP is the most metabolically active form of ATP in most biochemical reactions [224, 242]. Accordingly,  $Mg^{2+}$  deprivation will reduce MgATP levels and slow down cellular energy metabolism [242]. Besides, a single ribosome binds around ~170  $Mg^{2+}$  ions [242, 244] and a reduction in free cytosolic  $Mg^{2+}$  causes a suppression of the synthesis [245]. Since the primary

function of AT2 cells is constant massive production of surfactant lipids and proteins [82, 89, 90], it is well thinkable that the whole metabolism of AT2 cells relies on a tight cellular balance of intracellular  $Mg^{2+}$ .

## 6.6. $Mg^{2+}$ homeostasis and COPD

$Mg^{2+}$  is implicated in many physiological processes in the airways such as bronchodilation and contraction of smooth airway muscles [246]. There is growing evidence that  $Mg^{2+}$  deficiency contributes to exacerbations and readmissions in patients with chronic lung diseases [247, 248]. Hypomagnesemia associated with lower serum  $Mg^{2+}$  levels is observed in COPD patients with severe symptoms compared to stable patients [247-249]. Clinical studies suggest that hypomagnesemia is very common in chronic pulmonary disease patients (accounting up to 60%) [248, 250, 251]. Moreover, the mortality rate was found higher in patients with hypomagnesemia compared to patients with normal  $Mg^{2+}$  balance [248, 250].

COPD patients, including subjects with emphysema, suffer from bronchospasms, defined as the inability of clear secretions causing reduced pulmonary gas exchange [252-255]. Furthermore,  $Mg^{2+}$  administration is useful in alleviating symptoms in these patients [246, 256]. Similarly, dietary  $Mg^{2+}$  intake has been related to improved lung function, reduced airway hyperreactivity and respiratory symptoms in COPD patients [257, 258]. In addition, inhaled  $Mg^{2+}$  (as nebulized  $MgSO_4$ ) and intravenous  $Mg^{2+}$  administration have been shown to promote better lung function and bronchodilation [259-263]. Additionally, another clinical study [252] suggested a positive correlation between the serum  $Mg^{2+}$  levels and the number of acute exacerbations. Finally, disease progression has been associated with serum  $Mg^{2+}$  levels in patients with COPD [252]. Along these lines, systemic or lung-restricted  $Mg^{2+}$  deficiency can be considered as the risk factor of COPD. Therefore, improved nutritional  $Mg^{2+}$  uptake, intravenous  $Mg^{2+}$  administration and inhaled  $Mg^{2+}$  salts can be considered as therapeutic treatment of patients with chronic lung diseases including COPD [248, 257].

## 6.7. The suggested model for the role of TRPM6 in AT2 cells

Based on our results, we suggest the following model for the role of TRPM6 in the alveolar epithelium (Figure 44). We propose that TRPM6 is required for  $Mg^{2+}$  uptake in AT2 cells and that such a mechanism is crucial for alveolar homeostasis of  $Mg^{2+}$  and respiratory surfactants. Consequently, genetic inactivation of *Trpm6* results in abnormally high concentrations of  $Mg^{2+}$  in ALF likely due to a defect in transcellular  $Mg^{2+}$  exchange between the blood and ALF. Moreover,  $Mg^{2+}$  deprivation of AT2 cells leads to declined metabolic activity of these cells and inability to properly produce and/or release respiratory surfactants in ALF. Consequently, such alterations trigger the development of pulmonary emphysema. We also suggest that the respiratory phenotype of the *Trpm6*-deficient mice is primarily attributed to the lack of TRPM6 channel activity rather than its kinase moiety and that dietary  $Mg^{2+}$  supplementation is sufficient to fully reverse the lung emphysema in the *Trpm6*-deficient mice.

Our findings also stress new intriguing questions to be addressed in follow-up studies. For, instance, it will be crucial to investigate the role of related TRPM7 channels in AT2 cells. Previous publications [23, 35, 36] have shown that TRPM6 and TRPM7 functionally interplay in the control of the transcellular transport of divalent cations and we anticipate that conditional AT2-restricted inactivation of TRPM7 will have a substantial impact on the homeostatic balance of divalent cations in the alveolar airspace. Our experiments revealed that expression patterns of respiratory TRPM6 are limited to AT2 cells and bronchial epithelial cells. While the channel's role in AT2 cells was analysed in this thesis, TRPM6 function in bronchial epithelial cells needs to be elucidated in the future. Hence, it will be interesting to compare the respiratory characteristics of mice strains carrying cell type-restricted ablation of *Trpm6*. Finally, our results proposed that systemic  $Mg^{2+}$  deficiency, a surprisingly frequent situation in humans [223], is a risk factor for emphysema and that new clinical studies can be designed to elucidate the impact of  $Mg^{2+}$  balance on prevention and treatment of COPD.

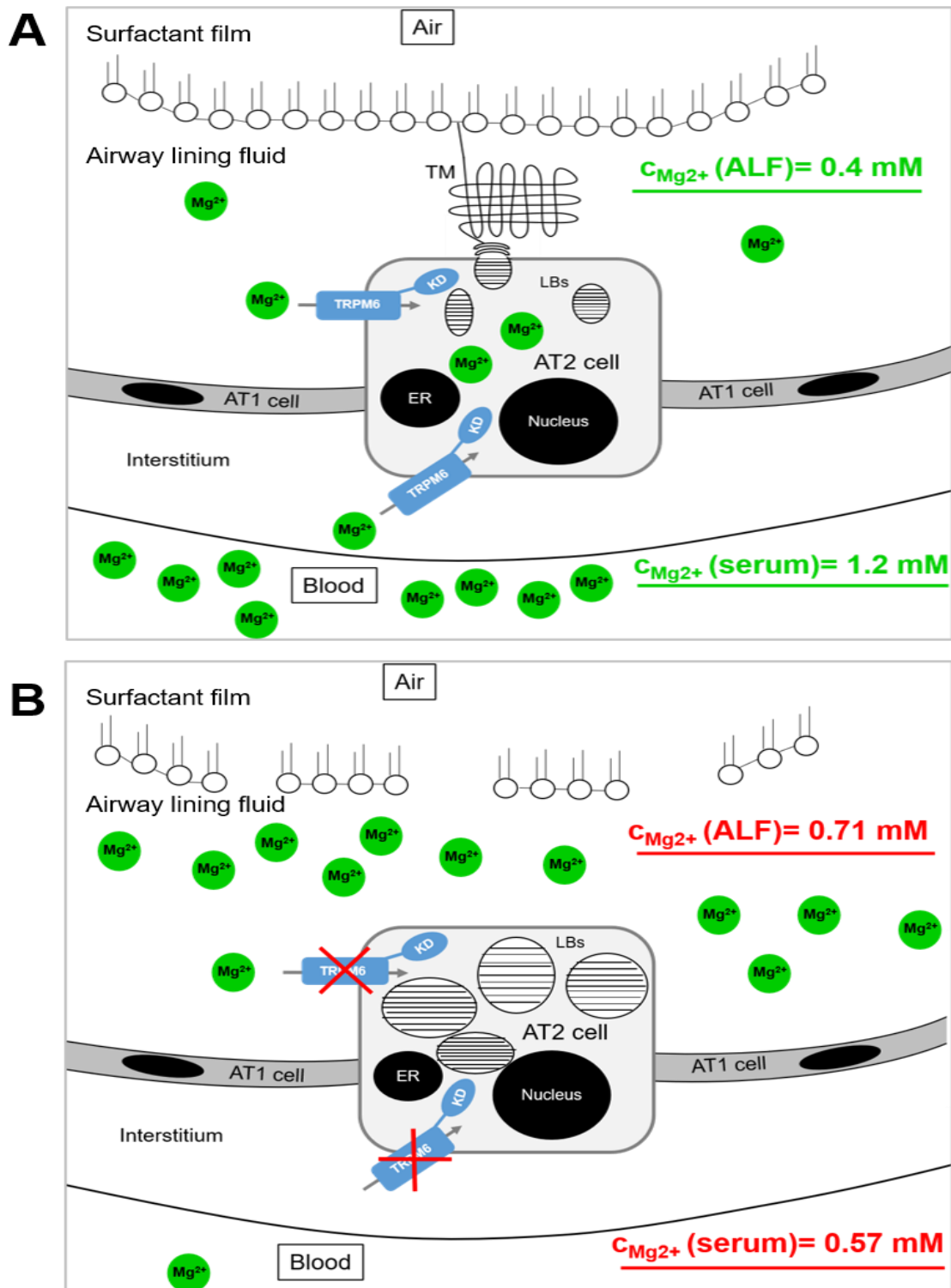


**Figure 44. A proposed model for the role of TRPM6 channels in respiratory balance of  $Mg^{2+}$ .** (A) In *Trpm6<sup>fl/+</sup>* (Control) AT2 cells, TRPM6 regulates  $Mg^{2+}$  uptake in highly metabolically active AT2 cells. (B) In *Trpm6 <sup>$\Delta$ 17/ $\Delta$ 17</sup>;Sox2-Cre* (KO) mice,  $Mg^{2+}$  influx in AT2 cells is suppressed associated with accumulation of  $Mg^{2+}$  in ALF. Consequently,  $Mg^{2+}$ -deprived AT2 cells shut down production of pulmonary surfactants leading to disruption of liquid-air interface in alveoli. AT1 = alveolar epithelial cells type 1, AT2 = alveolar epithelial cells type 2, LB = lamellar bodies, TM = tubular myelin, ER = endoplasmic reticulum, ALF = alveolar lining fluid, KD = kinase-domain.

## 7. Conclusions

The present study aimed to define the pathophysiological role of the channel-kinase TRPM6 in the lung by systemic assessment of mouse strains with a global null mutation disrupting the whole *Trpm6* gene and kinase-dead point mutation affecting the kinase moiety of *Trpm6*.

Accordingly, we draw the following conclusions:

1. TRPM6 is explicitly expressed in bronchial epithelial cells and alveolar type 2 (AT2) cells.
2. Global deletion of *Trpm6* in mice resulted in progressive alterations in morphology, biochemical characteristics and function of the lung indicative of pulmonary emphysema.
3. Dietary Mg<sup>2+</sup> supplementations rescued the respiratory phenotype of *Trpm6*-deficient mice.
4. Global ablation of TRPM6 kinase activity in mice did not cause changes in morphology or function of the lung reinforcing the critical role of the lack of TRPM6 channel activity in the development of emphysema in *Trpm6*-deficient mice.
5. Examination of tissue sections and cultured AT2 cells isolated from *Trpm6*-deficient mice revealed abnormal production and release of pulmonary surfactants likely in an ATP-dependent fashion.

---

## References

1. Clapham, D.E., *TRP channels as cellular sensors*. Nature, 2003. **426**(6966): p. 517-24.
2. Gees, M., B. Colson, and B. Nilius, *The role of transient receptor potential cation channels in Ca<sup>2+</sup> signaling*. Cold Spring Harb Perspect Biol, 2010. **2**(10): p. a003962.
3. Venkatachalam, K. and C. Montell, *TRP channels*. Annu Rev Biochem, 2007. **76**: p. 387-417.
4. Montell, C., *Physiology, phylogeny, and functions of the TRP superfamily of cation channels*. Sci STKE, 2001. **2001**(90): p. re1.
5. Hoenderop, J.G., B. Nilius, and R.J. Bindels, *Calcium absorption across epithelia*. Physiol Rev, 2005. **85**(1): p. 373-422.
6. Wu, L.J., Sweet, T. B., & Clapham, D. E., *Current progress in the mammalian TRP ion channel family*. International Union of Basic and Clinical Pharmacology. LXXVI.Pharmacological reviews, 2010. **62**(3): p. 381–404.
7. Montell, C., *The TRP superfamily of cation channels*. Sci STKE, 2005. **2005**(272): p. re3.
8. Nilius, B., *TRP channels in disease*. Biochim Biophys Acta, 2007. **1772**(8): p. 805-12.
9. Nilius, B. and G. Owsianik, *The transient receptor potential family of ion channels*. Genome Biol, 2011. **12**(3): p. 218.
10. Zhang, X., et al., *Organelle TRP channels*. Nat Struct Mol Biol, 2018. **25**(11): p. 1009-1018.
11. Owsianik, G., et al., *Structure-function relationship of the TRP channel superfamily*. Rev Physiol Biochem Pharmacol, 2006. **156**: p. 61-90.
12. Vriens, J., et al., *Invertebrate TRP proteins as functional models for mammalian channels*. Pflugers Arch, 2004. **449**(3): p. 213-26.
13. Montell, C., L. Birnbaumer, and V. Flockerzi, *The TRP channels, a remarkably functional family*. Cell, 2002. **108**(5): p. 595-8.
14. Fleig, A. and V. Chubanov, *Trpm7*. Handb Exp Pharmacol, 2014. **222**: p. 521-46.
15. Mei, Z.Z., et al., *Intracellular coiled-coil domain engaged in subunit interaction and assembly of melastatin-related transient receptor potential channel 2*. J Biol Chem, 2006. **281**(50): p. 38748-56.
16. Tsuruda, P.R., D. Julius, and D.L. Minor, Jr., *Coiled coils direct assembly of a cold-activated TRP channel*. Neuron, 2006. **51**(2): p. 201-12.
17. Schlingmann, K.P., et al., *TRPM6 and TRPM7--Gatekeepers of human magnesium metabolism*. Biochim Biophys Acta, 2007. **1772**(8): p. 813-21.

18. Pedersen, S.F., G. Owsianik, and B. Nilius, *TRP channels: an overview*. Cell Calcium, 2005. **38**(3-4): p. 233-52.
19. Nadler, M.J., et al., *LTRPC7 is a Mg.ATP-regulated divalent cation channel required for cell viability*. Nature, 2001. **411**(6837): p. 590-5.
20. Schlingmann, K.P., et al., *Hypomagnesemia with secondary hypocalcemia is caused by mutations in TRPM6, a new member of the TRPM gene family*. Nat Genet, 2002. **31**(2): p. 166-70.
21. Walder, R.Y., et al., *Mutation of TRPM6 causes familial hypomagnesemia with secondary hypocalcemia*. Nat Genet, 2002. **31**(2): p. 171-4.
22. Chubanov, V., et al., *Disruption of TRPM6/TRPM7 complex formation by a mutation in the TRPM6 gene causes hypomagnesemia with secondary hypocalcemia*. Proc Natl Acad Sci U S A, 2004. **101**(9): p. 2894-9.
23. Chubanov, V. and T. Gudermann, *Trpm6*. Handb Exp Pharmacol, 2014. **222**: p. 503-20.
24. Riazanova, L.V., et al., *[Novel type of signaling molecules: protein kinases covalently linked to ion channels]*. Mol Biol (Mosk), 2001. **35**(2): p. 321-32.
25. Runnels, L.W., L. Yue, and D.E. Clapham, *TRP-PLIK, a bifunctional protein with kinase and ion channel activities*. Science, 2001. **291**(5506): p. 1043-7.
26. Chubanov, V., L. Mittermeier, and T. Gudermann, *Role of kinase-coupled TRP channels in mineral homeostasis*. Pharmacol Ther, 2018. **184**: p. 159-176.
27. Voets, T., et al., *TRPM6 forms the Mg<sup>2+</sup> influx channel involved in intestinal and renal Mg<sup>2+</sup> absorption*. J Biol Chem, 2004. **279**(1): p. 19-25.
28. Groenestege, W.M., et al., *The epithelial Mg<sup>2+</sup> channel transient receptor potential melastatin 6 is regulated by dietary Mg<sup>2+</sup> content and estrogens*. J Am Soc Nephrol, 2006. **17**(4): p. 1035-43.
29. Fonfria, E., et al., *Tissue distribution profiles of the human TRPM cation channel family*. J Recept Signal Transduct Res, 2006. **26**(3): p. 159-78.
30. Kunert-Keil, C., et al., *Tissue-specific expression of TRP channel genes in the mouse and its variation in three different mouse strains*. BMC Genomics, 2006. **7**: p. 159.
31. Mittermeier, L., et al., *TRPM7 is the central gatekeeper of intestinal mineral absorption essential for postnatal survival*. Proc Natl Acad Sci U S A, 2019. **116**(10): p. 4706-4715.
32. Chubanov, V., et al., *Emerging roles of TRPM6/TRPM7 channel kinase signal transduction complexes*. Naunyn Schmiedebergs Arch Pharmacol, 2005. **371**(4): p. 334-41.
33. Ramsey, I.S., M. Delling, and D.E. Clapham, *An introduction to TRP channels*. Annu Rev Physiol, 2006. **68**: p. 619-47.

34. Ferioli, S., et al., *TRPM6 and TRPM7 differentially contribute to the relief of heteromeric TRPM6/7 channels from inhibition by cytosolic Mg(2+) and Mg.ATP*. *Sci Rep*, 2017. **7**(1): p. 8806.
35. Monteilh-Zoller, M.K., et al., *TRPM7 provides an ion channel mechanism for cellular entry of trace metal ions*. *J Gen Physiol*, 2003. **121**(1): p. 49-60.
36. Chubanov, V., et al., *Epithelial magnesium transport by TRPM6 is essential for prenatal development and adult survival*. *Elife*, 2016. **5**.
37. Walder, R.Y., et al., *Mice defective in Trpm6 show embryonic mortality and neural tube defects*. *Hum Mol Genet*, 2009. **18**(22): p. 4367-75.
38. Schmitz, C., et al., *Regulation of vertebrate cellular Mg2+ homeostasis by TRPM7*. *Cell*, 2003. **114**(2): p. 191-200.
39. Ryazanova, L.V., et al., *TRPM7 is essential for Mg(2+) homeostasis in mammals*. *Nat Commun*, 2010. **1**: p. 109.
40. Sahni, J. and A.M. Scharenberg, *TRPM7 ion channels are required for sustained phosphoinositide 3-kinase signaling in lymphocytes*. *Cell Metab*, 2008. **8**(1): p. 84-93.
41. Clark, K., et al., *TRPM7, a novel regulator of actomyosin contractility and cell adhesion*. *EMBO J*, 2006. **25**(2): p. 290-301.
42. Su, L.T., et al., *TRPM7 regulates cell adhesion by controlling the calcium-dependent protease calpain*. *J Biol Chem*, 2006. **281**(16): p. 11260-70.
43. Wei, C., et al., *Calcium flickers steer cell migration*. *Nature*, 2009. **457**(7231): p. 901-5.
44. Oancea, E., J.T. Wolfe, and D.E. Clapham, *Functional TRPM7 channels accumulate at the plasma membrane in response to fluid flow*. *Circ Res*, 2006. **98**(2): p. 245-53.
45. Numata, T., T. Shimizu, and Y. Okada, *Direct mechano-stress sensitivity of TRPM7 channel*. *Cell Physiol Biochem*, 2007. **19**(1-4): p. 1-8.
46. Zierler, S., et al., *Waixenicin A inhibits cell proliferation through magnesium-dependent block of transient receptor potential melastatin 7 (TRPM7) channels*. *J Biol Chem*, 2011. **286**(45): p. 39328-35.
47. Du, J., et al., *TRPM7-mediated Ca2+ signals confer fibrogenesis in human atrial fibrillation*. *Circ Res*, 2010. **106**(5): p. 992-1003.
48. Hanano, T., et al., *Involvement of TRPM7 in cell growth as a spontaneously activated Ca2+ entry pathway in human retinoblastoma cells*. *J Pharmacol Sci*, 2004. **95**(4): p. 403-19.
49. Jiang, J., et al., *Transient receptor potential melastatin 7-like current in human head and neck carcinoma cells: role in cell proliferation*. *Cancer Res*, 2007. **67**(22): p. 10929-38.
50. Kim, B.J., et al., *Suppression of transient receptor potential melastatin 7 channel induces cell death in gastric cancer*. *Cancer Sci*, 2008. **99**(12): p. 2502-9.

51. Touyz, R.M., *Transient receptor potential melastatin 6 and 7 channels, magnesium transport, and vascular biology: implications in hypertension*. Am J Physiol Heart Circ Physiol, 2008. **294**(3): p. H1103-18.
52. Tseveleki, V., et al., *Comparative gene expression analysis in mouse models for multiple sclerosis, Alzheimer's disease and stroke for identifying commonly regulated and disease-specific gene changes*. Genomics, 2010. **96**(2): p. 82-91.
53. Hermosura, M.C., et al., *A TRPM7 variant shows altered sensitivity to magnesium that may contribute to the pathogenesis of two Guamanian neurodegenerative disorders*. Proc Natl Acad Sci U S A, 2005. **102**(32): p. 11510-5.
54. Jin, J., et al., *Deletion of Trpm7 disrupts embryonic development and thymopoiesis without altering Mg<sup>2+</sup> homeostasis*. Science, 2008. **322**(5902): p. 756-60.
55. Kaitsuka, T., et al., *Inactivation of TRPM7 kinase activity does not impair its channel function in mice*. Sci Rep, 2014. **4**: p. 5718.
56. Ryazanova, L.V., et al., *Elucidating the role of the TRPM7 alpha-kinase: TRPM7 kinase inactivation leads to magnesium deprivation resistance phenotype in mice*. Sci Rep, 2014. **4**: p. 7599.
57. Jin, J., et al., *The channel kinase, TRPM7, is required for early embryonic development*. Proc Natl Acad Sci U S A, 2012. **109**(5): p. E225-33.
58. Vogelmeier, C.F., et al., *Global Strategy for the Diagnosis, Management, and Prevention of Chronic Obstructive Lung Disease 2017 Report: GOLD Executive Summary*. Eur Respir J, 2017. **49**(3).
59. Singh, D., et al., *Global Strategy for the Diagnosis, Management, and Prevention of Chronic Obstructive Lung Disease: the GOLD science committee report 2019*. Eur Respir J, 2019. **53**(5).
60. Jia, J., et al., *Cholesterol metabolism promotes B-cell positioning during immune pathogenesis of chronic obstructive pulmonary disease*. EMBO Mol Med, 2018. **10**(5).
61. Sharafkhaneh, A., N.A. Hanania, and V. Kim, *Pathogenesis of emphysema: from the bench to the bedside*. Proc Am Thorac Soc, 2008. **5**(4): p. 475-7.
62. Quaderi, S.A. and J.R. Hurst, *The unmet global burden of COPD*. Glob Health Epidemiol Genom, 2018. **3**: p. e4.
63. Diaz-Guzman, E. and D.M. Mannino, *Epidemiology and prevalence of chronic obstructive pulmonary disease*. Clin Chest Med, 2014. **35**(1): p. 7-16.
64. Pauwels, R.A., et al., *Global strategy for the diagnosis, management, and prevention of chronic obstructive pulmonary disease. NHLBI/WHO Global Initiative for Chronic Obstructive Lung Disease (GOLD) Workshop summary*. Am J Respir Crit Care Med, 2001. **163**(5): p. 1256-76.

65. John-Schuster, G., et al., *Cigarette smoke-induced iBALT mediates macrophage activation in a B cell-dependent manner in COPD*. *Am J Physiol Lung Cell Mol Physiol*, 2014. **307**(9): p. L692-706.
66. Cavailles, A., et al., *Comorbidities of COPD*. *Eur Respir Rev*, 2013. **22**(130): p. 454-75.
67. Zholos, A.V., *TRP Channels in Respiratory Pathophysiology: the Role of Oxidative, Chemical Irritant and Temperature Stimuli*. *Curr Neuropharmacol*, 2015. **13**(2): p. 279-91.
68. Grace, M.S., et al., *Transient receptor potential (TRP) channels in the airway: role in airway disease*. *Br J Pharmacol*, 2014. **171**(10): p. 2593-607.
69. Donley, E.R., M.R. Holme, and J.W. Loyd, *Anatomy, Thorax, Wall Movements*, in *StatPearls*. 2020: Treasure Island (FL).
70. Burlew, J.T., C. Weber, and K.P. Banks, *Anatomy, Thorax, Mediastinal Lymph Nodes*, in *StatPearls*. 2020: Treasure Island (FL).
71. Tucker, W.D., C. Weber, and B. Burns, *Anatomy, Thorax, Heart Pulmonary Arteries*, in *StatPearls*. 2020: Treasure Island (FL).
72. Pan, H., et al., *Comprehensive anatomic ontologies for lung development: A comparison of alveolar formation and maturation within mouse and human lung*. *J Biomed Semantics*, 2019. **10**(1): p. 18.
73. Effros, R.M. *Anatomy, development and physiology of the lungs*. 2006. DOI: doi:10.1038/gimo73.
74. Ma, J., B.K. Rubin, and J.A. Voynow, *Mucins, Mucus, and Goblet Cells*. *Chest*, 2018. **154**(1): p. 169-176.
75. Whitsett, J.A., *Airway Epithelial Differentiation and Mucociliary Clearance*. *Ann Am Thorac Soc*, 2018. **15**(Suppl 3): p. S143-S148.
76. Chuquimia, O.D., et al., *Alveolar epithelial cells are critical in protection of the respiratory tract by secretion of factors able to modulate the activity of pulmonary macrophages and directly control bacterial growth*. *Infect Immun*, 2013. **81**(1): p. 381-9.
77. Ryu, J.H., C.H. Kim, and J.H. Yoon, *Innate immune responses of the airway epithelium*. *Mol Cells*, 2010. **30**(3): p. 173-83.
78. Hollenhorst, M.I., K. Richter, and M. Fronius, *Ion transport by pulmonary epithelia*. *J Biomed Biotechnol*, 2011. **2011**: p. 174306.
79. Heidemann, S.M., et al., *Pathophysiology and Management of Acute Respiratory Distress Syndrome in Children*. *Pediatr Clin North Am*, 2017. **64**(5): p. 1017-1037.
80. Nova, Z., H. Skovierova, and A. Calkovska, *Alveolar-Capillary Membrane-Related Pulmonary Cells as a Target in Endotoxin-Induced Acute Lung Injury*. *Int J Mol Sci*, 2019. **20**(4).

81. Crandall, E.D. and M.A. Matthay, *Alveolar epithelial transport. Basic science to clinical medicine*. Am J Respir Crit Care Med, 2001. **163**(4): p. 1021-9.
82. Castranova, V., et al., *The alveolar type II epithelial cell: a multifunctional pneumocyte*. Toxicol Appl Pharmacol, 1988. **93**(3): p. 472-83.
83. Williams, M.C., *Alveolar type I cells: molecular phenotype and development*. Annu Rev Physiol, 2003. **65**: p. 669-95.
84. Fereol, S., et al., *Cell mechanics of alveolar epithelial cells (AECs) and macrophages (AMs)*. Respir Physiol Neurobiol, 2008. **163**(1-3): p. 3-16.
85. Stone, K.C., et al., *Allometric relationships of cell numbers and size in the mammalian lung*. Am J Respir Cell Mol Biol, 1992. **6**(2): p. 235-43.
86. Fehrenbach, H., *Alveolar epithelial type II cell: defender of the alveolus revisited*. Respir Res, 2001. **2**(1): p. 33-46.
87. Olajuyin, A.M., X. Zhang, and H.L. Ji, *Alveolar type 2 progenitor cells for lung injury repair*. Cell Death Discov, 2019. **5**: p. 63.
88. Devendra, G. and R.G. Spragg, *Lung surfactant in subacute pulmonary disease*. Respir Res, 2002. **3**: p. 19.
89. Lopez-Rodriguez, E., et al., *Lung surfactant metabolism: early in life, early in disease and target in cell therapy*. Cell Tissue Res, 2017. **367**(3): p. 721-735.
90. Daniels, C.B. and S. Orgeig, *Pulmonary surfactant: the key to the evolution of air breathing*. News Physiol Sci, 2003. **18**: p. 151-7.
91. Perez-Gil, J., *Structure of pulmonary surfactant membranes and films: the role of proteins and lipid-protein interactions*. Biochim Biophys Acta, 2008. **1778**(7-8): p. 1676-95.
92. Gordon, S.B. and R.C. Read, *Macrophage defences against respiratory tract infections*. Br Med Bull, 2002. **61**: p. 45-61.
93. Cheung, D.O., K. Halsey, and D.P. Speert, *Role of pulmonary alveolar macrophages in defense of the lung against Pseudomonas aeruginosa*. Infect Immun, 2000. **68**(8): p. 4585-92.
94. Rennard, S.I., et al., *Estimation of volume of epithelial lining fluid recovered by lavage using urea as marker of dilution*. J Appl Physiol (1985), 1986. **60**(2): p. 532-8.
95. Boucher, R.C., *Human airway ion transport. Part one*. Am J Respir Crit Care Med, 1994. **150**(1): p. 271-81.
96. Moliva, J.I., et al., *Molecular composition of the alveolar lining fluid in the aging lung*. Age (Dordr), 2014. **36**(3): p. 9633.
97. Griese, M., *Pulmonary surfactant in health and human lung diseases: state of the art*. Eur Respir J, 1999. **13**(6): p. 1455-76.

98. Frerking, I., et al., *Pulmonary surfactant: functions, abnormalities and therapeutic options*. Intensive Care Med, 2001. **27**(11): p. 1699-717.
99. Christmann, U., et al., *Role of lung surfactant in respiratory disease: current knowledge in large animal medicine*. J Vet Intern Med, 2009. **23**(2): p. 227-42.
100. Kuroki, Y. and D.R. Voelker, *Pulmonary surfactant proteins*. J Biol Chem, 1994. **269**(42): p. 25943-6.
101. Wright, J.R., *Immunoregulatory functions of surfactant proteins*. Nat Rev Immunol, 2005. **5**(1): p. 58-68.
102. McCormack, F.X., et al., *The structure and function of surfactant protein A. Hydroxyproline- and carbohydrate-deficient mutant proteins*. J Biol Chem, 1994. **269**(8): p. 5833-41.
103. Kuroki, Y., et al., *Surfactant proteins A and D: disease markers*. Biochim Biophys Acta, 1998. **1408**(2-3): p. 334-45.
104. Johansson, J. and T. Curstedt, *Molecular structures and interactions of pulmonary surfactant components*. Eur J Biochem, 1997. **244**(3): p. 675-93.
105. Sano, H. and Y. Kuroki, *The lung collectins, SP-A and SP-D, modulate pulmonary innate immunity*. Mol Immunol, 2005. **42**(3): p. 279-87.
106. Fisher, A.B., et al., *Pathway to lamellar bodies for surfactant protein A*. Am J Physiol Lung Cell Mol Physiol, 2010. **299**(1): p. L51-8.
107. Jain, D., et al., *SP-A is necessary for increased clearance of alveolar DPPC with hyperventilation or secretagogues*. Am J Physiol Lung Cell Mol Physiol, 2003. **284**(5): p. L759-65.
108. Kuroki, Y., R.J. Mason, and D.R. Voelker, *Alveolar type II cells express a high-affinity receptor for pulmonary surfactant protein A*. Proc Natl Acad Sci U S A, 1988. **85**(15): p. 5566-70.
109. Palaniyar, N., et al., *The role of pulmonary collectin N-terminal domains in surfactant structure, function, and homeostasis in vivo*. J Biol Chem, 2002. **277**(30): p. 26971-9.
110. Wu, Y.Z., et al., *Interaction of surfactant protein A with peroxiredoxin 6 regulates phospholipase A2 activity*. J Biol Chem, 2006. **281**(11): p. 7515-25.
111. Hartl, D. and M. Griese, *Surfactant protein D in human lung diseases*. Eur J Clin Invest, 2006. **36**(6): p. 423-35.
112. Botas, C., et al., *Altered surfactant homeostasis and alveolar type II cell morphology in mice lacking surfactant protein D*. Proc Natl Acad Sci U S A, 1998. **95**(20): p. 11869-74.
113. Tafel, O., et al., *Surfactant proteins SP-B and SP-C and their precursors in bronchoalveolar lavages from children with acute and chronic inflammatory airway disease*. BMC Pulm Med, 2008. **8**: p. 6.

114. Whitsett, J.A. and T.E. Weaver, *Hydrophobic surfactant proteins in lung function and disease*. N Engl J Med, 2002. **347**(26): p. 2141-8.
115. Hawgood, S., *Surfactant protein B: structure and function*. Biol Neonate, 2004. **85**(4): p. 285-9.
116. Mulugeta, S. and M.F. Beers, *Surfactant protein C: its unique properties and emerging immunomodulatory role in the lung*. Microbes Infect, 2006. **8**(8): p. 2317-23.
117. Wright, J.R., *Clearance and recycling of pulmonary surfactant*. Am J Physiol, 1990. **259**(2 Pt 1): p. L1-12.
118. Veldhuizen, R. and F. Possmayer, *Phospholipid metabolism in lung surfactant*. Subcell Biochem, 2004. **37**: p. 359-88.
119. Whitsett, J.A., S.E. Wert, and T.E. Weaver, *Alveolar surfactant homeostasis and the pathogenesis of pulmonary disease*. Annu Rev Med, 2010. **61**: p. 105-19.
120. Qamar, W., et al., *Analysis of Trace Elements in Rat Bronchoalveolar Lavage Fluid by Inductively Coupled Plasma Mass Spectrometry*. Biol Trace Elem Res, 2017. **178**(2): p. 246-252.
121. Suzuki, K., et al., *Trace and major elements status in bronchoalveolar lavage fluid in dogs with or without bronchopneumonia*. Biol Trace Elem Res, 2008. **124**(1): p. 92-6.
122. Lu, H., et al., *Zinc suppressed the airway inflammation in asthmatic rats: effects of zinc on generation of eotaxin, MCP-1, IL-8, IL-4, and IFN-gamma*. Biol Trace Elem Res, 2012. **150**(1-3): p. 314-21.
123. Govindaraju, K., et al., *Microanalysis of lung airway surface fluid by capillary electrophoresis with conductivity detection*. Anal Chem, 1997. **69**(14): p. 2793-7.
124. Nielson, D.W., *Electrolyte composition of pulmonary alveolar subphase in anesthetized rabbits*. J Appl Physiol (1985), 1986. **60**(3): p. 972-9.
125. Juettner, F.M., et al., *Pulmonary exchange of solutes during experimental lung lavage in pigs*. Respiration, 1988. **54**(4): p. 226-34.
126. Bargagli, E., et al., *Analysis of trace elements in bronchoalveolar lavage of patients with diffuse lung diseases*. Biol Trace Elem Res, 2008. **124**(3): p. 225-35.
127. *Standards for the diagnosis and care of patients with chronic obstructive pulmonary disease. American Thoracic Society*. Am J Respir Crit Care Med, 1995. **152**(5 Pt 2): p. S77-121.
128. Kim, V. and G.J. Criner, *Chronic bronchitis and chronic obstructive pulmonary disease*. Am J Respir Crit Care Med, 2013. **187**(3): p. 228-37.
129. Kim, V., et al., *The chronic bronchitic phenotype of COPD: an analysis of the COPD Gene Study*. Chest, 2011. **140**(3): p. 626-633.

130. Vestbo, J., E. Prescott, and P. Lange, *Association of chronic mucus hypersecretion with FEV1 decline and chronic obstructive pulmonary disease morbidity. Copenhagen City Heart Study Group.* Am J Respir Crit Care Med, 1996. **153**(5): p. 1530-5.
131. Yildirim, A.O., et al., *Palifermin induces alveolar maintenance programs in emphysematous mice.* Am J Respir Crit Care Med, 2010. **181**(7): p. 705-17.
132. Pauwels, R.A., et al., *Global strategy for the diagnosis, management, and prevention of chronic obstructive pulmonary disease: National Heart, Lung, and Blood Institute and World Health Organization Global Initiative for Chronic Obstructive Lung Disease (GOLD): executive summary.* Respir Care, 2001. **46**(8): p. 798-825.
133. Barnes, P.J., S.D. Shapiro, and R.A. Pauwels, *Chronic obstructive pulmonary disease: molecular and cellular mechanisms.* Eur Respir J, 2003. **22**(4): p. 672-88.
134. Thurlbeck, W.M. and N.L. Muller, *Emphysema: definition, imaging, and quantification.* AJR Am J Roentgenol, 1994. **163**(5): p. 1017-25.
135. Thurlbeck, W.M., *The incidence of pulmonary emphysema, with observations on the relative incidence and spatial distribution of various types of emphysema.* Am Rev Respir Dis, 1963. **87**: p. 206-15.
136. Gould, N.S., et al., *Aging adversely affects the cigarette smoke-induced glutathione adaptive response in the lung.* Am J Respir Crit Care Med, 2010. **182**(9): p. 1114-22.
137. Guerra, S., *Overlap of asthma and chronic obstructive pulmonary disease.* Curr Opin Pulm Med, 2005. **11**(1): p. 7-13.
138. Martinez, F.D., *The origins of asthma and chronic obstructive pulmonary disease in early life.* Proc Am Thorac Soc, 2009. **6**(3): p. 272-7.
139. Tudor, R.M., S. McGrath, and E. Neptune, *The pathobiological mechanisms of emphysema models: what do they have in common?* Pulm Pharmacol Ther, 2003. **16**(2): p. 67-78.
140. Hersh, C.P., D.L. DeMeo, and E.K. Silverman, *National Emphysema Treatment Trial state of the art: genetics of emphysema.* Proc Am Thorac Soc, 2008. **5**(4): p. 486-93.
141. Shapiro, S.D., *Elastolytic metalloproteinases produced by human mononuclear phagocytes. Potential roles in destructive lung disease.* Am J Respir Crit Care Med, 1994. **150**(6 Pt 2): p. S160-4.
142. Barnes, P.J., *Mediators of chronic obstructive pulmonary disease.* Pharmacol Rev, 2004. **56**(4): p. 515-48.
143. Barnes, P.J., *Mechanisms in COPD: differences from asthma.* Chest, 2000. **117**(2 Suppl): p. 10S-4S.
144. Pryor, W.A. and K. Stone, *Oxidants in cigarette smoke. Radicals, hydrogen peroxide, peroxyxynitrate, and peroxyxynitrite.* Ann N Y Acad Sci, 1993. **686**: p. 12-27; discussion 27-8.

145. Church, D.F. and W.A. Pryor, *Free-radical chemistry of cigarette smoke and its toxicological implications*. Environ Health Perspect, 1985. **64**: p. 111-26.
146. Kode, A., S.R. Yang, and I. Rahman, *Differential effects of cigarette smoke on oxidative stress and proinflammatory cytokine release in primary human airway epithelial cells and in a variety of transformed alveolar epithelial cells*. Respir Res, 2006. **7**: p. 132.
147. Hellermann, G.R., et al., *Mechanism of cigarette smoke condensate-induced acute inflammatory response in human bronchial epithelial cells*. Respir Res, 2002. **3**: p. 22.
148. Mio, T., et al., *Cigarette smoke induces interleukin-8 release from human bronchial epithelial cells*. Am J Respir Crit Care Med, 1997. **155**(5): p. 1770-6.
149. Chen, Q., et al., *TRPC6-dependent Ca(2+) signaling mediates airway inflammation in response to oxidative stress via ERK pathway*. Cell Death Dis, 2020. **11**(3): p. 170.
150. Chun, J. and A. Prince, *Ca<sup>2+</sup> signaling in airway epithelial cells facilitates leukocyte recruitment and transepithelial migration*. J Leukoc Biol, 2009. **86**(5): p. 1135-44.
151. Ribeiro, C.M., *The role of intracellular calcium signals in inflammatory responses of polarised cystic fibrosis human airway epithelia*. Drugs R D, 2006. **7**(1): p. 17-31.
152. Ratner, A.J., et al., *Cystic fibrosis pathogens activate Ca<sup>2+</sup>-dependent mitogen-activated protein kinase signaling pathways in airway epithelial cells*. J Biol Chem, 2001. **276**(22): p. 19267-75.
153. Crystal, R.G., *Alpha 1-antitrypsin deficiency, emphysema, and liver disease. Genetic basis and strategies for therapy*. J Clin Invest, 1990. **85**(5): p. 1343-52.
154. Janus, E.D., N.T. Phillips, and R.W. Carrell, *Smoking, lung function, and alpha 1-antitrypsin deficiency*. Lancet, 1985. **1**(8421): p. 152-4.
155. Senn, O., et al., *alpha1-Antitrypsin deficiency and lung disease: risk modification by occupational and environmental inhalants*. Eur Respir J, 2005. **26**(5): p. 909-17.
156. Holm, K.E., et al., *The impact of age on outcomes in chronic obstructive pulmonary disease differs by relationship status*. J Behav Med, 2014. **37**(4): p. 654-63.
157. Gramegna, A., et al., *Alpha-1 antitrypsin deficiency as a common treatable mechanism in chronic respiratory disorders and for conditions different from pulmonary emphysema? A commentary on the new European Respiratory Society statement*. Multidiscip Respir Med, 2018. **13**: p. 39.
158. Berndt, A., A.S. Leme, and S.D. Shapiro, *Emerging genetics of COPD*. EMBO Mol Med, 2012. **4**(11): p. 1144-55.
159. Diaz, P.T., et al., *Optimizing bronchodilator therapy in emphysema*. Proc Am Thorac Soc, 2008. **5**(4): p. 501-5.
160. Shafazand, S., *ACP Journal Club. Review: inhaled medications vary substantively in their effects on mortality in COPD*. Ann Intern Med, 2013. **158**(12): p. JC2.

161. Decramer, M., W. Janssens, and M. Miravittles, *Chronic obstructive pulmonary disease*. Lancet, 2012. **379**(9823): p. 1341-51.
162. Brusselle, G.G., et al., *Murine models of COPD*. Pulm Pharmacol Ther, 2006. **19**(3): p. 155-65.
163. Campbell, E.J., *Animal models of emphysema: the next generations*. J Clin Invest, 2000. **106**(12): p. 1445-6.
164. Ghorani, V., et al., *Experimental animal models for COPD: a methodological review*. Tob Induc Dis, 2017. **15**: p. 25.
165. Wright, J.L., M. Cosio, and A. Churg, *Animal models of chronic obstructive pulmonary disease*. Am J Physiol Lung Cell Mol Physiol, 2008. **295**(1): p. L1-15.
166. Mahadeva, R. and S.D. Shapiro, *Chronic obstructive pulmonary disease \* 3: Experimental animal models of pulmonary emphysema*. Thorax, 2002. **57**(10): p. 908-14.
167. Fehrenbach, H., *Animal models of chronic obstructive pulmonary disease: some critical remarks*. Pathobiology, 2002. **70**(5): p. 277-83.
168. Liang, G.B. and Z.H. He, *Animal models of emphysema*. Chin Med J (Engl), 2019. **132**(20): p. 2465-2475.
169. Longhini-Dos-Santos, N., et al., *Cell therapy with bone marrow mononuclear cells in elastase-induced pulmonary emphysema*. Stem Cell Rev Rep, 2013. **9**(2): p. 210-8.
170. Busch, R.H., et al., *Experimental pulmonary emphysema induced in the rat by intratracheally administered elastase: morphogenesis*. Environ Res, 1984. **33**(2): p. 497-513.
171. Abboud, R.T. and S. Vimalanathan, *Pathogenesis of COPD. Part I. The role of protease-antiprotease imbalance in emphysema*. Int J Tuberc Lung Dis, 2008. **12**(4): p. 361-7.
172. Leberl, M., A. Kratzer, and L. Taraseviciene-Stewart, *Tobacco smoke induced COPD/emphysema in the animal model-are we all on the same page?* Front Physiol, 2013. **4**: p. 91.
173. van der Strate, B.W., et al., *Cigarette smoke-induced emphysema: A role for the B cell?* Am J Respir Crit Care Med, 2006. **173**(7): p. 751-8.
174. Churg, A., M. Cosio, and J.L. Wright, *Mechanisms of cigarette smoke-induced COPD: insights from animal models*. Am J Physiol Lung Cell Mol Physiol, 2008. **294**(4): p. L612-31.
175. Valenca, S.S., et al., *Emphysema and metalloelastase expression in mouse lung induced by cigarette smoke*. Toxicol Pathol, 2004. **32**(3): p. 351-6.

176. Eltom, S., C. Stevenson, and M.A. Birrell, *Cigarette smoke exposure as a model of inflammation associated with COPD*. Curr Protoc Pharmacol, 2013. **Chapter 5**: p. Unit5 64.
177. Suga, T., et al., *Disruption of the klotho gene causes pulmonary emphysema in mice. Defect in maintenance of pulmonary integrity during postnatal life*. Am J Respir Cell Mol Biol, 2000. **22**(1): p. 26-33.
178. Glasser, S.W., et al., *Altered stability of pulmonary surfactant in SP-C-deficient mice*. Proc Natl Acad Sci U S A, 2001. **98**(11): p. 6366-71.
179. *The definition of emphysema. Report of a National Heart, Lung, and Blood Institute, Division of Lung Diseases workshop*. Am Rev Respir Dis, 1985. **132**(1): p. 182-5.
180. Hawgood, S., et al., *Sequential targeted deficiency of SP-A and -D leads to progressive alveolar lipoproteinosis and emphysema*. Am J Physiol Lung Cell Mol Physiol, 2002. **283**(5): p. L1002-10.
181. Korfhagen, T.R., et al., *Altered surfactant function and structure in SP-A gene targeted mice*. Proc Natl Acad Sci U S A, 1996. **93**(18): p. 9594-9.
182. Korfhagen, T.R., et al., *Surfactant protein-D regulates surfactant phospholipid homeostasis in vivo*. J Biol Chem, 1998. **273**(43): p. 28438-43.
183. Glasser, S.W., et al., *Pneumonitis and emphysema in sp-C gene targeted mice*. J Biol Chem, 2003. **278**(16): p. 14291-8.
184. Knudsen, L., et al., *Truncated recombinant human SP-D attenuates emphysema and type II cell changes in SP-D deficient mice*. Respir Res, 2007. **8**: p. 70.
185. Tokieda, K., et al., *Surfactant protein-B-deficient mice are susceptible to hyperoxic lung injury*. Am J Respir Cell Mol Biol, 1999. **21**(4): p. 463-72.
186. Mukhopadhyay, I., et al., *Expression of functional TRPA1 receptor on human lung fibroblast and epithelial cells*. J Recept Signal Transduct Res, 2011. **31**(5): p. 350-8.
187. Dietrich, A., *Modulators of Transient Receptor Potential (TRP) Channels as Therapeutic Options in Lung Disease*. Pharmaceuticals (Basel), 2019. **12**(1).
188. Nassini, R., et al., *Transient receptor potential ankyrin 1 channel localized to non-neuronal airway cells promotes non-neurogenic inflammation*. PLoS One, 2012. **7**(8): p. e42454.
189. Conklin, D.J., et al., *Role of TRPA1 in acute cardiopulmonary toxicity of inhaled acrolein*. Toxicol Appl Pharmacol, 2017. **324**: p. 61-72.
190. Lin, A.H., et al., *Lung Epithelial TRPA1 Transduces the Extracellular ROS into Transcriptional Regulation of Lung Inflammation Induced by Cigarette Smoke: The Role of Influxed Ca(2)(+)*. Mediators Inflamm, 2015. **2015**: p. 148367.

191. Corteling, R.L., et al., *Expression of transient receptor potential C6 and related transient receptor potential family members in human airway smooth muscle and lung tissue*. *Am J Respir Cell Mol Biol*, 2004. **30**(2): p. 145-54.
192. Finney-Hayward, T.K., et al., *Expression of transient receptor potential C6 channels in human lung macrophages*. *Am J Respir Cell Mol Biol*, 2010. **43**(3): p. 296-304.
193. Caterina, M.J., et al., *The capsaicin receptor: a heat-activated ion channel in the pain pathway*. *Nature*, 1997. **389**(6653): p. 816-24.
194. Reilly, C.A., et al., *Capsaicinoids cause inflammation and epithelial cell death through activation of vanilloid receptors*. *Toxicol Sci*, 2003. **73**(1): p. 170-81.
195. Baxter, M., et al., *Role of transient receptor potential and pannexin channels in cigarette smoke-triggered ATP release in the lung*. *Thorax*, 2014. **69**(12): p. 1080-9.
196. Choi, J.Y., et al., *TRPV1 Blocking Alleviates Airway Inflammation and Remodeling in a Chronic Asthma Murine Model*. *Allergy Asthma Immunol Res*, 2018. **10**(3): p. 216-224.
197. Groneberg, D.A., et al., *Increased expression of transient receptor potential vanilloid-1 in airway nerves of chronic cough*. *Am J Respir Crit Care Med*, 2004. **170**(12): p. 1276-80.
198. Garcia-Elias, A., et al., *The TRPV4 channel*. *Handb Exp Pharmacol*, 2014. **222**: p. 293-319.
199. Dietrich, A., et al., *Cation channels of the transient receptor potential superfamily: their role in physiological and pathophysiological processes of smooth muscle cells*. *Pharmacol Ther*, 2006. **112**(3): p. 744-60.
200. Jia, Y., et al., *Functional TRPV4 channels are expressed in human airway smooth muscle cells*. *Am J Physiol Lung Cell Mol Physiol*, 2004. **287**(2): p. L272-8.
201. Weber, J., et al., *TRPV4 channels are essential for alveolar epithelial barrier function as protection from lung edema*. *JCI Insight*, 2020. **5**(20).
202. Hayashi, S., T. Tenzen, and A.P. McMahon, *Maternal inheritance of Cre activity in a Sox2Cre deleter strain*. *Genesis*, 2003. **37**(2): p. 51-3.
203. Wyatt, A., et al., *Genetic strategies to analyze primary TRP channel-expressing cells in mice*. *Cell Calcium*, 2017. **67**: p. 91-104.
204. Dawson, P.A., J. Rakoczy, and D.G. Simmons, *Placental, renal, and ileal sulfate transporter gene expression in mouse gestation*. *Biol Reprod*, 2012. **87**(2): p. 43.
205. Mutze, K., et al., *Enolase 1 (ENO1) and protein disulfide-isomerase associated 3 (PDIA3) regulate Wnt/beta-catenin-driven trans-differentiation of murine alveolar epithelial cells*. *Dis Model Mech*, 2015. **8**(8): p. 877-90.
206. Keshavarz, M., et al., *Caveolin-1: Functional Insights into Its Role in Muscarine- and Serotonin-Induced Smooth Muscle Constriction in Murine Airways*. *Front Physiol*, 2017. **8**: p. 295.

207. Fois, G., et al., *ATP is stored in lamellar bodies to activate vesicular P2X4 in an autocrine fashion upon exocytosis*. J Gen Physiol, 2018. **150**(2): p. 277-291.
208. Mishra, A., et al., *Purinergic P2X7 receptor regulates lung surfactant secretion in a paracrine manner*. J Cell Sci, 2011. **124**(Pt 4): p. 657-68.
209. Miklavc, P., et al., *Fusion-activated Ca<sup>2+</sup> entry via vesicular P2X4 receptors promotes fusion pore opening and exocytotic content release in pneumocytes*. Proc Natl Acad Sci U S A, 2011. **108**(35): p. 14503-8.
210. Suki, B., et al., *Mechanical failure, stress redistribution, elastase activity and binding site availability on elastin during the progression of emphysema*. Pulm Pharmacol Ther, 2012. **25**(4): p. 268-75.
211. Churg, A., et al., *Tumor necrosis factor-alpha drives 70% of cigarette smoke-induced emphysema in the mouse*. Am J Respir Crit Care Med, 2004. **170**(5): p. 492-8.
212. Vlahovic, G., et al., *Cellular and connective tissue changes in alveolar septal walls in emphysema*. Am J Respir Crit Care Med, 1999. **160**(6): p. 2086-92.
213. Devos, F.C., et al., *Forced expiration measurements in mouse models of obstructive and restrictive lung diseases*. Respir Res, 2017. **18**(1): p. 123.
214. Papandrinopoulou, D., V. Tzouda, and G. Tsoukalas, *Lung compliance and chronic obstructive pulmonary disease*. Pulm Med, 2012. **2012**: p. 542769.
215. Kannler, M., et al., *TRPA1 channels: expression in non-neuronal murine lung tissues and dispensability for hyperoxia-induced alveolar epithelial hyperplasia*. Pflugers Arch, 2018. **470**(8): p. 1231-1241.
216. Cheong, N., et al., *Functional and trafficking defects in ATP binding cassette A3 mutants associated with respiratory distress syndrome*. J Biol Chem, 2006. **281**(14): p. 9791-800.
217. Bodin, P. and G. Burnstock, *Purinergic signalling: ATP release*. Neurochem Res, 2001. **26**(8-9): p. 959-69.
218. Praetorius, H.A. and J. Leipziger, *ATP release from non-excitabile cells*. Purinergic Signal, 2009. **5**(4): p. 433-46.
219. Haanes, K.A. and I. Novak, *ATP storage and uptake by isolated pancreatic zymogen granules*. Biochem J, 2010. **429**(2): p. 303-11.
220. Lazarowski, E.R., et al., *Molecular mechanisms of purine and pyrimidine nucleotide release*. Adv Pharmacol, 2011. **61**: p. 221-61.
221. Frick, M., et al., *Secretion in alveolar type II cells at the interface of constitutive and regulated exocytosis*. Am J Respir Cell Mol Biol, 2001. **25**(3): p. 306-15.
222. Haller, T., et al., *Dynamics of surfactant release in alveolar type II cells*. Proc Natl Acad Sci U S A, 1998. **95**(4): p. 1579-84.

- 
223. de Baaij, J.H., J.G. Hoenderop, and R.J. Bindels, *Magnesium in man: implications for health and disease*. *Physiol Rev*, 2015. **95**(1): p. 1-46.
224. Romani, A.M., *Cellular magnesium homeostasis*. *Arch Biochem Biophys*, 2011. **512**(1): p. 1-23.
225. Akopova, I., et al., *Imaging exocytosis of ATP-containing vesicles with TIRF microscopy in lung epithelial A549 cells*. *Purinergic Signal*, 2012. **8**(1): p. 59-70.
226. Irvin, C.G. and J.H. Bates, *Measuring the lung function in the mouse: the challenge of size*. *Respir Res*, 2003. **4**: p. 4.
227. Fujita, M., et al., *Overexpression of tumor necrosis factor-alpha produces an increase in lung volumes and pulmonary hypertension*. *Am J Physiol Lung Cell Mol Physiol*, 2001. **280**(1): p. L39-49.
228. Bonnardel, E., et al., *Determination of reliable lung function parameters in intubated mice*. *Respir Res*, 2019. **20**(1): p. 211.
229. Bates, J.H. and C.G. Irvin, *Measuring lung function in mice: the phenotyping uncertainty principle*. *J Appl Physiol* (1985), 2003. **94**(4): p. 1297-306.
230. Vanoirbeek, J.A., et al., *Noninvasive and invasive pulmonary function in mouse models of obstructive and restrictive respiratory diseases*. *Am J Respir Cell Mol Biol*, 2010. **42**(1): p. 96-104.
231. Shalaby, K.H., et al., *Combined forced oscillation and forced expiration measurements in mice for the assessment of airway hyperresponsiveness*. *Respir Res*, 2010. **11**: p. 82.
232. Glaab, T., et al., *Invasive and noninvasive methods for studying pulmonary function in mice*. *Respir Res*, 2007. **8**: p. 63.
233. Matthay, M.A., H.G. Folkesson, and C. Clerici, *Lung epithelial fluid transport and the resolution of pulmonary edema*. *Physiol Rev*, 2002. **82**(3): p. 569-600.
234. O'Brodovich, H., et al., *Expression of the epithelial Na<sup>+</sup> channel in the developing rat lung*. *Am J Physiol*, 1993. **265**(2 Pt 1): p. C491-6.
235. Helms, M.N., et al., *Redox regulation of epithelial sodium channels examined in alveolar type 1 and 2 cells patch-clamped in lung slice tissue*. *J Biol Chem*, 2008. **283**(33): p. 22875-83.
236. Wynne, B.M., et al., *Regulation of Lung Epithelial Sodium Channels by Cytokines and Chemokines*. *Front Immunol*, 2017. **8**: p. 766.
237. Dietrich, A., V. Chubanov, and T. Gudermann, *Renal TRP channels*. *J Am Soc Nephrol*, 2010. **21**(5): p. 736-44.
238. Viering, D., et al., *Genetic causes of hypomagnesemia, a clinical overview*. *Pediatr Nephrol*, 2017. **32**(7): p. 1123-1135.

- 
239. Clark, K., et al., *Massive autophosphorylation of the Ser/Thr-rich domain controls protein kinase activity of TRPM6 and TRPM7*. PLoS One, 2008. **3**(3): p. e1876.
240. Hasan, D., et al., *Excessive Extracellular ATP Desensitizes P2Y2 and P2X4 ATP Receptors Provoking Surfactant Impairment Ending in Ventilation-Induced Lung Injury*. Int J Mol Sci, 2018. **19**(4).
241. Patel, A.S., et al., *Paracrine stimulation of surfactant secretion by extracellular ATP in response to mechanical deformation*. Am J Physiol Lung Cell Mol Physiol, 2005. **289**(3): p. L489-96.
242. Chubanov, V. and T. Gudermann, *Lactate as a new second messenger shaping intracellular Mg(2+) dynamics and bioenergetics*. Cell Calcium, 2021. **93**: p. 102329.
243. Gout, E., et al., *Interplay of Mg2+, ADP, and ATP in the cytosol and mitochondria: unravelling the role of Mg2+ in cell respiration*. Proc Natl Acad Sci U S A, 2014. **111**(43): p. E4560-7.
244. Nierhaus, K.H., *Mg2+, K+, and the ribosome*. J Bacteriol, 2014. **196**(22): p. 3817-9.
245. Pontes, M.H., J. Yeom, and E.A. Groisman, *Reducing Ribosome Biosynthesis Promotes Translation during Low Mg(2+) Stress*. Mol Cell, 2016. **64**(3): p. 480-492.
246. Gourgoulianis, K.I., et al., *Magnesium as a relaxing factor of airway smooth muscles*. J Aerosol Med, 2001. **14**(3): p. 301-7.
247. Bhatt, S.P., et al., *Serum magnesium is an independent predictor of frequent readmissions due to acute exacerbation of chronic obstructive pulmonary disease*. Respir Med, 2008. **102**(7): p. 999-1003.
248. Aziz, H.S., et al., *Serum magnesium levels and acute exacerbation of chronic obstructive pulmonary disease: a retrospective study*. Ann Clin Lab Sci, 2005. **35**(4): p. 423-7.
249. Rolla, G., et al., *Hypomagnesemia in chronic obstructive lung disease: effect of therapy*. Magnes Trace Elem, 1990. **9**(3): p. 132-6.
250. Nagorni-Obradovic, L., et al., *Evaluation of magnesium in serum and urine in patients with pulmonary diseases*. Clin Lab, 2005. **51**(11-12): p. 647-52.
251. Landon, R.A. and E.A. Young, *Role of magnesium in regulation of lung function*. J Am Diet Assoc, 1993. **93**(6): p. 674-7.
252. Gumus, A., M. Haziroglu, and Y. Gunes, *Association of serum magnesium levels with frequency of acute exacerbations in chronic obstructive pulmonary disease: a prospective study*. Pulm Med, 2014. **2014**: p. 329476.
253. Hurst, J.R. and J.A. Wedzicha, *Management and prevention of chronic obstructive pulmonary disease exacerbations: a state of the art review*. BMC Med, 2009. **7**: p. 40.

- 
254. Vestbo, J., et al., *Global strategy for the diagnosis, management, and prevention of chronic obstructive pulmonary disease: GOLD executive summary*. Am J Respir Crit Care Med, 2013. **187**(4): p. 347-65.
255. Wedzicha, J.A., et al., *Acute exacerbations of chronic obstructive pulmonary disease are accompanied by elevations of plasma fibrinogen and serum IL-6 levels*. Thromb Haemost, 2000. **84**(2): p. 210-5.
256. Alter, H.J., T.D. Koepsell, and W.M. Hilty, *Intravenous magnesium as an adjuvant in acute bronchospasm: a meta-analysis*. Ann Emerg Med, 2000. **36**(3): p. 191-7.
257. Britton, J., et al., *Dietary magnesium, lung function, wheezing, and airway hyperreactivity in a random adult population sample*. Lancet, 1994. **344**(8919): p. 357-62.
258. Gilliland, F.D., et al., *Dietary magnesium, potassium, sodium, and children's lung function*. Am J Epidemiol, 2002. **155**(2): p. 125-31.
259. Amaral, A.F., et al., *The effect of acute magnesium loading on the maximal exercise performance of stable chronic obstructive pulmonary disease patients*. Clinics (Sao Paulo), 2012. **67**(6): p. 615-22.
260. Cheuk, D.K., T.C. Chau, and S.L. Lee, *A meta-analysis on intravenous magnesium sulphate for treating acute asthma*. Arch Dis Child, 2005. **90**(1): p. 74-7.
261. Blitz, M., et al., *Aerosolized magnesium sulfate for acute asthma: a systematic review*. Chest, 2005. **128**(1): p. 337-44.
262. Abreu Gonzalez, J., et al., *[Effect of intravenous magnesium sulfate on chronic obstructive pulmonary disease exacerbations requiring hospitalization: a randomized placebo-controlled trial]*. Arch Bronconeumol, 2006. **42**(8): p. 384-7.
263. Davalos Bichara, M. and R.D. Goldman, *Magnesium for treatment of asthma in children*. Can Fam Physician, 2009. **55**(9): p. 887-9.

# Acknowledgements

First of all, I am very thankful to my main supervisor, Prof. Dr. Thomas Gudermann for being my doctor father and for his scientific guidance and also supporting me from the first time until the end as a young woman with a child in the academic career.

I would like to express my profound gratitude to Dr. Vladimir Chubanov who gave me the opportunity to perform this PhD project in his lab. I am very grateful for his permanent support, excellent supervision, great scientific enthusiasm and encouragement throughout this long walk. I deeply appreciate his careful revision of all my work including thesis and the publications.

I also want to thank Prof. Alexander Dietrich, Prof. Nikolaus Kneidinger and Prof. Tobias Heer for their willingness to be a member of my examination board.

My sincere thanks go to Dr. Sabine Bauer whom I met during my master thesis at Roche and inspired me to start with PhD, for the constant motivation, encouragement and her trust in me.

I am also very glad and thankful for having met and worked with Dr. Ali Önder Yildirim who is experienced in lung diseases at Helmholtz Zentrum Neuherberg, for his willing collaboration, advices offering a valuable view and for his important considerations and suggestions with animal experiments and many thanks to his team who helped me during all animal experiments at Helmholtz Zentrum.

Moreover, I also want to thank our cooperation partners Prof. Ulrich Böhm for the generation of a new mouse line, Dr. David Simmons for helping us with in situ hybridization, Dr. Ilia Rodushkin for his support in ICP-MS analysis and Dr. Gabriela Krasteva-Christ for her support in electron microscopic analysis of lung samples.

I deeply appreciate and thank to the team of our animal facility, especially Clarinda Hofer, Sandra Barfuß and Petra Eigner for being good organized, their help and support.

Especially, I would like to thank all the previous and present members of my group: Silvia Ferioli, Lorenz Mittermeier, Eva Schmidt, Miyuki Egawa, Anna Rössig and Angel Tseung for the friendly atmosphere in the lab and for their support. For the valuable technical assistance in the laboratory and the excellent experimental contribution, I am deeply grateful to Joanna Zaißerer and Anna Erbacher for the preparation of most part of my experiments, and also for patiently supporting me and for their encouragement during this journey. Particularly, I am deeply thankful to Anna who became a very good friend throughout the years, for her contribution to my project as a research assistance, always being extremely good organized and for her excellent support with animal experiments.

I would also to extend my thanks to all members of secretariat team for the outstanding administrative support, especially to Jutta Schreier, for her unlimited help in all occasions.

I would like to thank all members of Walther Straub Institute, for the support I have received during these years.

I would like to express my gratitude to my parents for their constant support, love, patience and encouragement throughout the whole time of my life. I thank them for always being there for me whenever I needed.

Last but not least, I would like to thank to my beloved husband, Arda Akdogan, for his never-ending patience, encouragement and for being a constant source of support during the challenges of PhD journey. I am truly thankful for having you in my life! I also would like to express my deepest thanks to my little daughter, Hazal, who came in the middle of my thesis, for giving me unlimited happiness, pleasure and motivation. Without the love of my treasures Arda and Hazal, this work would never have been possible.

# Eidesstattliche Versicherung

Akdogan, Banu

Ich erkläre hiermit an Eides statt, dass ich die vorliegende Dissertation mit dem Titel:

**”Role of kinase-coupled TRPM6 ion channels in the lung”**

selbständig verfasst, mich außer der angegebenen keiner weiteren Hilfsmittel bedient und alle Erkenntnisse, die aus dem Schrifttum ganz oder annähernd übernommen sind, als solche kenntlich gemacht und nach ihrer Herkunft unter Bezeichnung der Fundstelle einzeln nachgewiesen habe.

Ich erkläre des Weiteren, dass die hier vorgelegte Dissertation nicht in gleicher oder in ähnlicher Form bei einer anderen Stelle zur Erlangung eines akademischen Grades eingereicht wurde.

München, 20.01.2021

Banu Akdogan

---

---

# Curriculum vitae

## **Personal data:**

Name: Banu Akdogan  
Date of birth: 09.06.1988  
Place of birth: Karabük, Turkey  
Citizenship: German  
Address: Cimbernstr. 74B, 81377 München  
Mobile phone: +49 172 2013303  
E-mail: banuakdogan72@gmail.com

## **Scientific education:**

06/2014 – 12/2020 Dissertation at Walther-Straub-Institute of Pharmacology and Toxicology, Ludwig Maximilians University of Munich, Germany  
Doctoral thesis: Role of kinase-coupled ion channel TRPM6 in the lung  
Supervisors: Prof. Dr. med. Thomas Gudermann, Dr. Vladimir Chubanov

03/2016 – 08/2016 Maternal leave

09/2011 - 11/2013 Master of Science in Advanced Materials Science at Technical University of Munich, Germany  
Master's thesis: Surface characterization of stainless steel surfaces in pharma industry by electrochemical methods and XRD  
Supervisors: Prof. Dr. Hubert A. Gasteiger, Dipl. Ing. Michael Clever

09/2006 - 06/2011 Bachelor of Science in Chemistry (Major: biochemistry) at Middle East Technical University of Ankara, Turkey  
Bachelor's thesis: Surface enhanced Raman spectroscopy (SERS) applications for DNA detection on gold surfaces  
Supervisors: Prof. Dr. Mürvet Volkan, Prof. Dr. Semra Tuncel

## **Secondary education:**

09/2002 - 06/2006 High school diploma (Abitur) at Karabük Anatolian School, Turkey

**Publications:**

**Epithelial magnesium transport by TRPM6 is essential for prenatal development and adult survival.**

Chubanov V, Ferioli S, Wisnowsky A, Simmons DG, Leitzinger C, Einer C, Jonas W, Shymkiv Y, Bartsch H, Braun A, **Akdogan B**, Mittermeier L, Sytik L, Torben F, Jurinovic V, van der Vorst EP, Weber C, Yildirim ÖA, Sotlar K, Schürmann A, Zierler S, Zischka H, Ryazanov AG, Gudermann T.

*eLife*. 2016; ;5:e20914 doi: 10.7554/eLife.20914

**Disruption of TRPM6 uncovers a critical role of respiratory Mg<sup>2+</sup> balance for alveolar tissue homeostasis**

The paper is in progress and will be submitted parallel to thesis.

**Talks and posters:**

**Walther Straub Institute, 2015-2019**

Role of the kinase-coupled ion channel TRPM6 in the lung

**Regulation of cell functions by transient receptor potential channels, Herrsching, Germany; September 2016**

A role of the kinase-coupled ion channel TRPM6 in the lung, poster

**Practical course human biology: Heart, Lung and Metabolisms, 2019**

Assessment of living alveolar epithelial cells by fluorescent markers